Fall 12-18-2017

Displacement Measurement Using a Laser Doppler Vibrometer Mounted on an Unmanned Aerial Vehicles

Piyush Garg
University of New Mexico

Follow this and additional works at: https://digitalrepository.unm.edu/ece_etds

Part of the Electrical and Computer Engineering Commons

Piyush Garg

Candidate

Electrical and Computer Engineering

Department

This thesis is approved, and it is acceptable in quality and form for production:

Approved by the Thesis Committee:

Dr. Rafael Fierro, Co-Chair

Dr. Fernando Moreu, Co-Chair

Dr. Su Zhang

Dr. David Mascareñas

**DISPLACEMENT MEASUREMENT USING A LASER DOPPLER VIBROMETER
MOUNTED ON AN UNMANNED AERIAL VEHICLES**

by

**PIYUSH GARG
B.E., ELECTRONICS AND TELECOMMUNICATION,
UNIVERSITY OF MUMBAI, INDIA 2010**

THESIS

Submitted in Partial Fulfillment of the
Requirements for the Degree of

Master of Science

Electrical Engineering

The University of New Mexico
Albuquerque, New Mexico

May 2018

To my parents, thank you for always supporting my dreams

To my sister, I wouldn't have been here without you

To Upasana, thank you for being my rock

To my BiL, you motivate me always

To Tashvi, you are my inspiration

ACKNOWLEDGEMENT

DISPLACEMENT MEASUREMENT USING A LASER DOPPLER VIBROMETER MOUNTED ON AN UNMANNED AERIAL SYSTEM

by

Piyush Garg

B.E., Electronics and Telecommunication, University of Mumbai, India, 2010

M.S., Electrical Engineering, University of New Mexico, USA, 2017

ABSTRACT

The railroad network in the united states is one of the best in the world, handling around 40 percent of all US freight movement. To maintain the serviceability and cost-effective operation of the railway infrastructure, regular monitoring is essential. Bridges are a critical part of the railway infrastructure and their timely maintenance and repair is important. Measuring transverse bridge displacement under train loading can assist to determine the bridge condition. The traditional methods available for transverse displacement measurement include Linear Variable Differential Transducers (LVDT). However, irregular terrain, remote and inaccessible locations, and the height of railroad bridges make implementation of these sensors for transverse displacement measurement either inadequate, or risky and time-consuming, and sometimes not possible altogether. Alternatively, railroads can monitor transverse bridge displacement using non-contact sensing with instruments such as robotic total station (RTS) and high-

speed cameras. In recent years, the use of Laser Doppler Vibrometers (LDV) has started to draw some attention in the field of non-contact transverse bridge displacement measurement. However, in these applications, the instruments are generally placed on a fixed reference close to the bridge. It is not always possible to find this fixed reference point, especially when a bridge is spanning over a large opening, like a water body. In addition, a fixed reference point would require calibration of the measurement for every different bridge individually. Researchers use Unmanned Aerial Systems (UAS) to acquire aerial images for Structural Health Monitoring (SHM). However, this approach requires extensive image post-processing, and in general, complex algorithms development. More importantly, current systems are not capable of measuring dynamic transverse displacements. This MS Thesis presents a novel approach to measure transverse bridge dynamic displacements using non-contact vibrometers mounted on unmanned aerial system. This research proposes algorithms for compensating the measurement errors due to the angular and linear movement vibrometer to obtain accurate transverse bridge displacement measurements. These algorithms are verified in the laboratory using a shake table simulating bridge vibration, and vibrometer movement simulating the motions of a UAS. The results of these tests show that the signal difference between the measured displacements of a moving LDV system and a LVDT are less than 10%. The Root mean squared (RMS) differences are less than 5%. This research also implements and tests the UAV-LDV system in the field. The results of these experiments show that the signal difference between LVDT and the UAS-LDV system is 10%. The RMS difference between

the two systems is 8%. The results of this research show that the UAS and LDV

can be used together to measure the dynamic transverse bridge displacements

and could become and effective tool for campaign monitoring of railroad bridges

with application for railroad bridge maintenance and repair prioritization.

TABLE OF CONTENTS

List of Figures

List of Tables

Chapter 1: Introduction

This chapter focuses on the motivation driving this research. This research proposes and implements a new method of transverse displacement measurement using an unmanned aerial system (UAS). The outcome of this work are: (1) a new method for using laser doppler vibrometer (LDV) as an aerial subsystem instead of a ground based system, and (2) methods and algorithms to correct the errors in the output signal due to the motion of the vibrometer. The first part of this research focuses on measurement of simulated bridge movements under dynamic train loading under laboratory conditions using a moving vibrometer. The corrections to the signal are based on the trigonometric relations to obtain the correct readings using the angle made by the vibrometer to the target. The second part of the research focuses on mounting the vibrometer to the UAS and flying it in the field to collect the target's transverse displacements. The displacements collected are compared to the measurements obtained using an LVDT.

1.1 US Infrastructure Decay

As of 2017, according to the American Society of Civil Engineers (ASCE) infrastructure report card, the majority of the infrastructure in the US received a grade of D or less with an overall grade of D+ (ASCE 2017). For the past decade, the infrastructure in the US has constantly received poor grades (ASCE 1988, 1998, 2001, 2005, 2009, 2013, 2017). The overview of the American infrastructure grade performance over the last couple of decades is summarized in Table 1-1.

Table 1-1. US infrastructure grade performance 1988 – 2017 (ASCE 1988,1998, 2001, 2005, 2009, 2013, 2017)

Year	1988	1998	2001	2005	2009	2013	2017
Roads	C+	D-	D+	D	D-	D	D
Bridges	-	C-	C	C	C	C+	C+
Transit	C-	C	C-	D+	D	D	D-
Aviation	B-	C-	D	D+	D	D	D
School	-	F	D-	D	D	D	D+
Railways	-	-	-	C-	C-	C+	B
Waterways	-	-	D+	D-	D-	D-	D
Energy	-	-	D+	D	D+	D+	D+
Dams	B	D	D	D	D	D	D
Cumulative	**C**	**D**	**D+**	**D**	**D**	**D+**	**D+**

Figure 1-1 shows the estimated investment required for maintenance of the infrastructure over the past 15 years. The investment required to maintain the infrastructure has been constantly on the rise. The investment estimate required for maintaining the infrastructure by 2025 currently stands at 4.59 trillion, with an available investment of 2.526 trillion and an investment gap of 2.064 trillion (ASCE 2017).

There is a need to prioritize the maintenance and repair within the infrastructure network. Engineers and managers are looking for data acquisition that inform their decisions about the safety and maintenance prioritization (Moreu 2015). Collecting data about the health of individual structures within the network can inform managers on which structures to prioritize first.

TOTAL ESTIMATED INVESTMENT PROJECTION FOR INFRASTRUCTURE MAINTENANCE BY YEAR ($ TRILLION)
(ASCE 2001,2005,2009,2013,2017)
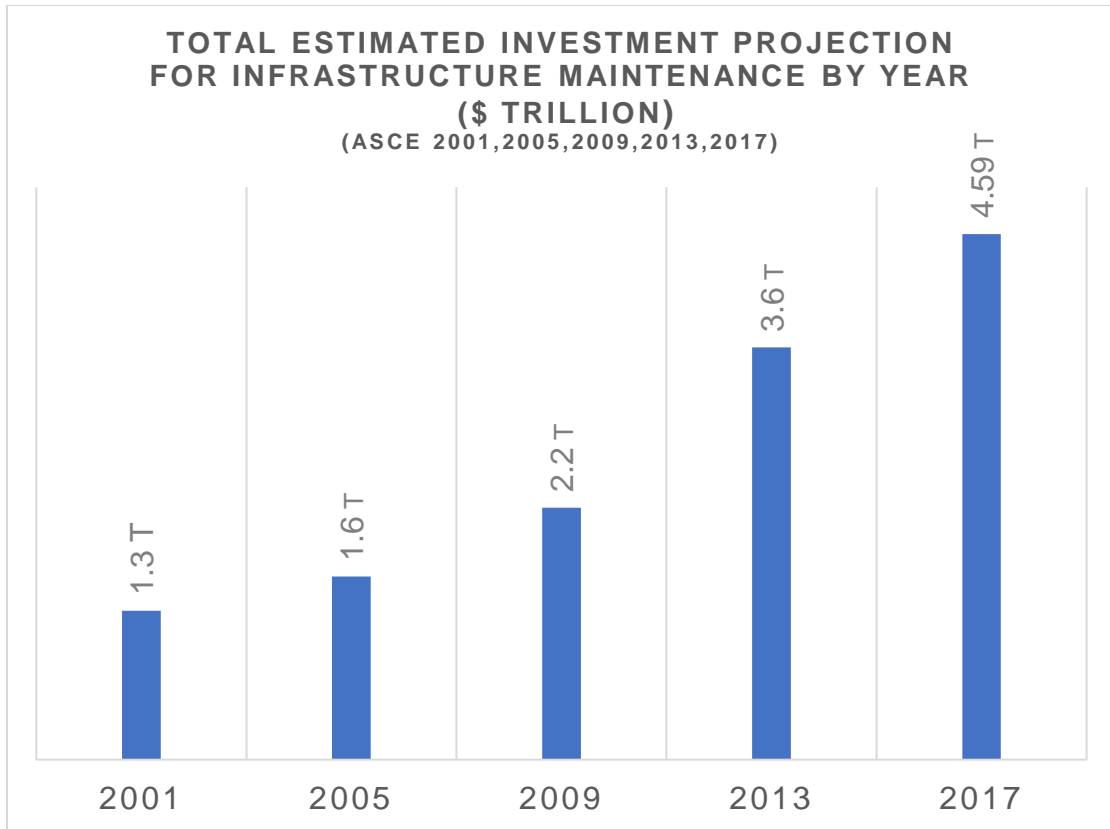
Figure 1-1. Total estimated investment projection for infrastructure maintenance by year (ASCE 2001, 2005, 2009, 2013, 2017)

1.2 Structural Health Monitoring: Displacements

Structural health monitoring (SHM) of an infrastructure includes monitoring dynamic movements as indicators of the health of the system (Nagayama and Spencer, 2007). According to a survey conducted in 2010, displacement measurement under dynamic loading is an important aspect for SHM of railroad bridges and provides objective information about the performance of bridges (Moreu and LaFave 2012). Table 1-2 shows the result of the survey ranking railroad bridge research topics.

Table 1-2. Ranking of 2010 railroad bridge research topics (Moreu and LaFave 2012)

Topics	Fields
Deflection measurement	1
High speed trains	2
Long span bridges	3
Approaches	4
Longitudinal forces	5
New design loads	6

1.3 Railroad Bridge Displacement and Monitoring

The US railroad network is one of the best freight systems in the world (FRA 2015). Railroads in America carry up to 40% of the total cross-country freight (FRA 2010). The network of railways is 140,000 miles long (AAR 2013, AAR 2015) with approximately 100,000 bridges (Infrastructure Report Card (IRC) 2017). In other words, on average there is one bridge every 1.4 mile. Thus, the performance of the bridges is very critical for the safe operation of the rail networks.

In US, more than 50% of the railroad bridges are more than 100 years old (AREMA 2003), making the maintenance of bridges a top priority for railroad bridge engineers (Moreu, 2015). The under-maintenance of the railroad bridges could pose a significant threat to the safety of train operations, cause derailments, delay network operations, and losses in terms of valuable time, resources, and costs. To

pro-actively avoid any of these and plan accordingly, bridge engineers and managers make regular bridge inspections a priority across their network. Figure 1-2 shows a crew inspecting a railroad bridge.

Figure 1-2. Inspectors monitoring a railway bridge (Bridge access specialties 2017)

1.4 Sensors

Researchers use different sensors to monitor of the infrastructure performance. These sensors range from traditional contact sensors like LVDT and accelerometers, to modern smart sensors which use wireless communication and microcontroller based data acquisition. Other sensors like robotic total stations, high speed cameras, and global positioning systems have been used to measure infrastructure performance as well. However, each of these methods have their limitations. Laser based systems such as laser doppler vibrometers (LDV), laser triangulation sensors, and light detection and ranging (LiDAR) are used for infrastructure monitoring. LiDAR technologies can measure slow changes in a

structure or environment, but are not capable of measuring real-time dynamic responses. Following research from Morey et al. (2014), the measurement of the dynamic transverse displacements of railroad bridges can inform railroad managers of the condition of the bridges. LDVs are good for measuring dynamic transverse displacements, however, these systems need to be installed on a ground surface close to the bridges, which might not always be possible. Thus, the need for accessing the structure, when installing these sensors limits their field implementation.

1.5 Unmanned Aerial System (UAS)

UAS platforms are being used in several areas including inspection, photography, surveillance, data collection, and remote sensing (Blanks. M, 2016). The use of UAS offers more flexibility and access to the structures, which was previously not possible (Cummings et al. 2017). Due to their agility UAS have found their use in several applications such as disaster management (Restas 2015), oil spill surveillance and detection (Allen and Walsh 2008), soil erosion monitoring (d'Oleire-Oltmanns et al. 2012), forest ecosystem and biodiversity monitoring (Getzin et al. 2014), and deforestation detection (Paneque-Gálvez et al. 2014).

Structural engineers and managers are interested in UAS based systems implementing image processing and 3D mapping the structures being inspected (Yoon et al. 2017). UAS systems have also been in SHM in form of novel methods like checking the quality of the concrete by tap testing it with a hammer mounted UAS due to their accessibility (Mason et al. 2016, Moreu et al. 2017). Other

researchers have used digital image correlation (DIC) methods using UAS to collect vertical and longitudinal displacements (Yoon et al. 2016) There is an intensive post processing involved with this technique which makes data acquisition slow, and real-time solutions currently do not exist. Thus, while the UAS based data acquisition solves the problems of displacement acquisition in the vertical and transverse directions, the onboard technology is not capable of measuring real-time and dynamic transverse displacements. In summary, current UAS innovations can measure vertical and longitudinal displacements and cannot obtain the real-time responses during the train crossing event, which may be needed in the field.

1.6 Thesis Outline

This research proposes a new method to measure real-time transverse bridge displacements with a LDV mounted on a UAS. The author of this research uses transverse bridge displacement data under train loading for validating the method. This research first proposes and tests the method of measuring transverse bridge displacements using a moving vibrometer in the laboratory, including the algorithms to compensate for the vibrometer movement. The author then measures transverse bridge displacements in the field using a LDV mounted on a UAS. The measured displacements are compared with the actual displacement obtained from the LVDT to validate the output of the vibrometer.

Chapter 2 explores the current efforts and methods for bridge displacement measurement, and identifies the research needs based on the capabilities of the existing systems.

Chapter 3 studies the capabilities of the LDV to measure transverse displacements in laboratory conditions. The output of the vibrometer is first analyzed for different vibrations: (1) sinusoidal, (2) earthquake (zero mean), and (3) train loading of bridge (non-zero mean). The author then proposes algorithms using a vibrometer to measure transverse displacements when in moving conditions. These algorithms are then tested in the laboratory environment and the results are analyzed.

Chapter 4 describes the tests using a LDV mounted on a UAS for measuring transverse displacements in the field. The LDV is mounted on the UAS and tested for measuring the dynamic transverse displacements of the target moving with a bridge displacement. The results are analyzed to evaluate the ability of the new system to measure dynamic displacements in the transverse direction under train crossing events.

Chapter 5 summarizes the results of this research and draws conclusions from the experiments. The future work on this technology, limitations of the technique, and applications in other fields are also discussed in this chapter.

Chapter 2: Literature Review

2.1 Introduction

This chapter provides an overview of the current methods for measuring transverse bridges displacements, discusses their inadequacy, and provides the motivation behind the new technique proposed in this research. First, the author discusses the importance of displacement measurement in the railway industry. Then, the current techniques and their shortcomings are listed. After that, the recent trends in the field of railway bridge monitoring and new techniques are discussed. The last part of this chapter discusses the proposed solution.

2.2 Railroad Bridge Displacement Measurement

To ensure operation safety, the railroad owners inspect bridges regularly. Currently, most of the methods for bridge inspection either involve visual inspection (AAR 2016), or mounting of sensors on railway bridges. Figure 2-1 shows a railway bridge inspection during a train passing event. Visual inspection, however, do not always provide the reliable information (Agdas 2015).

According to a survey conducted in 2010, displacement measurements under dynamic loading are an important aspect of railroad bridge performance and provide objective information about the safety the bridges and railroad operations (Moreu and LaFave 2012).

Figure 2-1. Visual inspection of railroad bridges.

2.3 Monitoring Bridge Displacements using Contact Sensors

The railroad industry is interested in measuring the transverse displacement of the bridges. There are different places to measure transverse displacement in different types of bridges. For short span timber bridges, the ideal place to measure the transverse bridge displacement in at the top of the pile, and for long span steel bridges the location ideal to measure the displacements mid-span. To collect the data on the field is cumbersome and complex because collecting displacements require a fixed point. Moreu et al. (2014) demonstrated the use of LVDT transverse bridge displacement measurements under dynamic train loading. This approach of physically mounting the sensor to the bridge and repeating the procedure for every test takes time, and in many situations, is very challenging for bridges spanning over large openings, such as a water body or a deep gorge. Figure 2-2 shows an attempt to measure transverse bridge displacement using a LVDT (Moreu et al. 2015a).

Figure 2-2. Transverse bridge displacement using a LVDT (Moreu et al. 2015a)

Alternative to LVDT, researchers have used accelerometers as contact sensors to collect reference free transverse bridge displacements. Use of accelerometers to double integrate their accelerations readings and to obtain displacement, as demonstrated by Yang et al. (2005). This method has been used for displacement measurement (Hoag et al. 2017, Ozdagli et al. 2017, Gomez et al. 2017). Figure 2-3 shows two accelerometers installed on a bridge to measure transverse bridge displacements (Sheppard 2010). Although mounting an accelerometer is easier compared to an LVDT, it still requires physical installation of the sensor on the bridge which is not always possible and involves safety concerns for bridge engineers. Moreover, the output of an accelerometer is acceleration data which needs to be integrated to obtain the displacement data hence adding a drift to the data, and not always reliable.

Figure 2-3. Accelerometers installed on a bridge to measure bridge displacements (Sheppard 2010)

In recent years, researchers have used global positioning systems (GPS) as contact sensors to measure displacements (Wang et al. 1991, Ashkenazi and Roberts 1997, Meng, et al. 2007, Watson et al. 2007, Yi et al. 2013). Figure 2-4 shows the monitoring of displacements of highway bridge using GPS (Carnenbroeck 2015).

Figure 2-4. GPS for bridge displacement measurement (Carnenbroeck 2015)

However, the readings from a GPS unit are not accurate for detecting small displacements, as in the case of train crossing events over the railway bridges. Smyth and Wu (2007), Kogan et al. (2008), and Moschas and Stiros (2013) fused GPS data along with the measurement captured with accelerometers and inertial measurement unit (IMU) for the purpose of accuracy. However, this setup still needs installation in the field which is not always feasible.

2.4 Bridge Displacement Monitoring Using Non-Contact Sensors

To overcome the drawbacks of the contact sensors, a number of researchers studied the feasibility of non-contact sensors to measure transverse bridge displacements. For example, Panos and Stiros (2007, 2013) proposed the use of a robotic total station (RTS) for non-contact displacement detection of highway bridges. Figure 2-5 shows the use of a robotic total station for railway bridge monitoring (Psimoulis and Stiros, 2013).

Figure 2-5. Railway bridge monitoring using a robotic total station (Psimoulis and Stiros, 2013)

RTS monitors displacement by autonomously identifying and tracking the target. Nakamura (2000), and Moschas et al. (2013) proposed a solution pairing

RTS with GPS for more accurate displacement measurement. However, this system is dependent on right atmospheric conditions to give accurate output. While RTS is good for measuring static changes to the bridge structure over a long period of time, it cannot measure dynamic transverse bridge displacements. Also, RTS requires to be set up close to the target, which might not always be possible.

Another method for non-contact displacement measurement widely studied is image processing (Olaszek 1999, Lee and Shinozuka 2006, Fukuda et al. 2010, Feng et al. 2015, Feng et al. 2015a). Figure 2-6 shows the implementation of the high-speed camera for the structural health monitoring of a highway bridge.

Figure 2-6. High speed camera for highway bridge monitoring (iMetrum 2017)

However, there are several drawbacks to the aforementioned methods for measuring displacements. The instruments must be set up close to the target, which is not always possible, and the readings are not accurate if measured from a distance. The accuracy of measurement is also dependent on lighting and environmental conditions. Besides this, complex algorithm development is required for post-processing to extract information from the images captured. Another factor affecting the use of the methods is that they always require either

calibration of camera properties or some reference for comparison and displacement detection.

2.5 Light Detection and Ranging (LiDAR) and LDV for Bridge Monitoring

Light detection and ranging (LiDAR) is a laser light based sensor which gives a point cloud, and helps developing and analyzing the 3D modelling of the infrastructure (NOAA 2016). The UAS based LiDAR system has been researched as a low-cost sensor for infrastructure management (Zhang et al. 2014). Aerial LiDAR systems have been used in 3D detection and modelling of buildings (Verma et al. 2006) as well as for mapping topographical features (Siebert and Teizer 2014).

The airborne LiDAR systems have been used in detection of some dynamic activities such as landslide mapping and damage assessment (Liu et al. 2011), building and infrastructure change detection over time (Vu et al. 2004, Chen and Lin 2010), and volumetric changes in coastal dunes detection (Woolard and Colby 2002). Figure 2-7 (left) shows a 3-D point cloud image output from a LIDAR sensor and Figure 2-7 (right) shows the implementation and working of an aerial lidar system.
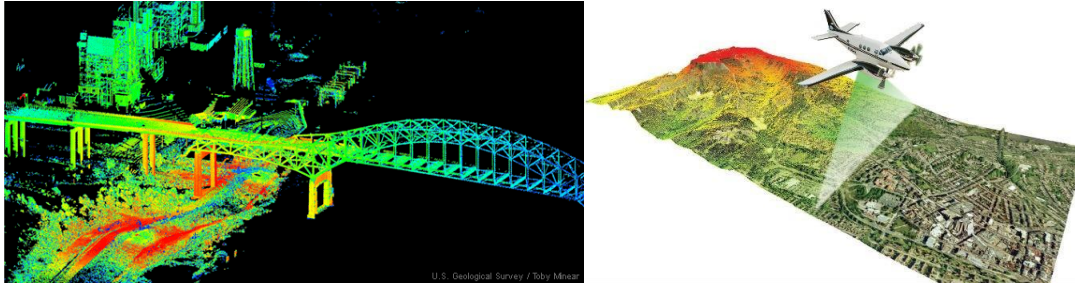
Figure 2-7. 3-D point cloud image output a lidar camera (left) (Marshall 2013), and implementation and working of an airborne lidar (right) (Brumm 2012)

These physical structures may change their coordinates over time due to long term decay of their structural properties. However, they are not real-time changes, and usually take years or decades to occur, or natural disasters. Thus, multiple flights spaced in time can help in change detection. However, transverse bridge displacements due to train loading is dynamic (seconds, or minutes under a long train) and cannot be detected using a LiDAR.

LDV measures target vibration using changes in frequency due to the Doppler Effect. Researchers have also LDV as a non-contact sensor to measure bridge displacements (Nassif et al. 2005). This device needs to be placed on a rigid surface near the target. However, the operation distance is usually long. Figure 2-8 shows the use of a Laser doppler vibrometer for structural health monitoring of a highway bridge (Mehrabi 2006)

Figure 2-8. Laser doppler vibrometer for structural health monitoring of a highway bridge (Mehrabi, 2006)

The output of LDV is not dependent on visibility and atmospheric conditions, and the output of a LDV is real-time requiring minimal post-processing. Although these advantages make the use of a LDV effective for transverse bridge displacement measurement, it still requires a surface close to the target and currently is not a reference free displacement sensor.

2.6 UAS for Bridge Monitoring

Researchers have used UAS based systems for bridge monitoring in recent years (Mascarenas et al. 2008, Kim et al. 2015, Ham et al. 2016, Hawken et al. 2017, Ellenberg 2017). UAS systems have also been used in form of novel methods like checking the quality of the concrete by tap testing it with a hammer mounted UAS (Mason et al. 2016). Figure 2-9 shows an aerial monitoring of a bridge (Smart Sensys 2017).

Figure 2-9. UAS for bridge monitoring (Smart Sensys 2017)

Researchers have uses camera mounted UAS for bridge structural health monitoring (Ellenberg et al. 2014, 2016, Yoon et al. 2016). 3D image correlation on images captured by cameras on the UAS (Reagan 2017) and photogrammetry using a UAS (Chan et al. 2017) have also been researched for SHM. Chen (2015) demonstrated the use of aerial photography in combination with GPS to detect sub-inch crack in concrete surfaces.

Using cameras and other devices mounted to UAS solves the problems related to accessibility in remote locations and hazardous conditions. However, this method still requires a reference for image processing, post processing of the captured data, and algorithms to extract valuable information from the collected data. Combining the agility and accessibility of the UAS with the real-time operation, ease of use, minimal post processing of LDV.

2.7 Proposed Research

It can be concluded from the previous research that the methods to collect transverse bridge displacements are of interest and can benefit owners. The use of non-contact sensors is an improvement over the contact method. The

integration of laser doppler vibrometer and unmanned aerial systems can overcome their respective drawbacks.

While an aerial system gives better reachability, more agility, and can be made autonomous, the current onboard technology for displacement measurement does not allow real-time measurements and cannot collect displacements perpendicular to the UAS. It can also be seen that the laser doppler vibrometer can measure displacements with high accuracy and in real-time, but lack the accessibility to bridges and need to be operated from the ground. This research explores using the advantages of the vibrometer to overcome the disadvantage of the aerial system, and vice versa. Thus, they can be used complimentary to each other. The summary of the advantages and disadvantages of both these systems can be seen in Table 2-1.

The ideal solution for the dynamic transverse bridge displacement monitoring is to combine the agility and accessibility of the aerial system with the displacement measurement capabilities of a vibrometer. In this research, an airborne vibrometer system is proposed for dynamic transverse bridge displacement measurement of railway bridges under train loading.

Table 2-1: Summary of advantages and disadvantages of an aerial system and a laser doppler vibrometer

	Unmanned Aerial Systems	Laser Doppler vibrometer
Advantages	• Accessibility • Agility • Autonomous	• Minimal post processing • Large stand-off distance • Real-time output • Non-contact displacement measurement.
Disadvantages	• No real-time output • Cannot measure displacement perpendicular to UAS • More post-processing time	• Requires mounting on ground • Less accessibility

The goal of this research can be summarized in four tasks (Figure 2-10). These tasks are: (1) displacement sensor selection, (2) development of correction algorithms, (3) UAS-LDV system integration, and (4) field testing using the integrated system.

Displacement sensor selection

Development of correction algorithms

Target Displacement
u

Sensor Perpendicular Location

Target Location

$u*cos(\vartheta)$

ϑ

φ

Measured Displacement
$u*cos(\vartheta)*cos(\varphi)$

Sensor Angular Location

UAS-LDV system integration

Field testing of UAS-LDV system

Target

UAS

LVDT

LDV

h = 1.5m

d = 4m or 7m

Tether

Weight kg
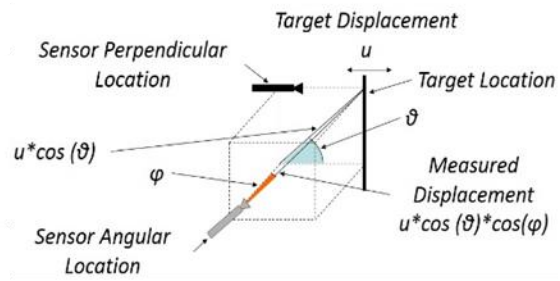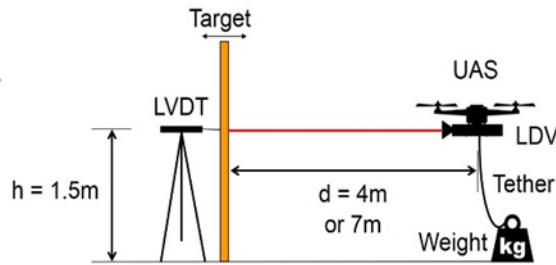
Figure 2-10: Integration of LDV and UAS for dynamic transverse displacement measurement

Chapter 3: Displacement Measurement Using a Moving Vibrometer

3.1 Introduction

This chapter covers the selection of laser sensor for the experiments, transverse displacement measurements using vibrometer, algorithms for correction of vibrometer motion, and the test methodology, setups, and results validating the use of vibrometer for transverse displacement measurement.

3.1.1 Laser Sensor

The selection of the sensor is critical for any application, and must meet some certain selection criteria. The basic need the research is to evaluate if the sensor can process the displacement in real-time with minimal error. It should also be able to measure displacements directly, with a capability to measure pseudo-static displacements for field applications. The sensor should also be able to work in various environmental conditions and not be affected by extreme weather such as heat, humidity, and fog. As a result, the author selected a laser based sensor for measuring transverse displacements of railroad bridges in the field.

Besides the measument requirements, the sensor should have other characteristics that support a UAS based sensing, including, but not limited to small dimensions and as discussed with railroad bridge inspectors and managers, the UAS should be able to collect data from a safe distance, so It should also have a large standoff distance. Considering all these requirements, the author of this research eliminated other advanced sensors and the other sensors considered are listed in Table 3-1.

Table 3-1. Laser sensor details and selection criteria

Name	IL2000	LP-01	OFV-534
Company	Keyence	OMS	Polytec
Image			
Website	www.keyence.com	www.omscorporation.com	www.polytec.com/us/
Type	Laser Triangulation	Laser Doppler Vibrometer	Laser Doppler Vibrometer
Positive Features	1. Light weight and small dimensions 2. Can measure displacements 3. Can measure pseudo-static displacements	1. Large standoff distance	--
Negative Features	1. Small standoff distance	1. Heavy for drone operation 2. Cannot measure displacements directly 3. Cannot measure pseudo-static displacements	1. Light weight and small dimensions 2. Can measure displacements 3. Can measure pseudo-static displacements 4. Large standoff distance

The author of this research evaluated the capabilities of the three options

and tested the two laser doppler vibrometers in the laboratory. The laser that was

best suited for the field application was Polytec laser doppler vibrometer OFV-534 (Figure 3-1).

Figure 3-1. OFV 534 - Laser Doppler Vibrometer (Polytec 2017)

The laser head of the sensor is.9in x 1.5in x 2.8in and its weight is 2.2 pounds. It also has a minimum stand-off distance of 200 mm and a maximum standoff distance of 2000m. The vibrometer controller, OFV-5000 Touch (Figure 3-2), is capable of measuring direct displacement and pseudo static displacements as well. Traditionally vibrometer output is only velocity. The vibrometer controller OFV-5000 however, is equipped with a velocity decoder as well as a displacement decoder. These decoders are independent of each other and simultaneously process the data output. In this research, the output of the velocity decoder is integrated to obtain the dynamic transverse displacements. The results of velocity decoder are analyzed only during the earlier stages of the experiments to compare the performance of the displacement decoders to the traditional sensors. Typically, the output of the velocity decoder is ideal to analyze the displacements at higher frequencies and displacement decoder is ideal for low frequency analysis.

Figure 3-2. OFV-5000 Touch - Vibrometer Controller (Polytec 2017)

3.1.2 Working of a Laser Doppler Vibrometer

The Laser doppler vibrometer (LDV) works on the principle of interferometry. The interference of reference and reflected beam causes light and dark pattern, which can be used to determine the transverse target displacement. The internal mechanism of a vibrometer is shown in Figure 3-3. The light emitted by the laser is split into a reference beam and a measuring beam. Since the distance covered by the reference signal is always constant within the vibrometer assembly, it is used to measure the movement of the target. The measuring beam is transmitted out of the vibrometer and reflected by the target. The frequency of the reflected signal changes due to the target movement. This reflected signal creates an interference pattern with the reference signal. The movement of the target towards and away from the vibrometer creates a similar interference pattern, so the frequency of the reference signal is increased by 40MHz using a Bragg cell, and this 40MHz is used to compare the reflected signal with the reference signal.
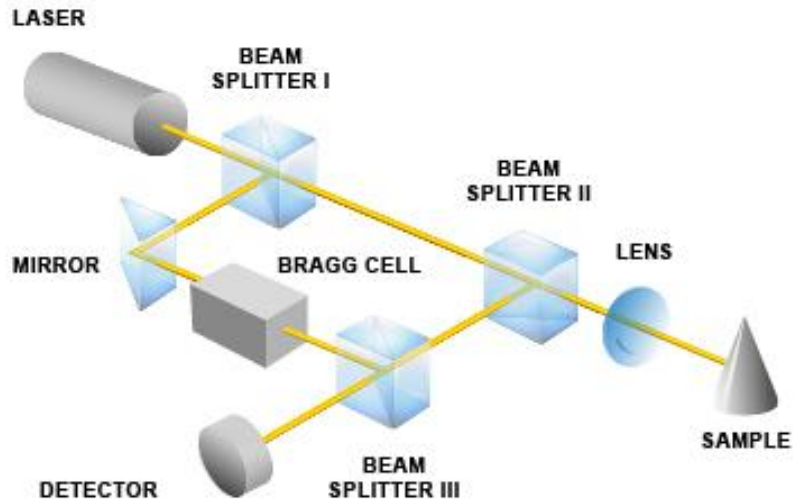
Figure 3-3. Working of a Vibrometer (Polytec 2017a)

3.2 Methodology

3.2.1 Vibrometer Movement Measurement

In principle, the laser doppler vibrometer reads the change in velocity as a vector quantity, and the angle that the target surface makes with the laser signal from the vibrometer is used to measure the transverse displacement. Thus, the output of the vibrometer reads the exact transverse displacement when the target surface is perpendicular to the laser. In Figure 3-4, the vibrometer will measure the exact target transverse displacement when it points along the x direction towards the target.

However, as the UAS moves along x direction, the distance of the vibrometer from the target changes and so does the vibrometer output. Also, with yaw and pitch motion the laser signal will not always be perpendicular to the target surface, thus changing the distance from the target. Changes in y and z direction, or the roll motion, do not affect the output of the vibrometer as the distance from

the target doesn't change. The aim of this research is to establish a framework to correct the readings for these angles and movement of drone along the x direction.
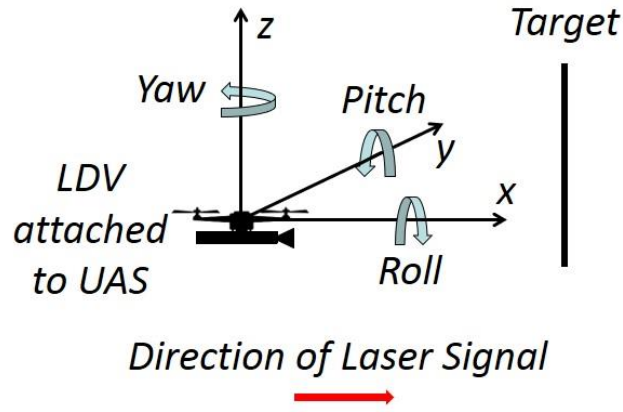
Figure 3-4. Motion of a UAS along six degrees of freedom.

3.2.2 Displacement Measurement Using a Vibrometer

For a static arrangement, if the vibrometer signal is perpendicular to the target, it measures the exact vibration. However, if it is at an angle to the target, the signal is attenuated by the cosine component of the angle. A vibrometer with a pitch angle of 'θ' and a yaw angle of 'φ' with the target surface can be visualized in Figure 3-5. In the figure, the "Sensor Perpendicular Location" is the point where the vibrometer reads the maximum transverse displacement, and the "Sensor Angular Location" is final position of the vibrometer.

When the sensor is at any location besides the perpendicular location, the equivalent readings by the vibrometer are to the product of the cosine of the pitch and the cosine of the yaw angles with the original signal. If the vibrometer reading at the perpendicular location is 'u', then at a pitch angle of 'θ' and a yaw angle of 'φ', the measured reading 'um' is represented as

27

$$u_m = u*cos(\theta)*cos(\varphi) \hspace{3cm} (3.1)$$
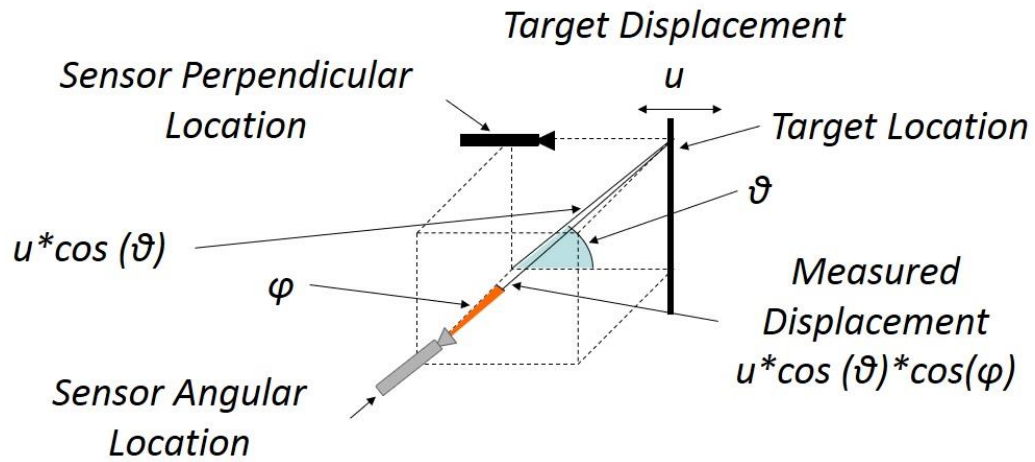
Figure 3-5. Reading by the vibrometer at an angular position.

Thus, the actual displacement 'u' can be obtained by using

$$u = \left(\frac{u_m}{cos(\theta)*cos(\varphi)} \right) \hspace{3cm} (3.2)$$

3.2.3 Vibrometer Movement Compensation Algorithms

It is important to analyze the dynamic motion of the vibrometer, as the UAS is a dynamic system, and the vibrometer is subject to these motions when attached to a UAS. The dynamic motion can be either a change in the distance from the target, or in the angles (roll, pitch, and yaw), or any combination of those two. The following sections describe the different considerations individually.

a. Change in Distance from Target

Of the three directions (x, y, and z) that a vibrometer can move in, only the movement in x direction changes the output of the vibrometer. This motion along x axis can be seen in Figure 3-6.
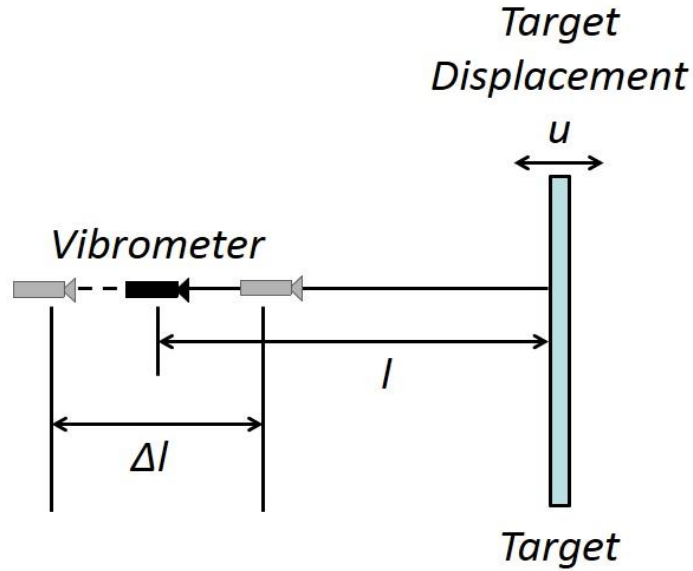
Figure 3-6. Dynamic displacement of vibrometer

Here, 'l' is the distance between the vibrometer and the target, while 'Δl' is the change in the distance. For the target vibration 'u', the measured vibration 'u_m' is calculated as

$$u_m = u + \Delta l \tag{3.3}$$

Thus, by measuring the change in the distance of the vibrometer from the target, the actual vibration can measures as

$$u = u_m - \Delta l \tag{3.4}$$

b. Change in Angle

Of the three angular motions (pitch, yaw, and roll), only the pitch and yaw motions of the vibrometer affects the displacement and velocity readings. When the vibrometer moves dynamically, the angle made by the laser signal with the target changes dynamically. Therefore, the distance travelled by the laser signal

between the vibrometer and target also changes. The change in this distance also depends on the angle that the laser makes with the target. This can be visualized from Figure 3-7. In this figure, 'l' is the distance between the vibrometer and the target, while 'Δl' is the change in the distance. The angle 'θ' is either the pitch angle, the yaw angle, or the combination of both angles.
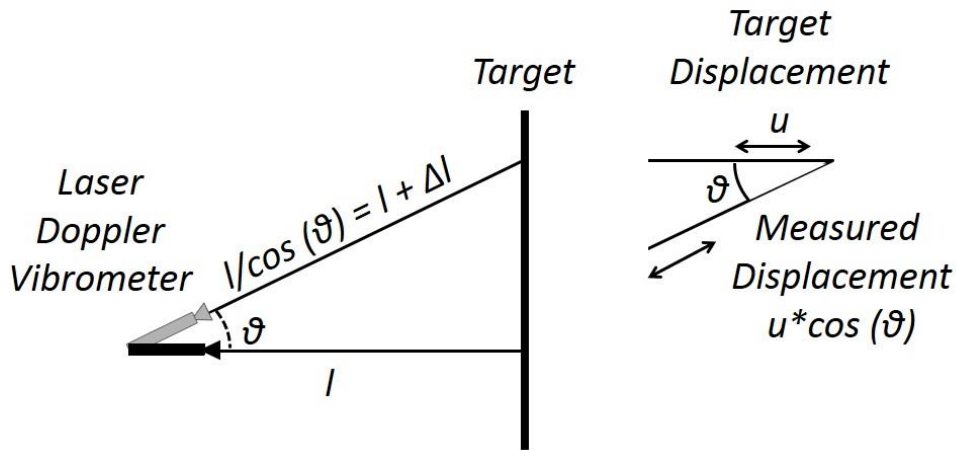
Figure 3-7. Dynamic pitching of vibrometer

The target vibration or movement to be recorded is given by 'u_m', where 'u_m', can be calculated by using the equation 3.2 as

$$u_m = u_c * cos(\theta) \tag{3.5}$$

Thus, the vibrations corrected 'u_c' for the change in angle can be obtained by

$$u_c = \left(\frac{u_m}{cos(\theta)}\right) \tag{3.6}$$

However, since the actual signal is affected by the change in angle as well as the apparent distance between the target and the vibrometer due to the angular motion, the final vibration signal can be written as

$$u = u_c - \Delta l \qquad (3.7)$$

Where 'Δl' is given by

$$\Delta l = \left(l - \left(\frac{l}{\cos(\theta)} \right) \right) \qquad (3.8)$$

c. Random Motion of Vibrometer

The random movement of a vibrometer includes both, the displacement, and the angular movement. For an actual vibration 'u', with angular movement 'θ', angular displacement 'Δd', and movement 'Δl', the measured displacement 'u_m' is given by

$$u_m = (u_c - \Delta d) * \cos(\theta) \qquad (3.9)$$

Where, u_c is the vibration measured from a laterally moving vibrometer, given by

$$u_c = u + \Delta l \qquad (3.10)$$

Thus, from equations 3.9 and 3.10, the actual vibration can be written as

$$u = \left(\frac{u_m}{\cos(\theta)} \right) - \Delta d - \Delta l \qquad (3.11)$$

3.2.4 Performance Evaluation Criteria

The readings of the vibrometer are compared to the measurements from the LVDT to benchmark the operation capabilities of the vibrometer for measuring transverse displacements. This MS thesis compares the measurements from the two different sensors as a percentage difference and not as a percentage error. For these experiments, the maximum difference (E1) and RMS difference (E3) between the two readings can be calculated.

The maximum difference between the signals is obtained by comparing the values at each of the sampling point and then finding the maximum of this value from these differences. For 'n' sampling points, the difference can be obtained as:

$$E_1(i) = (abs(LVDT(i) - LDV(i))), 1 \le i \le n \tag{3.12}$$

Thus, the percentage maximum difference from equation (13) is

$$E_1(\%) = \left(\frac{max(E_1)}{max(abs(LVDT))}\right) * 100 \tag{3.13}$$

The RMS difference for 'n' sampling points is

$$RMSD = \sqrt{\frac{\sum_{i=1}^{n}(LVDT(i) - LDV(i))^2}{n}} \tag{3.14}$$

Thus, by using equation 14, percentage RMS difference (normalized by range) is

$$E_2 = \left(\frac{RMSD}{max(LVDT) - min(LVDT)}\right) * 100 \tag{3.15}$$

These performance criteria were successfully used by Gomez et al. (2017) for quantifying effectiveness of a newly developed wireless low-cost displacement sensor on comparison with LVDT and commercial accelerometers, and will be used throughout this MS thesis.

3.3 Experiments

3.3.1 Instrumentation

The tests performed in this section require sensors for the measurement of the movement of the vibrometer using a shake table for target vibration simulating a railroad bridge moving during train crossing events and sensors for the measurement of the target movement.

Shake Table

A QUANSER Shake Table II is a vibration table with a single degree of freedom. This table can be programed to generate vibrations in a multitude of displacement patterns, including measured data from earthquakes or train loading of railroad bridges under train crossing events collected on the field. Figure 3-8 shows the shake table used for the experimental portion of this research.
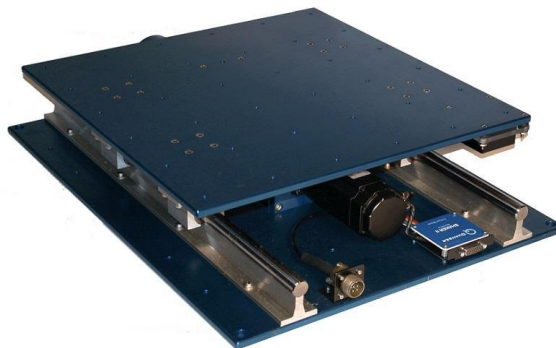
Figure 3-8. Quanser Shake Table II (Quanser 2017)

Linear Variable Differential Transducer (LVDT)

The Linear Variable Differential Transducer (LVDT) is a displacement transducer which converts mechanical displacement into voltage. In this experiment, LVDTs are used for tracking the actual displacement of any object on the shake table. The output of this LVDT is used as a reference displacement to determine the capabilities of the LDV to measure dynamic transverse displacements. The displacement output of the LDV is compared to the LVDT output. In the moving vibrometer setup, LVDT is also used to measure the lateral movements of the vibrometer. Figure 3-9 shows the LDVT used for the experimental portion of this research.

Figure 3-9. DCTH3000 Linear Variable Differential Transducer (RDP 2017)

Sensors for vibrometer motion detection

A rigid body in free space has basically six degrees of freedom: along the x-axis, y-axis, and z-axis, and the roll, pitch, and yaw. In other words, the motion can be either translational, or rotational, or the combination of both along one or multiple axes. Thus, the final solution needs to accurately measure the vibrometer motion along all three axes. In this set of experiments, the author uses the capacitive accelerometers to measure the rotation as well as translation of the vibrometer. Figure 3-10 shows the capacitive accelerometer used in the experimental part of this thesis.

Figure 3-10. Capacitive Accelerometer (PCB 2017)

Data Acquisition module

The vibpilot data acquisition system (DAQ) is used for processing the data output by sensors. This DAQ has 8 channels. For this research, the sensor outputs are sampled at 1024 samples/sec. Figure 3-11 shows the vibpilot DAQ used for data acquisition in these experiments.

Figure 3-11. Vibpilot: 8 Channel Data Acquisition System (M+P Intl., 2017)

3.3.2 Experimentation Layout

This section discusses the different laboratory arrangements and setup for this research. The experiments are divided into four sections depending on the positioning and motion of the vibrometer:

a. *Fixed Vibrometer with Laser Signal Perpendicular to the Target*

b. *Fixed Vibrometer with Laser Signal at an Angle to the Target*

c. *Dynamic Angular Motion of the Vibrometer*

d. *Random Dynamic Angular and Lateral Motions of the Vibrometer*

Table 3-2 describes the different states of motion for each setup.

Table 3-2. State of motion of vibrometer for the four experimental setups

Experiment	States of Motion					
	X direction	Y direction	Z direction	Roll	Pitch	Yaw
a	No motion	No motion	No motion	0°	0°	0°
b	No motion	No motion	No motion	0°	Fixed α°	Fixed θ°
c	No motion	No motion	No motion	0°	Δα°	Δθ°
d	Δx	No motion	No motion	0°	Δα°	Δθ°

Figure 3.12 shows the experimental layout of all the above configurations. These setups are discussed below in detail.

a. Fixed vibrometer with laser signal perpendicular to the target

In this setup, the vibrometer is arranged in such a way that the laser signal is directly perpendicular to the target, and therefore parallel to the plane of vibration of the target (Figure 3-12a). This arrangement gives the vibration of the target without any angular components, and the performance of the vibrometer can be benchmarked in comparison to the LVDT. Multiple tests were conducted using this setup to determine the response of the vibrometer for different signals, operating distances, and vibration frequencies and amplitudes. The aim of this test is to find the efficiency of the vibrometer in measuring signals with multi-frequency, multi-amplitude components such as earthquakes and transverse bridge displacements.

36
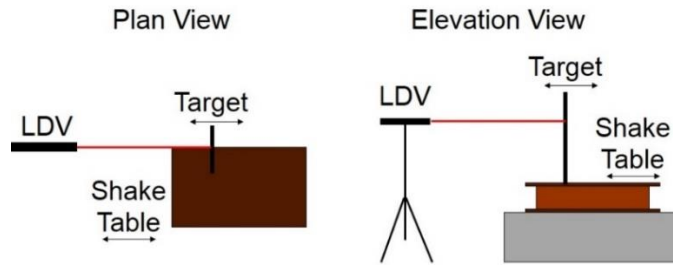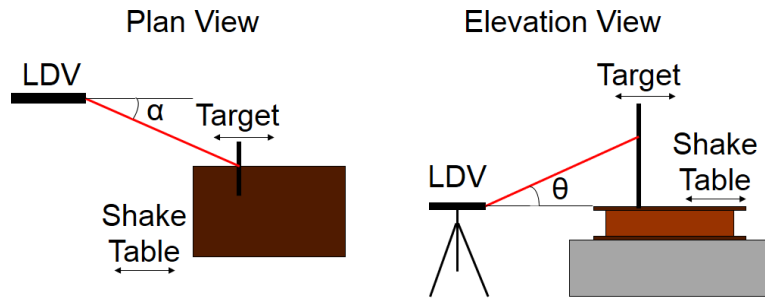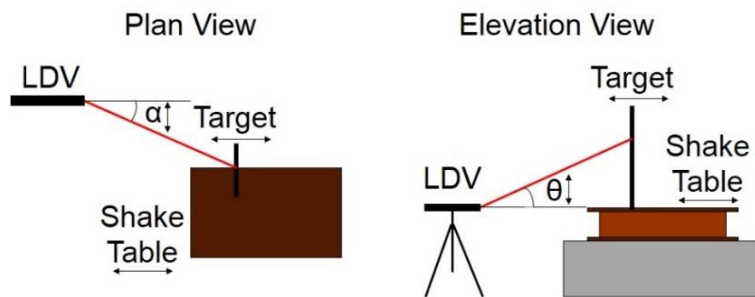
Figure 3-12. Experimental layout for different vibrometer for (a) vibrometer signal perpendicular to the target, (b) vibrometer at an angle to the target, (c) dynamic angular motion of the vibrometer, and (d) dynamic angular and translational motion of vibrometer

b. Fixed vibrometer with the laser signal at an angle to the target

In this setup, the vibrometer is arranged in such a way that the laser signal points to the target with an angle. This setup in Figure 3-12b, where the angles 'θ' and 'α' are the pitch angle and the yaw angle of the vibrometer respectively. These tests measure the pitch and yaw angles using capacitive accelerometers, and correct the readings of the vibrometer using these angles.

c. Dynamic angular motion of the vibrometer

It is essential to check the response of the vibrometer under a moving arrangement, check if the errors introduced due to the motion, and correct these errors. In this setup, the angle of the vibrometer will be changed dynamically. The capacitive accelerometer will measure the change in the vibrometer angle. The aim of this test is to use these calculated angles to correct the measured reading to get the actual vibration of the target after the correction.

d. Random dynamic angular and lateral motions of the vibrometer

In this section, a vibrometer is moved in a random lateral direction and at a random angle. This setup is as seen in Figure 3-13. The lateral movement of the vibrometer in any direction is measured with the LVDTs, and the capacitive accelerometers are used to measure the angular motion of the vibrometer in pitch and yaw. This test is the closest realization of the movement of the UAS which will be obtained from the UAS and used for corrections. The aim of this test is to design the framework to correct any movement of the vibrometer, and get the actual

vibration of the target. The final signal is corrected with the measured displacements.
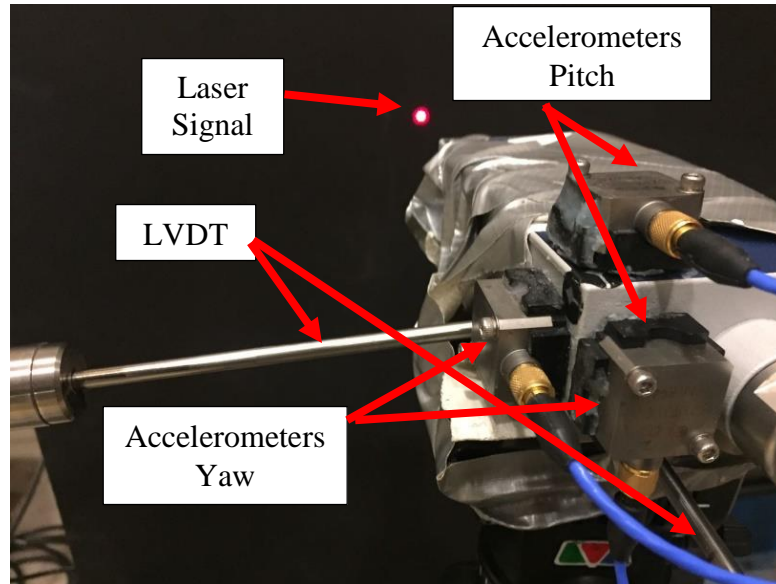
Figure 3-13. Randomly moving vibrometer with accelerometers measuring the angles and LVDT measuring the displacements.

Figure 3.14 shows the general laboratory setup of the experiments.
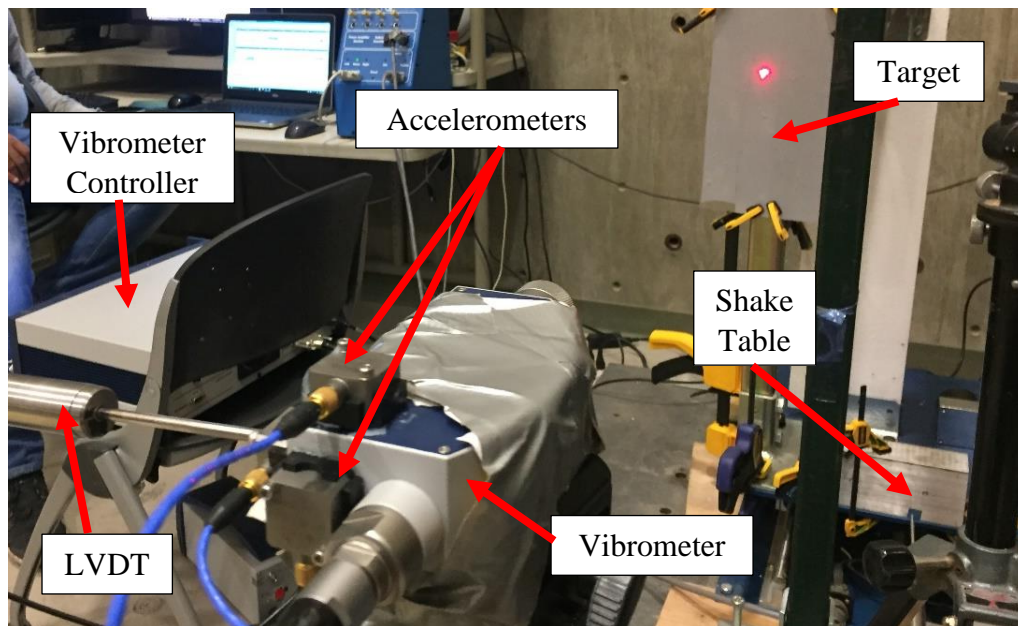
Figure 3-14. Laboratory Setup.

3.4 Results

3.4.1 *Fixed* **vibrometer** *with laser signal perpendicular to the target:*

These set of tests were conducted with the laser signal perpendicular to the target. The output seen in the Figure 3-15 shows the response collected by the velocity and displacement sensors of the vibrometer as compared to the actual output recorded by the LVDT.

(a)

(b)

(c)
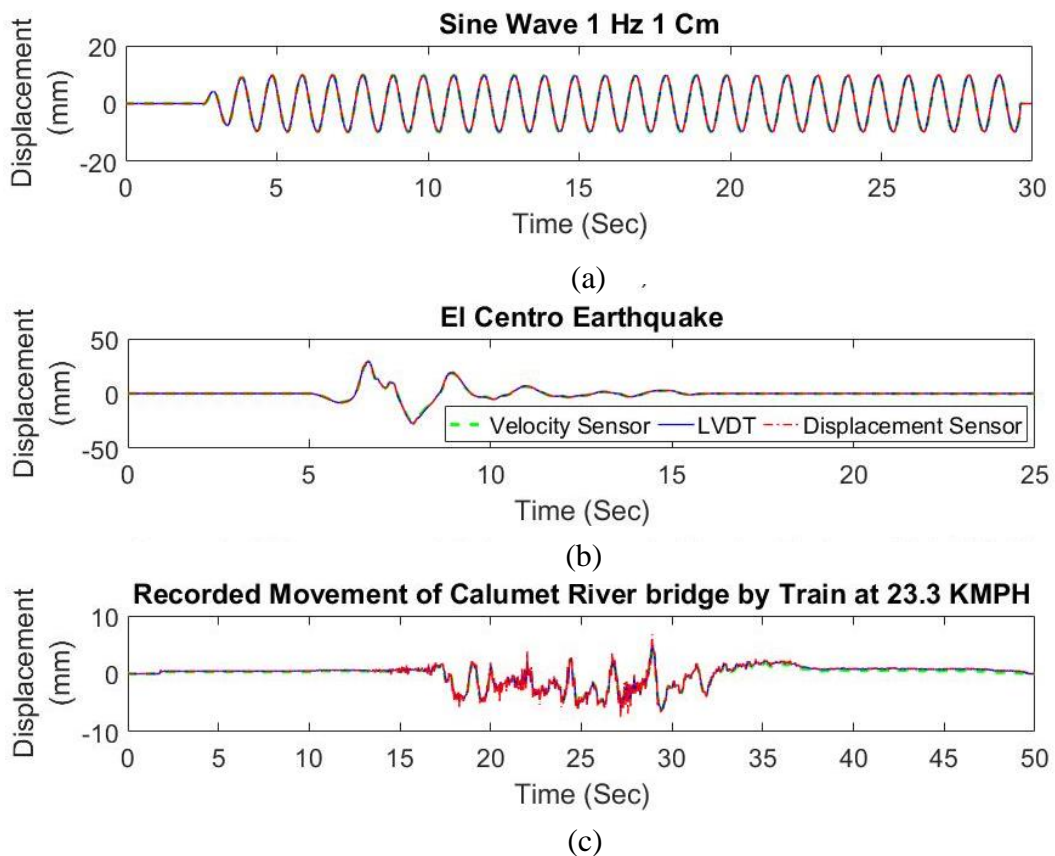
Figure 3-15. Response of displacement and velocity decoder of the vibrometer vs LVDT at 3 feet from the target for (a) sine wave 1Hz and 1cm, (b) El-Centro earthquake, and (c) Bridge displacement due to dynamic train loading

The results in Figure 3-15 show that the vibrometer follows the output of the LVDT closely in amplitude as well as phase but Figure 3-16 shows the RMS errors are around or below 2%. This shows that the vibrometer works well for single

frequency signal, as well as for multi frequency and multi amplitude signal with zero and non-zero mean.
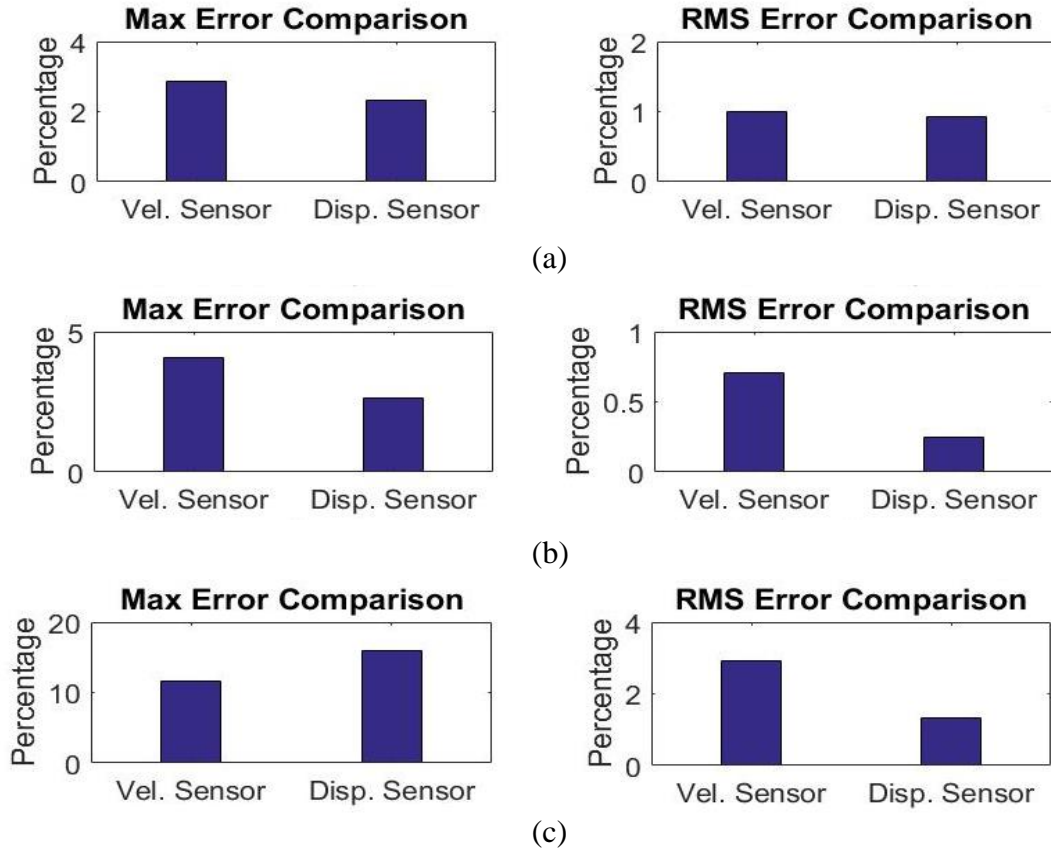
Figure 3-16. Peak and RMS signal difference between the outputs of the vibrometer vs LVDT at 3 feet from the target for (a) sine wave 1Hz and 1cm, (b) El-Centro earthquake, and (c) Bridge displacement due to dynamic train loading

Figure 3-17 shows the output of the vibrometer when it is placed at different distances from the target. The vibrometer velocity and displacement decoders are able to match the output of the LVDT in phase as well as amplitude, as shown for the different distances.
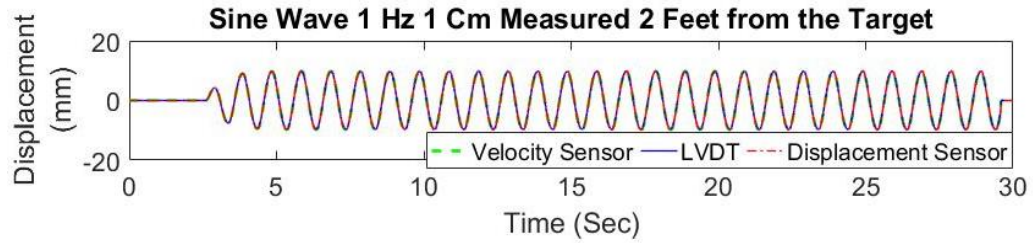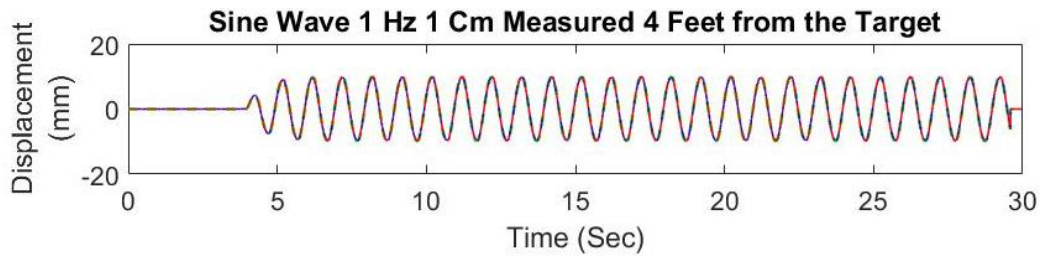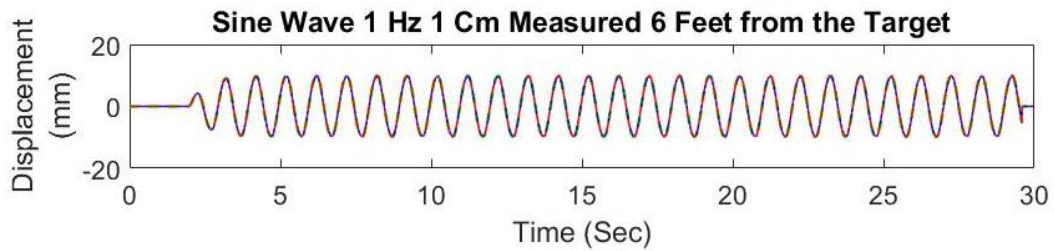
Figure 3-17. Response of displacement and velocity decoder of the vibrometer vs LVDT at (a) 2 feet from the target, (b) 4 feet from the target, and (c) 6 feet from the target

The maximum difference in all the three outputs are around 3% and the RMS difference is below 1% as seen in Figure 3-18. These results show that the output of the vibrometer does not increase significantly as the distance of vibrometer from the target increases.

Max Error Comparison | RMS Error Comparison

(a)

Max Error Comparison | RMS Error Comparison

(b)

Max Error Comparison | RMS Error Comparison

(c)
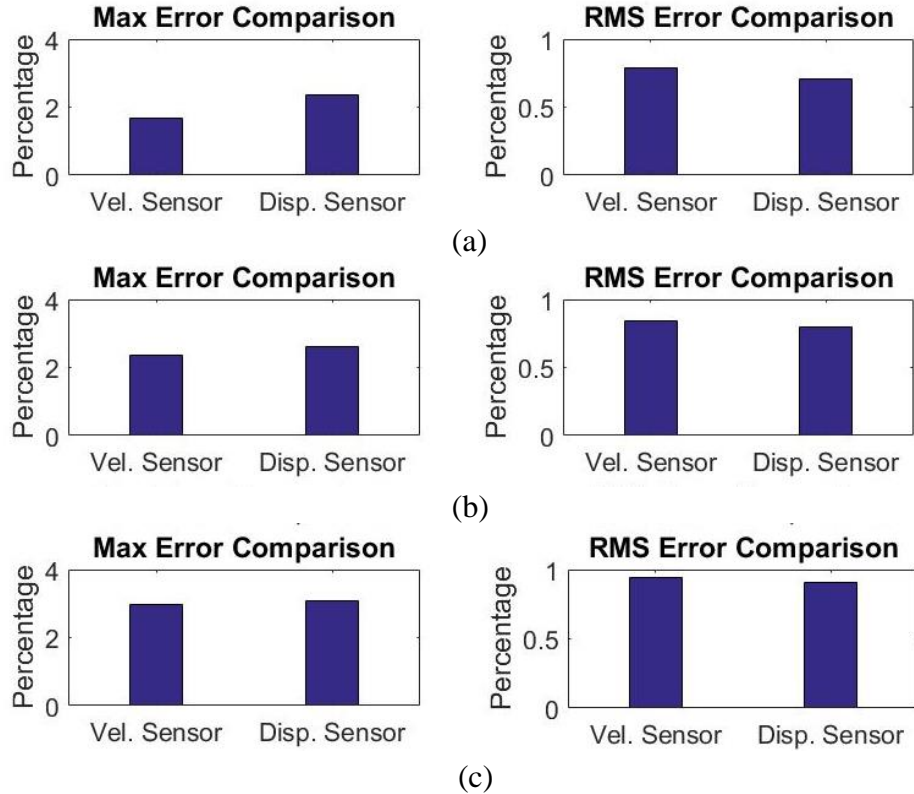
Figure 3-18. Signal difference between the output of the vibrometer vs LVDT at (a) 2 feet from the target, (b) 4 feet from the target, and (c) 6 feet from the target

Figure 3-19 shows the output of the vibrometer measuring different vibration frequencies. The vibrometer velocity and displacement decoders match the output of the LVDT in phase as well as amplitude

The maximum difference in all the three experiments are around 5% and the RMS difference is below 2% as seen in Figure 3-20. These results show that the output of the vibrometer does not change significantly with the change in frequency of the target being measured.
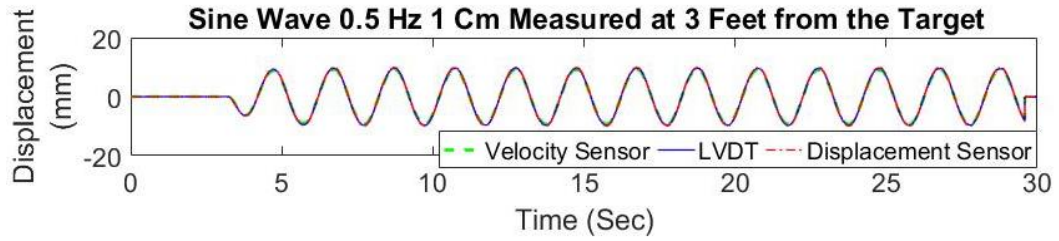
(a)
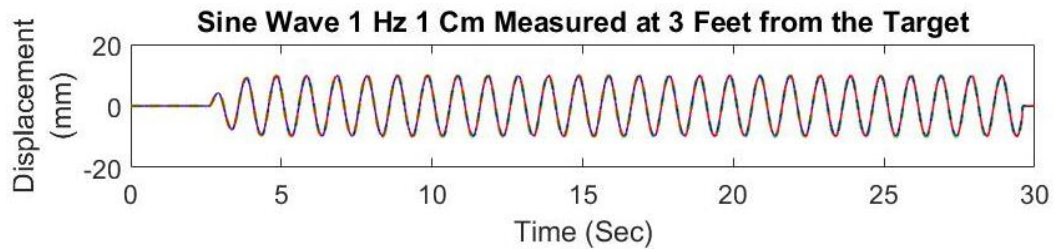
(b)
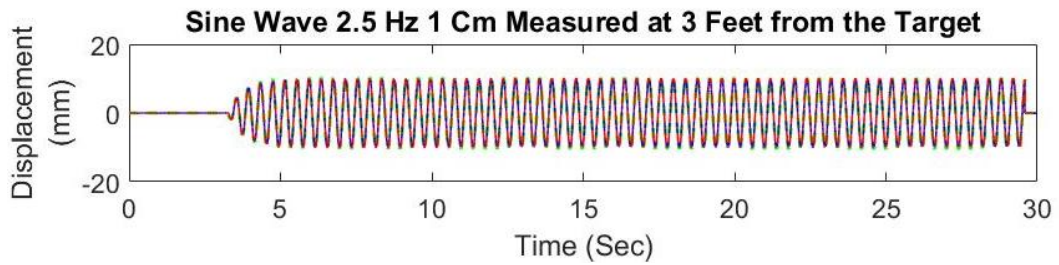
(c)

Figure 3-19. Response of displacement and velocity decoder of the vibrometer vs LVDT for sine wave of amplitude 1 cm and frequencieses (a) 0.5 Hz, (b) 1 Hz, (c) 2.5 Hz
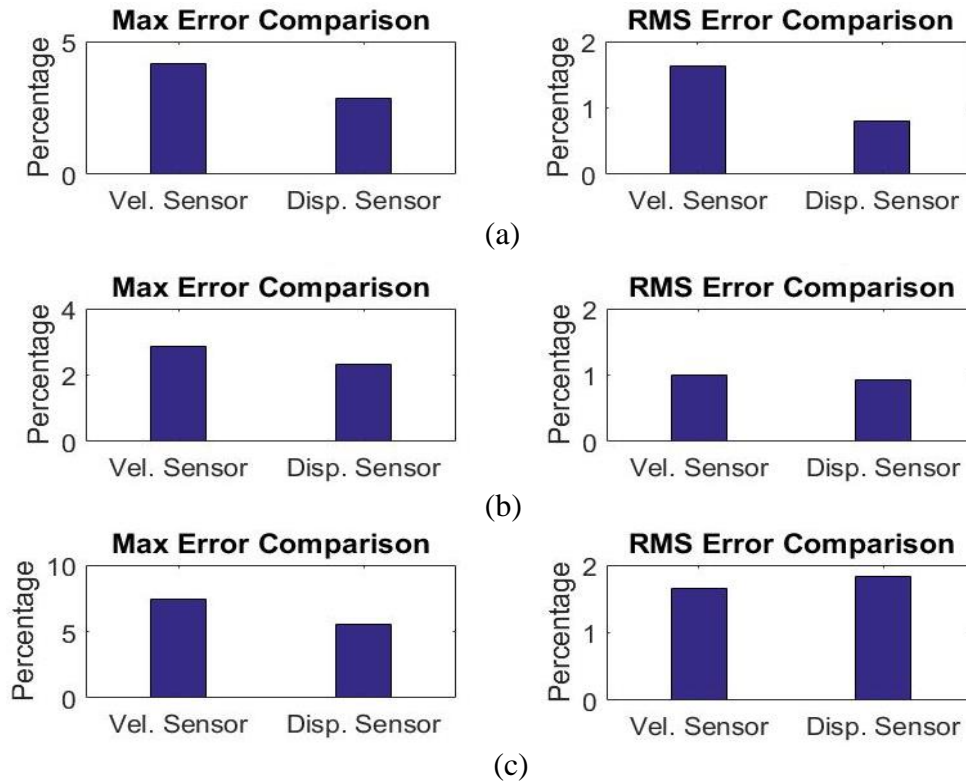
Figure 3-20. Signal difference between the output of the vibrometer vs LVDT for sine wave of amplitude 1 cm and frequencieses (a) 0.5 Hz, (b) 1 Hz, (c) 2.5 Hz

Three outputs of the vibrometer for different amplitudes (0.5cm, 1.5cm, and 2.5cm) of target vibration can be seen in Figure 3-21 for 1Hz signals. The vibrometer velocity and displacement decoders match the output of the LVDT in phase as well as amplitude.

Figure 3-22 shows that the maximum difference is below 4% and the RMS difference is around 1% for all the 3 outputs. Thus, it can be concluded that the output of the vibrometer does not change significantly with amplitude of target vibration.

(a)

(b)

(c)
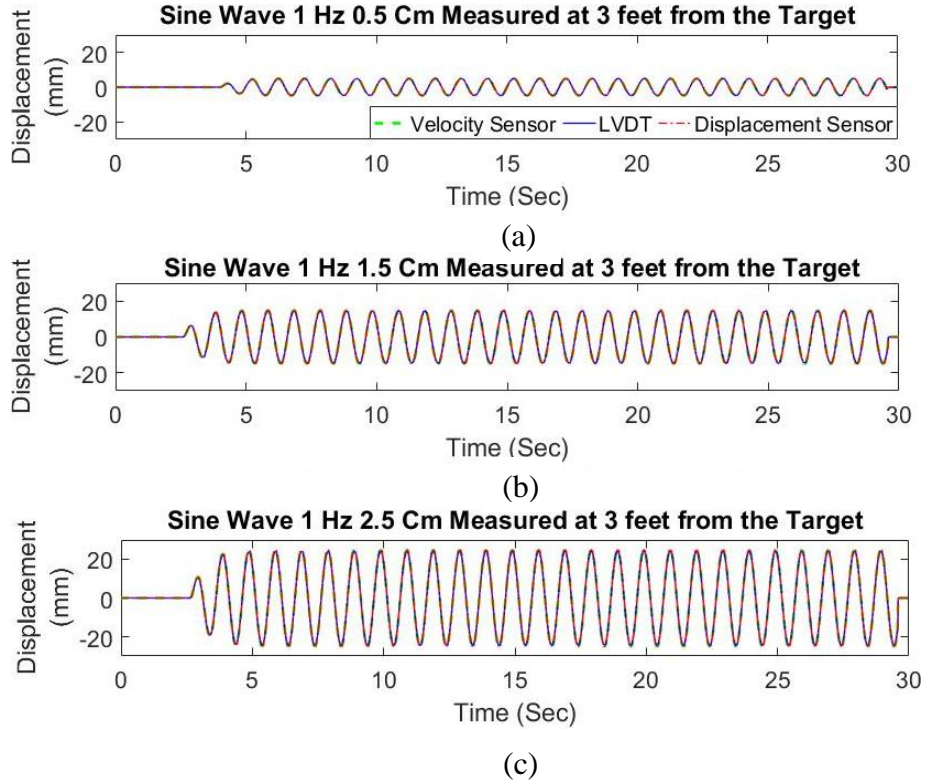
Figure 3-21. Response of displacement and velocity decoder of the vibrometer vs LVDT for sine wave of frequency 1 Hz and amplitudes (a) 0.5 cm, (b) 1.5 cm, (c) 2.5 cm

(a)

(b)

(c)
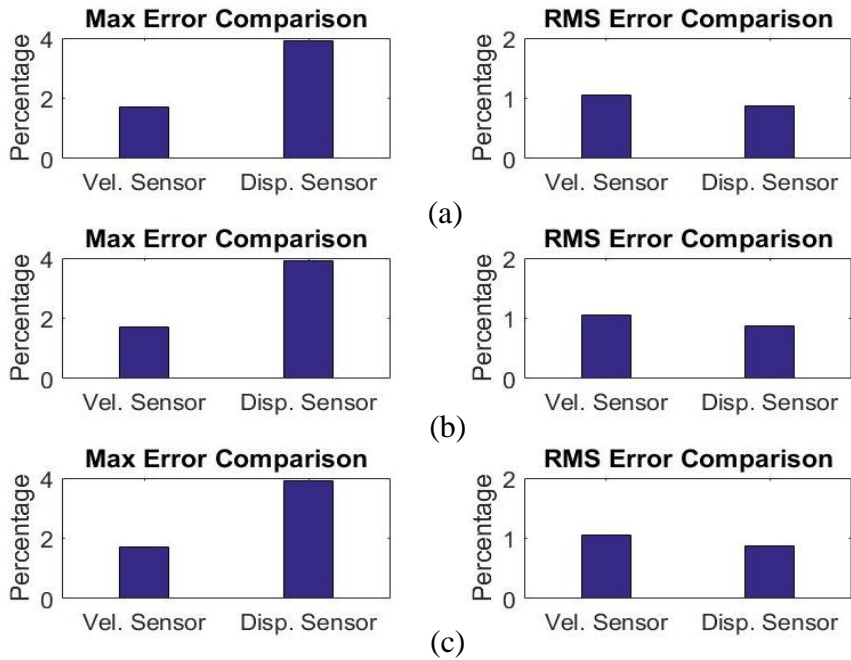
Figure 3-22. Signal difference between the output of the vibrometer vs LVDT for sine wave of frequency 1 Hz and amplitudes (a) 0.5 cm, (b) 1.5 cm, (c) 2.5 cm

Figure 3-23 shows the output of the vibrometer for multi-frequency and multi-amplitude signals with earthquake signals as compared to the LVDT output.

(a)

(b)

(c)
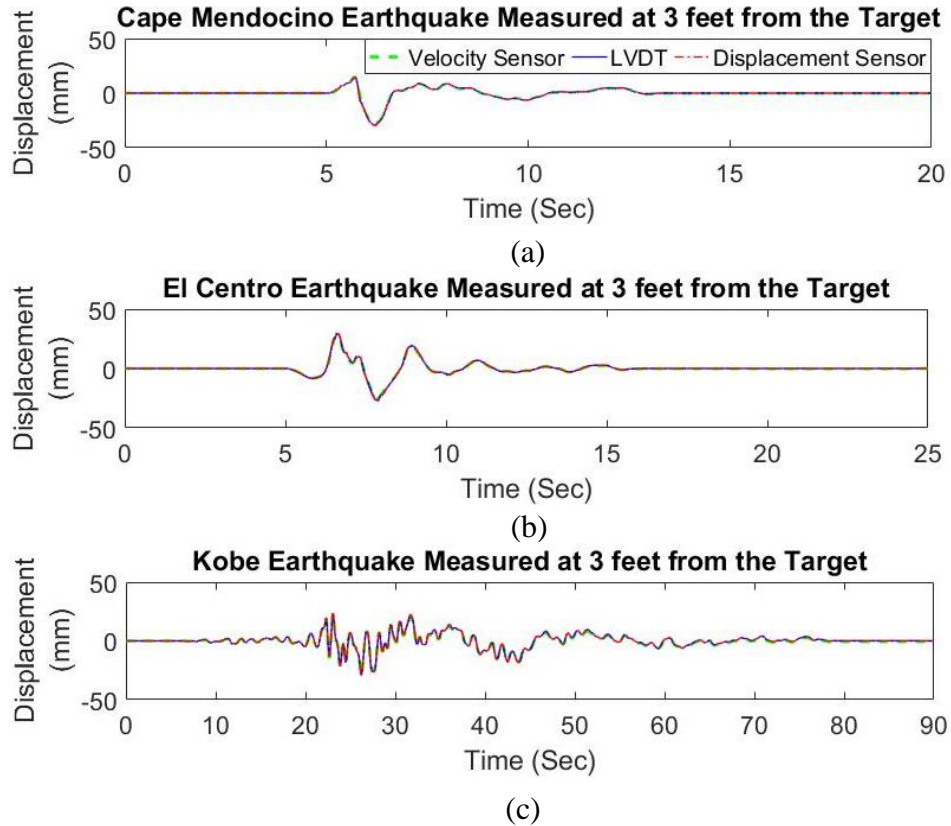
Figure 3-23. Response of displacement and velocity decoder of vibrometer vs LVDT, 3 feet from the target, for (a) Cape Mendocino earthquake, (b) El Centro earthquake, and (c) Kobe earthquake

It is observed from figure 3-24 that the maximum difference between the vibrometer and LVDT sensor outputs is less than 5% for all the earthquake signals, and the RMS difference is around or below 1%. Thus, it can be concluded that the vibrometer is able to track the signal with multiple amplitude and frequency components accurately for the three earthquakes tested.
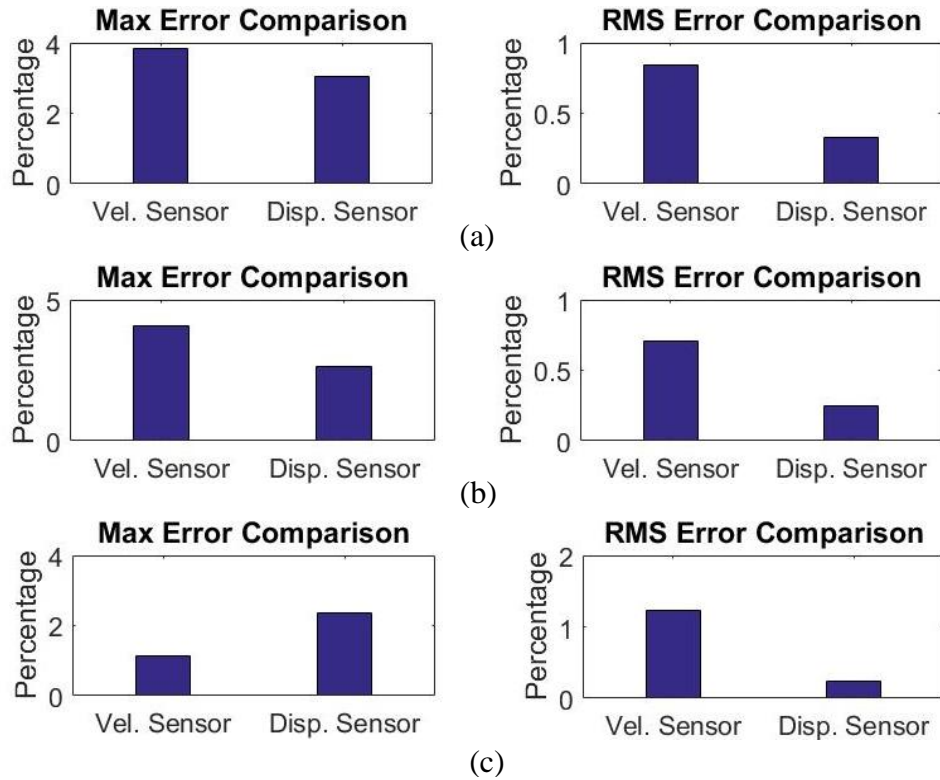
Figure 3-24. Signal difference between outputs of vibrometer vs LVDT, 3 feet from the target, for (a) Cape Mendocino earthquake, (b) El Centro earthquake, and (c) Kobe earthquake

The last test measures the ability of the vibrometer to measure transverse displacements of actual bridge responses under dynamic train loading. The transverse bridge displacement signal is a multi-frequency multi-amplitude signal with a non-zero mean, which means that there is a pseudo-static component in the signal. Figure 3-25 shows the response of the vibrometer for different train speeds compared with LVDT readings.
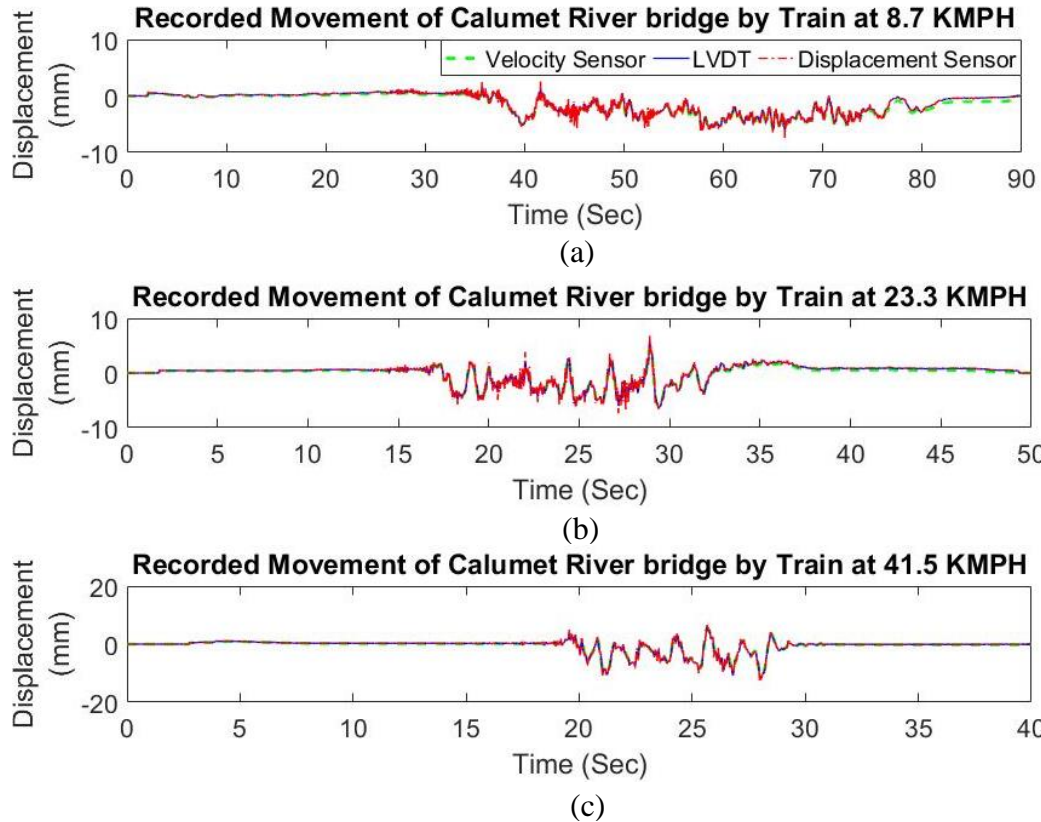
Figure 3-25. Response of displacement and velocity decoder of vibrometer vs LVDT, 3 feet from the target, and bridge displacements for dynamic train loading with train speeds (a) 8.7 kmph, (b) 23.3 kmph, and (c) 41.5 kmph

From these results, it can be concluded that the vibrometer can measure non-zero mean signals with a pseudo-static component with multiple frequencies and amplitudes accurately with maximum difference of less than 10%, and RMS differences below 5%, as seen in Figure 3-26.
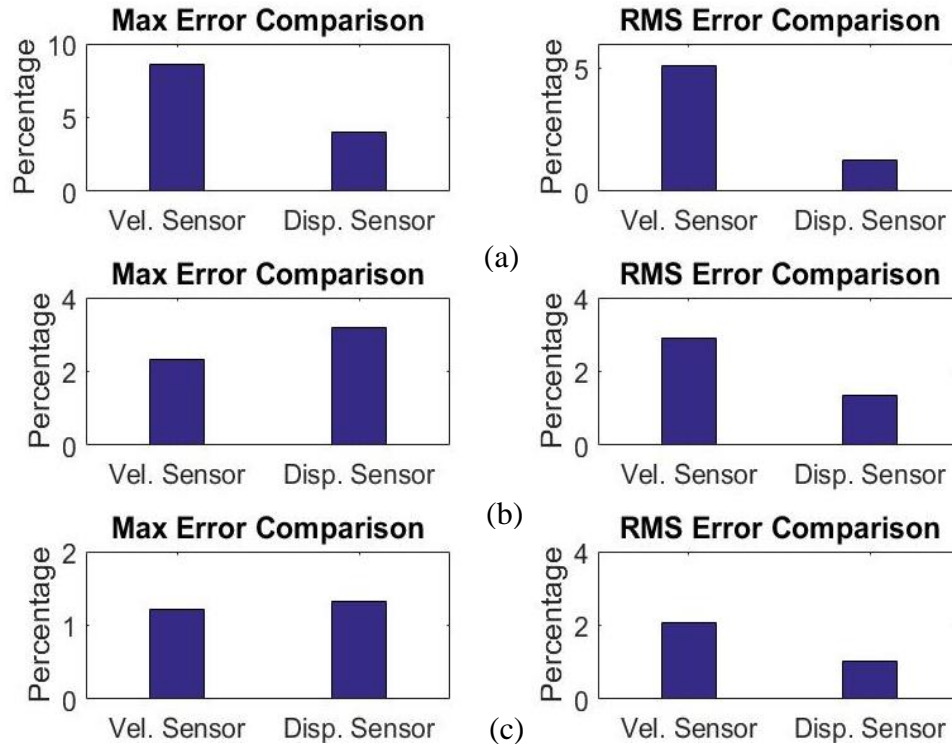
Figure 3-26. Signal difference between outputs of vibrometer vs LVDT, 3 feet from the target, and bridge displacements for dynamic train loading with train speeds (a) 8.7 kmph, (b) 23.3 kmph, and (c) 41.5 kmph

3.4.2 Fixed vibrometer with the laser signal at an angle to the target:

When the vibrometer is at an angle to the target, the vibrometer records the cosine component of the target vibration in the direction of the vibrometer. Therefore, the measured output is always less than the actual vibration. This measured vibration can be corrected by using the angle of the vibration as described in first section this MS thesis.

Figure 3-27 shows the output recorded by a vibrometer at a pitch angle of 30 degrees with the target. The vibration measured by the vibrometer is less than the actual vibration. When, it is corrected using the cosine of the pitch angle (30 degrees), the corrected output matches the output of the LVDT.

50
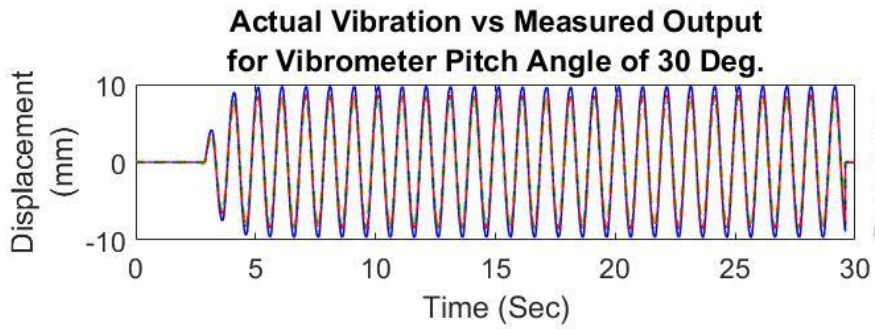
(a)
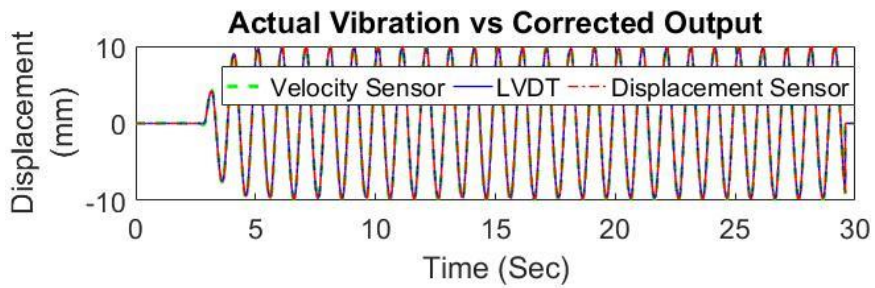
(b)

Figure 3-27. (a) Measured output and (b) corrected output from displacement and velocity decoder of vibrometer vs LVDT, 3 feet from the target, and at a 30 degrees pitch angle

The maximum difference in the corrected readings and the actual vibration is less than 2% and the RMS difference is less than 1% (Figure 3-28). From these results, it can be concluded that the correction algorithm for the angular position of the vibrometer works if the vibrometer makes only a pitch angle with the target, and not a yaw angle.

When the vibrometer is at a yaw angle of 30 degrees, the measurement of the vibrometer is similar to the measurement recorded for the 30 degrees pitch angle. It can be observed in Figure 3-29 that the vibrometer records the displacement signal with a value of much lower amplitude than the signal collected by the LVDT. After correcting the signal for the yaw angle, it matches that of the LVDT closely.

(a)

(b)
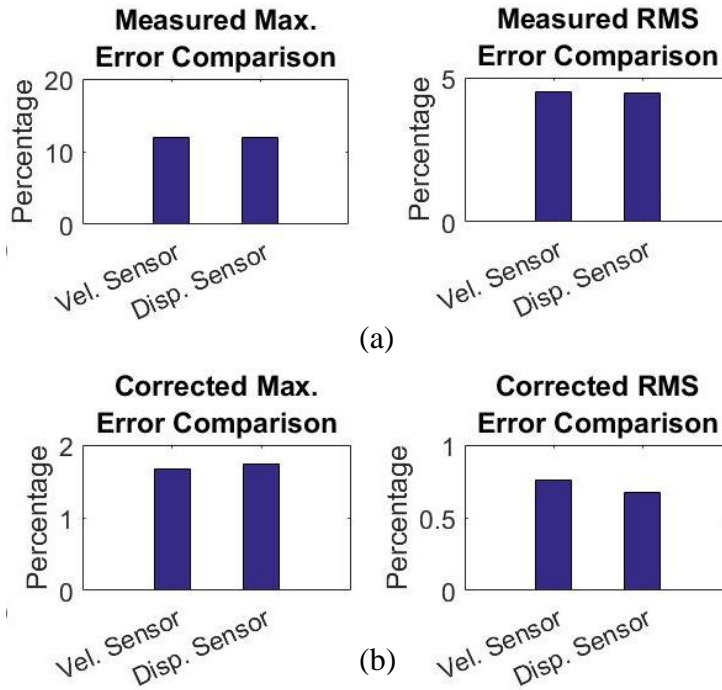
Figure 3-28. Signal difference of a) Measured output and (b) corrected output from vibrometer vs LVDT, 3 feet from the target, and at 30 degrees pitch angle

(a)

(b)
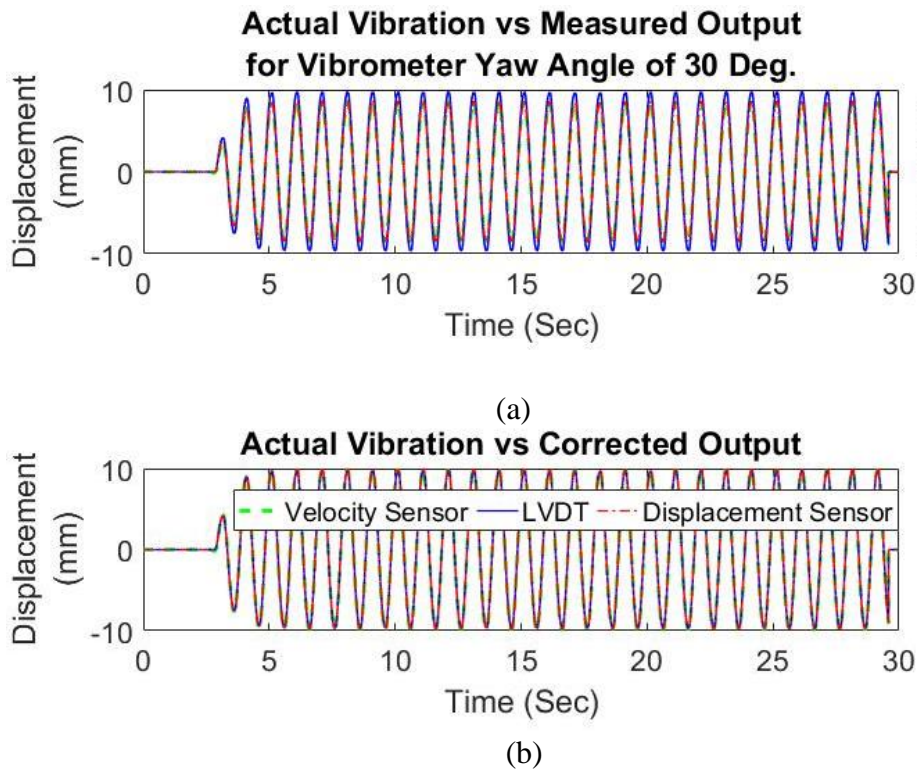
Figure 3-29. (a) Measured output and (b) corrected output from displacement and velocity decoder of vibrometer vs LVDT, 3 feet from the target, and at a 30 degrees yaw angle

Figure 3-30 shows that the maximum difference is below 2% for amplitude and the RMS difference is below 1%. As a result, it can be concluded that the correction algorithm works when vibrometer makes only a yaw angle with the target with no pitch angle.
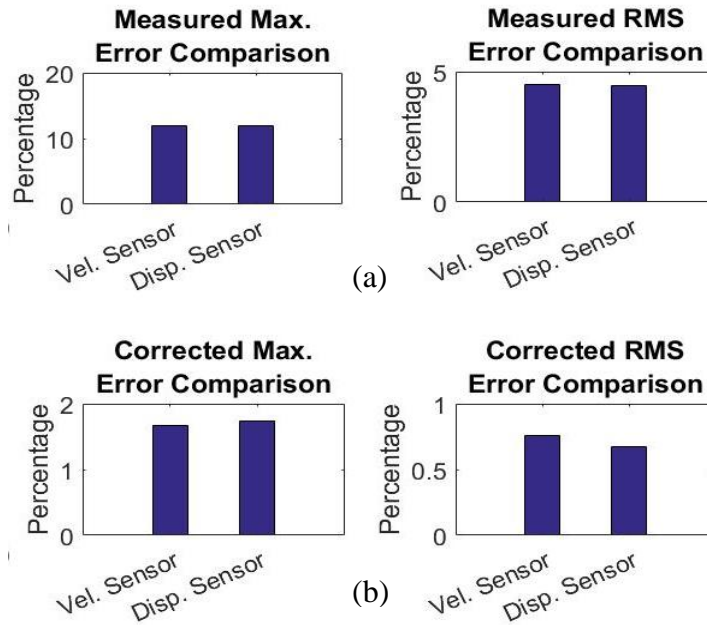
Figure 3-30. Signal difference of a) Measured output and (b) corrected output from vibrometer vs LVDT, 3 feet from the target, and at 30 degrees yaw angle

When the vibrometer is placed with both, a pitch and a yaw angle with the target, the measured output changes due to the error introduced by both these angles are greater than the error due to either pitch or yaw angles. These results can be seen in Figure 3-31. Figure 3-31(a) shows the output measured by the vibrometer at a pitch angle of 30 degree as well as a yaw angle of 30 degree vs the actual vibrations. Figure 3-31(b) shows the corrected output vs the actual vibrations.

The output has a maximum difference of less than 2% and a RMS difference is less than 1% as seen in Figure 3-32.
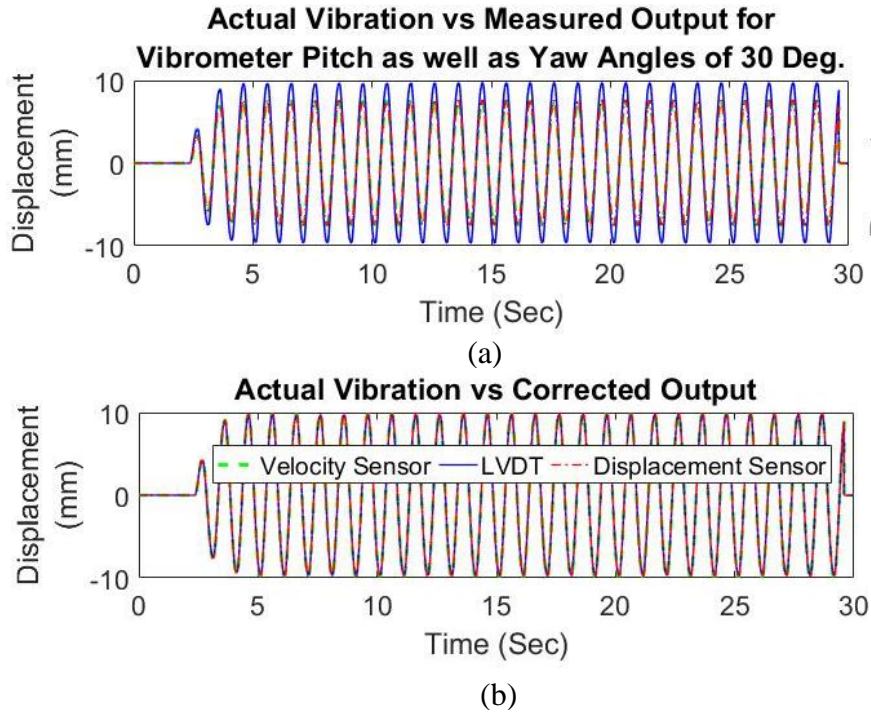
Figure 3-31. a) Measured output and (b) corrected output from displacement and velocity decoder of vibrometer vs LVDT, 3 feet from the target, and at 30 degrees pitch as well as yaw angles
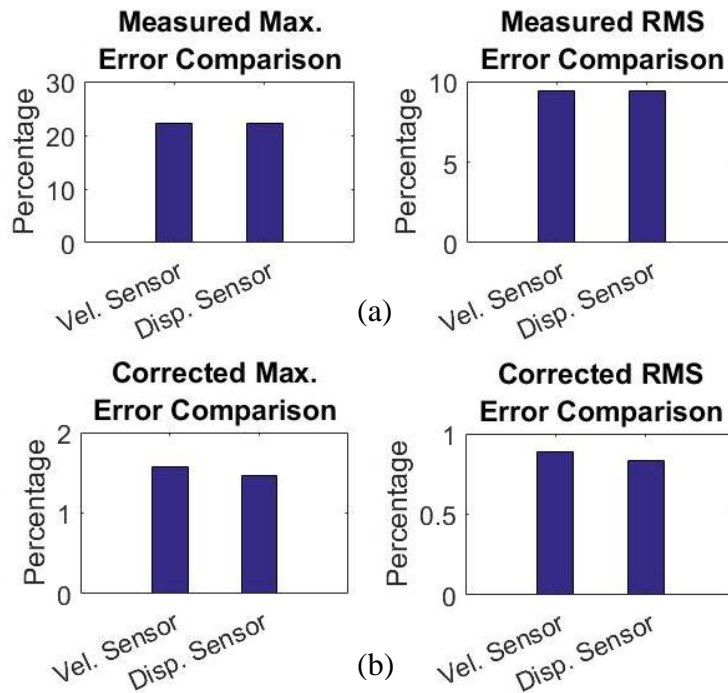
Figure 3-32. Signal difference of a) Measured output and (b) corrected output from vibrometer vs LVDT, 3 feet from the target, and at 30 degrees pitch as well as yaw angles

The algorithm is also tested for the earthquake and bridge loading signals. It can be seen from Figures 3-33, 3-34, 3-35, and 3-36, that the corrected vibrometer output matches the LVDT output in phase and amplitude for the different signals tested.

(a)

(b)

(c)
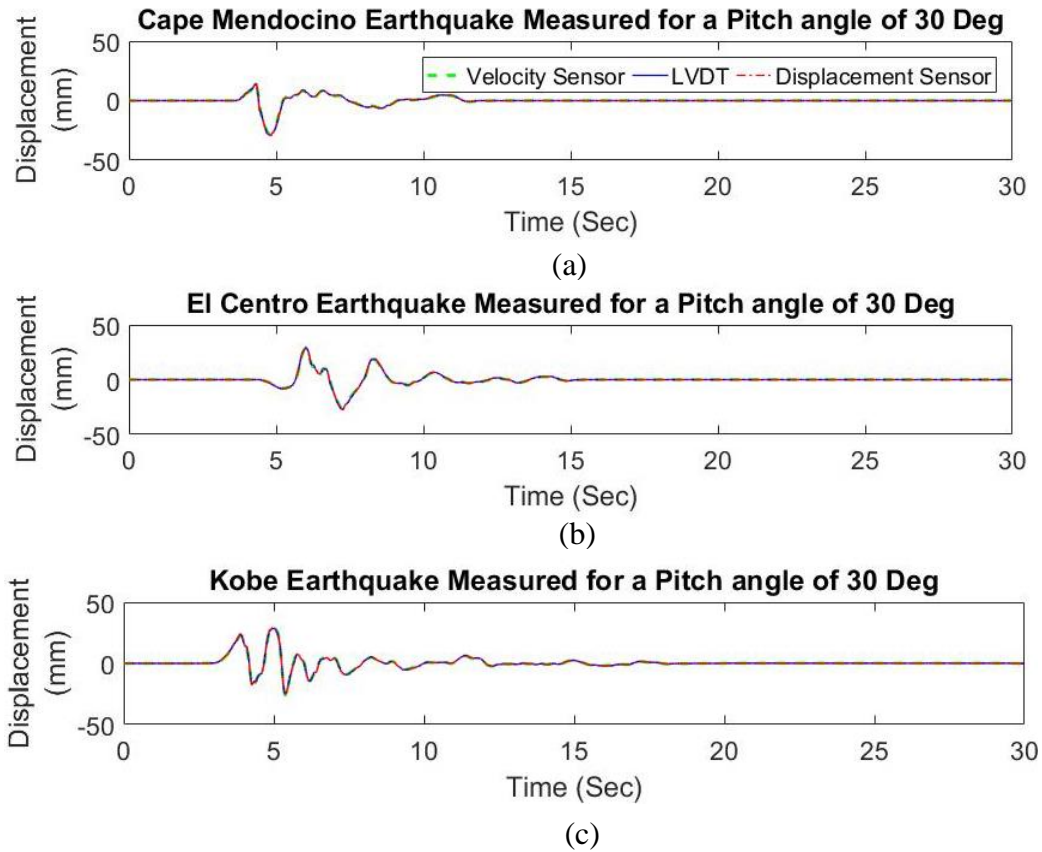
Figure 3-33. Response of vibrometer vs LVDT for (a) Cape Mendocino earthquake, (b) El Centro earthquake, and (c) Kobe earthquake and vibrometer pitch angle 30 degrees
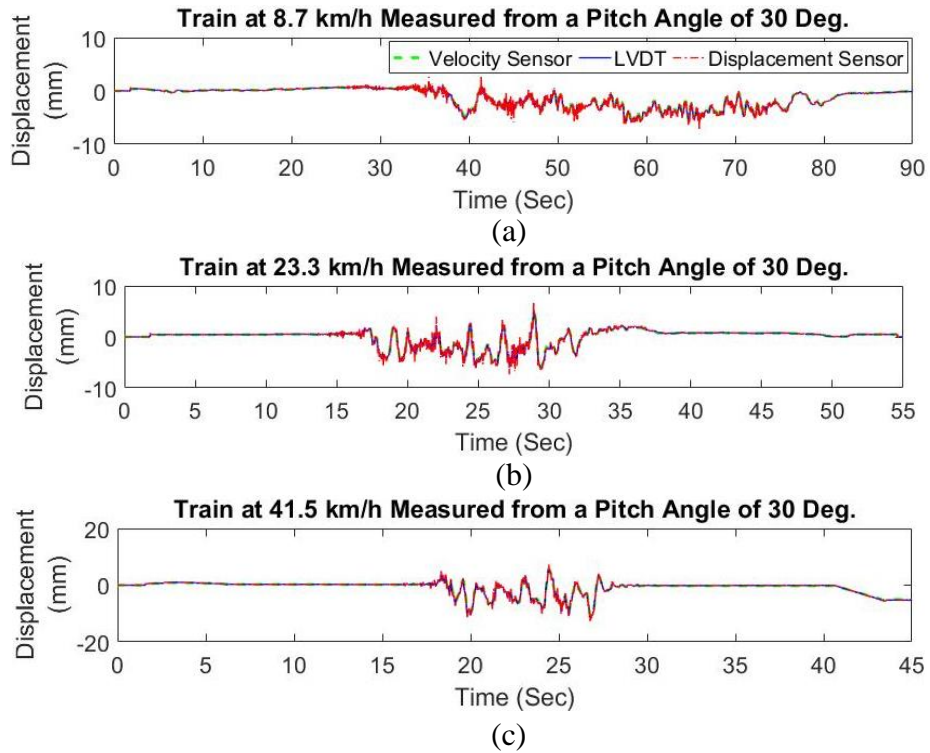
Figure 3-34. Response of vibrometer vs LVDT for bridge displacement signal, train speed (a) 8.7 kmph, (b) 23.3 kmph, and (c) 41.5 kmph and vibrometer pitch angle 30 degrees
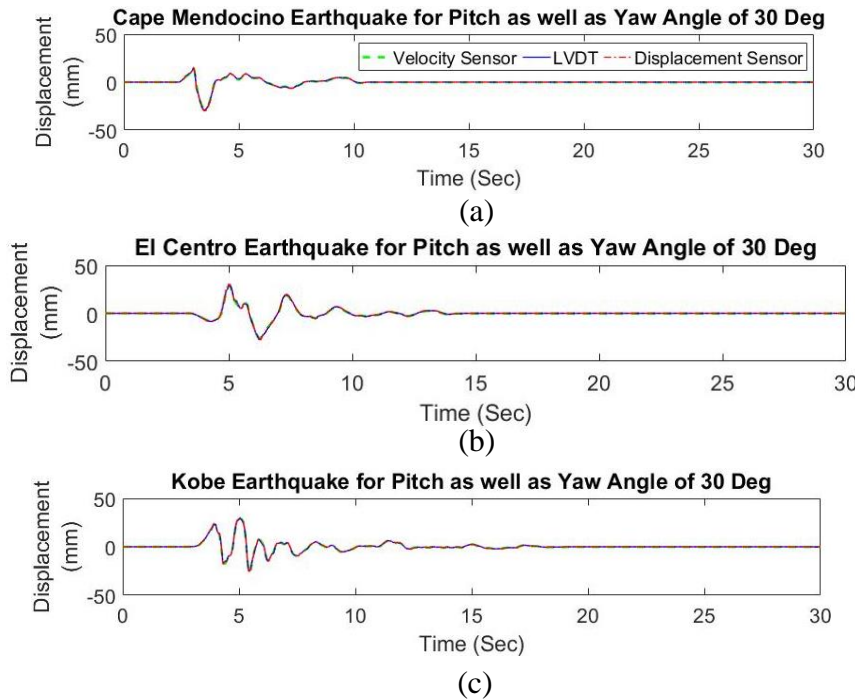
Figure 3-35. Response of vibrometer vs LVDT for Response of vibrometer vs LVDT for (a) Cape Mendocino earthquake, (b) El Centro earthquake, and (c) Kobe earthquake and vibrometer pitch and yaw angles 30 degrees
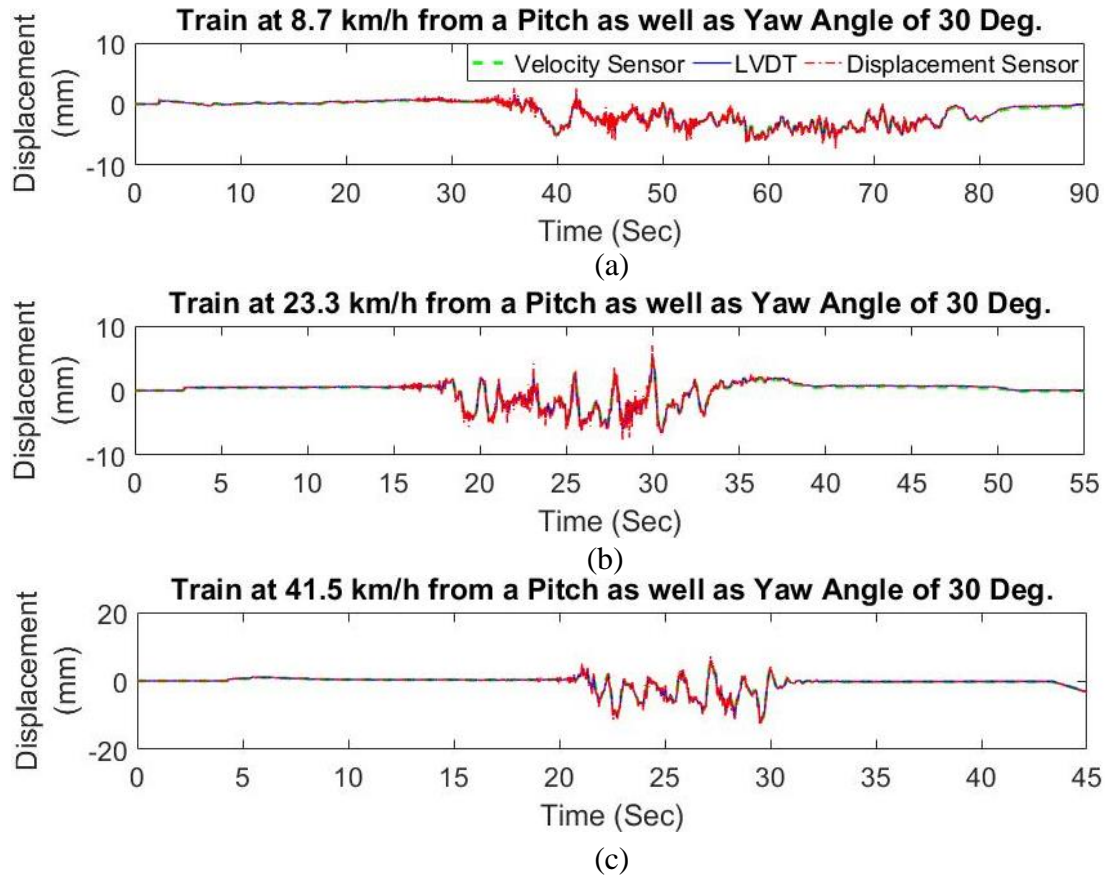
Figure 3-36. Response of vibrometer vs LVDT for bridge displacement signal, train speed (a) 8.7 kmph, (b) 23.3 kmph, and (c) 41.5 kmph and vibrometer pitch and yaw angles 30 degrees

The peak errors are below 5% and the RMS errors are below 2%. These tests prove that the correction algorithm for the angular location of the vibrometer work for the different signals tested. From all the experiments, it can be concluded that the algorithm for correction of the vibrometer output when it is at the angle to the target works in all the cases with RMS differences constantly less than 2%.

3.4.3 Dynamic angular motion of the vibrometer

To analyze the angular motion of the vibrometer, it is essential to measure the during the rotation. Figure 3-37 shows the readings measured by the capacitive accelerometer for dynamic pitching of the vibrometer during measurements
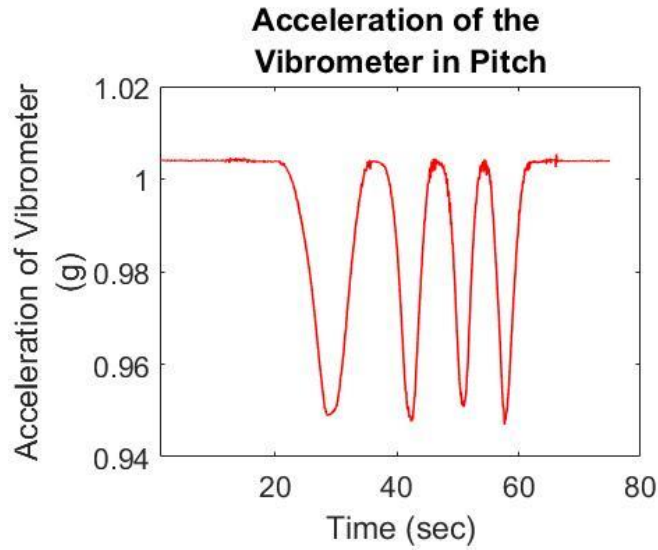
Figure 3-37. Gravitational force measured by the accelerometer in g

The calculated dynamic angles for the movement of the vibrometer can be seen in figure 3-35. it is observed that the vibrometer moves between 0 and 20 degrees.
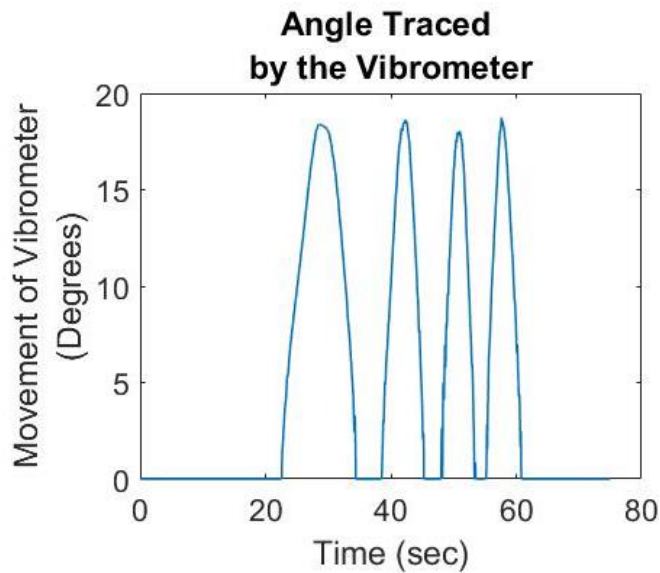
Figure 3-38. Angle calculated using the values of g force

Figure 3-39 shows the errors due to this movement, in the measured output. Figure 3-39 also shows the corrected readings obtained by correcting the signal

received by the vibrometer for the movement seen in Figure 3-38 using the equations 3.7 and 3.8.
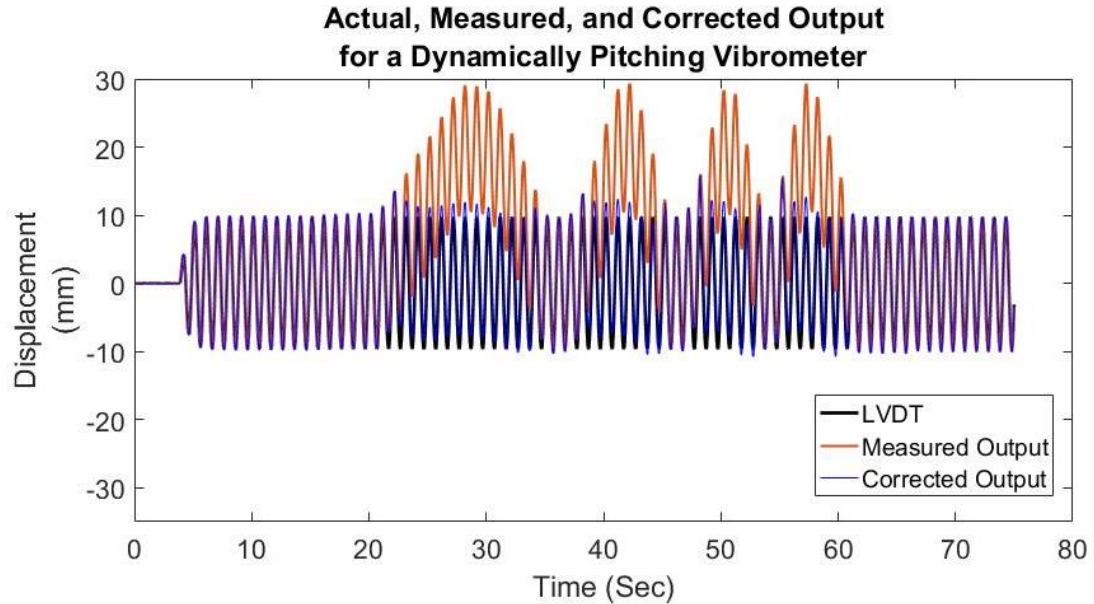
Figure 3-39. Measured and corrected value of the vibrometer displacement Output vs the actual output measured by the LVDT

The corrected readings from the vibrometer matches the LVDT reading in phase and is close to the amplitude of the actual signal. It is observed from Figure 3-37, that the maximum difference between the corrected output and the LVDT measurement is around 10% and the RMS difference is only around 5%.

Under these considerations, it can be concluded that the algorithm developed for the correction of a dynamically pitching vibrometer will be able to obtain the corrected displacement under small angles during UAS operations.

(a) (b)
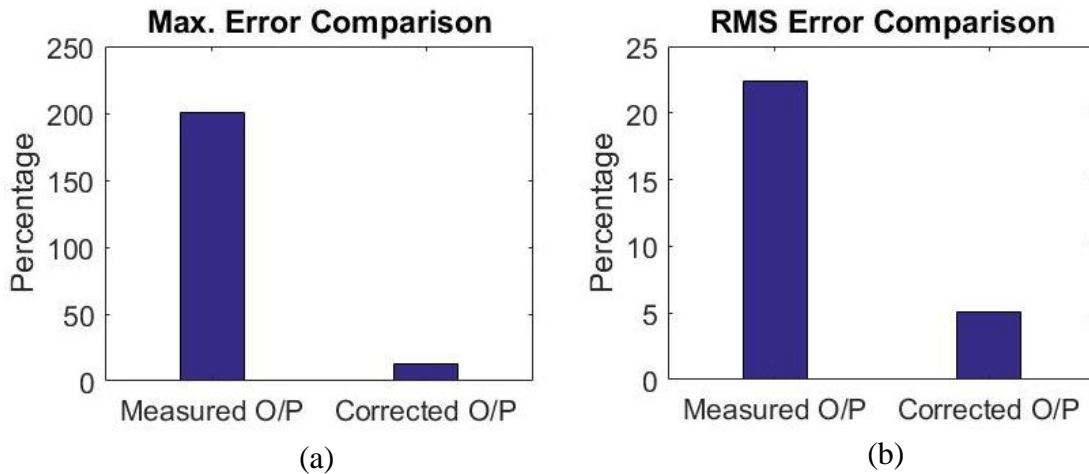
Figure 3-40. Maximum and RMS differences of measured vibrometer and corrected vibrometer outputs vs LVDT

3.4.4 Random dynamic angular and lateral motions of the vibrometer

The random motion of the vibrometer includes the linear motion of the vibrometer as well as its angular rotations. Figure 3-38 and Figure 3-39 show the linear movements of the vibrometer and the motion of the vibrometer in the angular directions respectively.
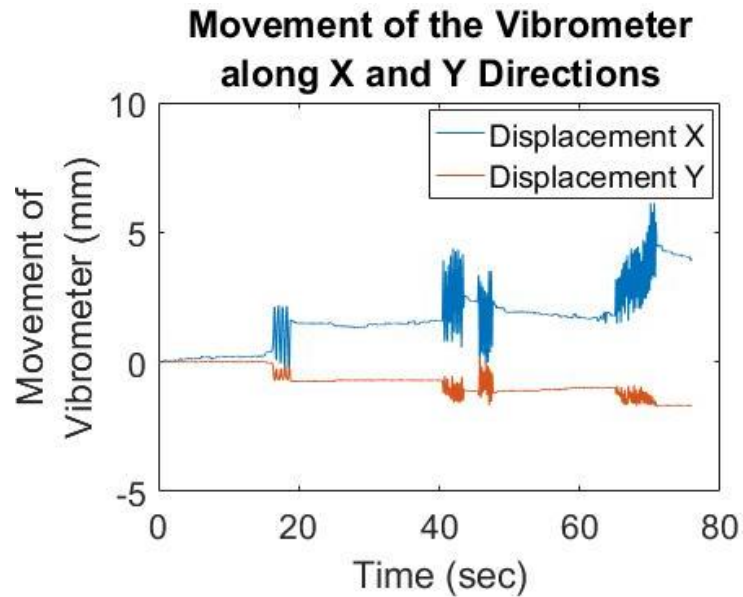
Figure 3-41. Motion of the vibrometer in linear directions.
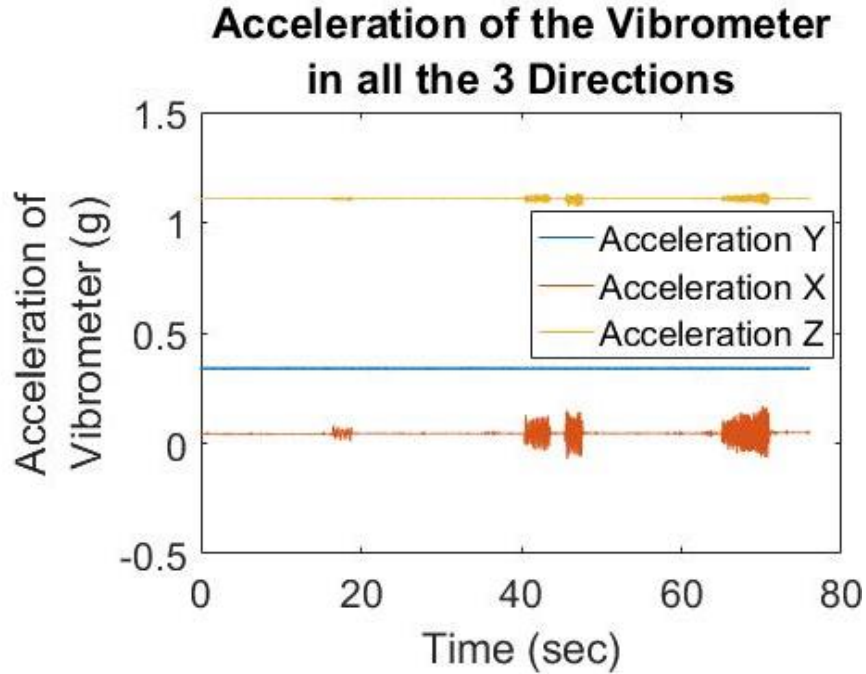
Figure 3-42. Motion along the angular directions (bottom)

Due to this random motion, the error is introduced in the measured signal. This can be seen in Figure 3-40, which shows the actual bridge vibration due to train loading as measured by the LVDT and the measured vibrometer displacement reading with errors due to the random motion.
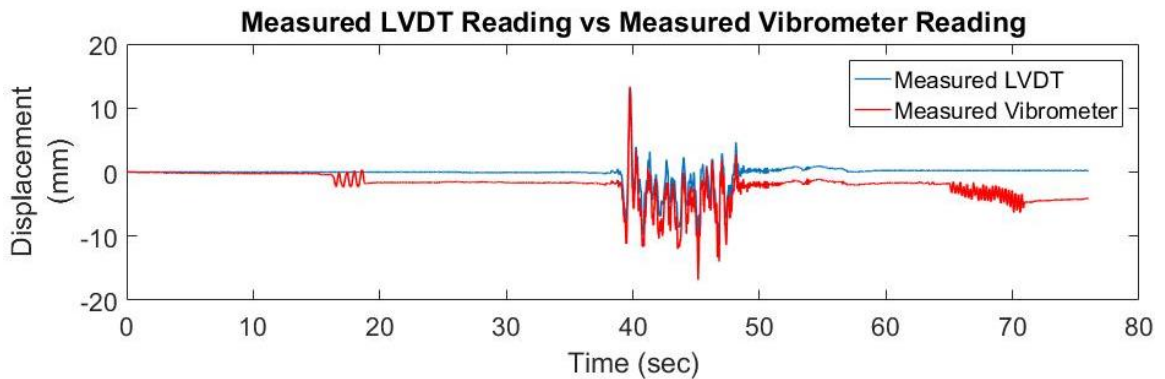
Figure 3-43. Measured reading of the vibrometer with error due to random motion vs the actual reading measured with the vibrometer

When this measured vibrometer reading is corrected for the motion recorded by the LVDT and the accelerometers, as seen in Figure 3-41, the corrected reading matches the actual reading both in amplitude and phase.
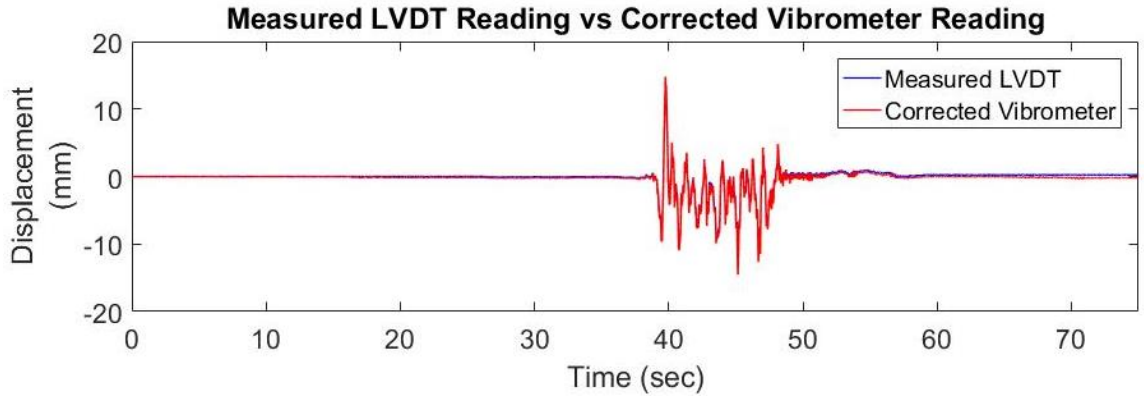
Figure 3-44. Corrected reading of the vibrometer vs LVDT

Figure 3-42 shows that the comparison of the maximum displacements and the RMS differences for the measured signal are high before correction. The maximum difference for corrected signal is around 12%, and the RMS difference is only around 1%. Thus, the algorithm for correction of the random motion the vibrometer works accurately.

(a)   (b)
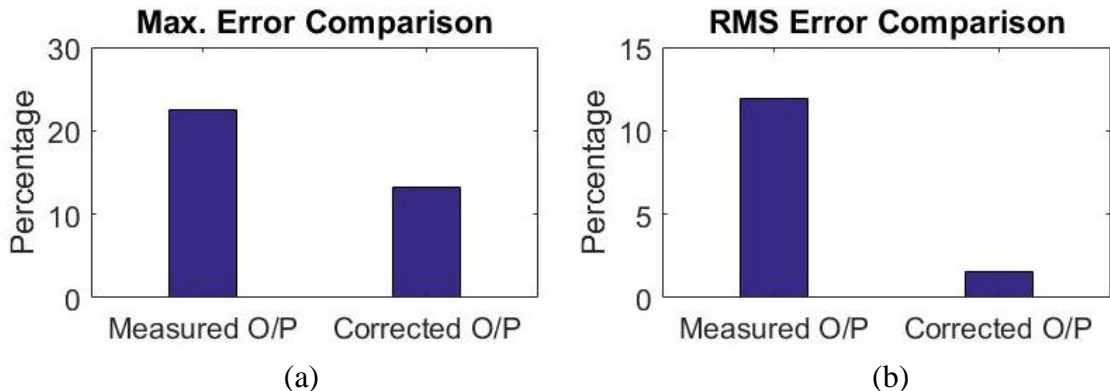
Figure 3-45. Signal difference between measured and corrected vibrometer vs LVDT for (a) peak differences and (b) RMS differences

From the results presented in this chapter, it can be claimed that the algorithms designed for the correction the vibrometer movement are correct.

3.5 Conclusions

This chapter focused on designing the framework for transverse displacement using a LDV in moving condition. The author selected the LDV OFV-534 by Polytec, with small dimensions and less weight for these experiments so the results can be carried forward to the UAS implementation. All tests in this section were carried out in the laboratory with vibrometer measuring the displacement of a target on the shake table simulating harmonic waves, earthquakes, and transverse bridge displacements under train loading. The author conducted the initial tests to validate the output response of the vibrometer compared to the LVDT. Algorithms were then developed to correct for various configurations of the vibrometer in moving and stationary conditions. These algorithms were tested and validated in the laboratory experiments. Table 3-3 shows the summary of the measured and corrected signal differences.

From the results, the author concluded that the vibrometer can measure the pseudo-static displacement of the railroad bridges, and that the algorithms developed for correction of movement of the vibrometer work for all the configurations as described in the test setups. Based on these tests and results, the author has demonstrated that the selected vibrometer can be used to measure transverse dynamic displacements, and can measure the accurate transverse displacements as long as the movement of the UAS is accurately measured and tracked as demonstrated in the laboratory.

Table 3-3 Summary of the LDV measured and corrected readings for different experimental setup

Vibrometer State	Measured Output		Corrected Output	
	Peak	RMS	Peak	RMS
Static Perpendicular	4%	1%	-	-
Pitch 30^0	12%	5%	2%	1%
Pitch 30^0 and Yaw 30^0	22%	10%	2%	1%
Dynamic Pitching	200%	22%	10%	5%
Random Motion	22%	12%	10%	2%

Chapter 4: Using Laser Doppler Vibrometers Mounted on Unmanned Aerial Systems for Measurement of Bridge Displacements

4.1 Introduction

This chapter covers the preliminary field testing for outdoor use of LDV to measure transverse displacements, selection of UAS, the dynamic transverse displacement measurements using vibrometer mounted on UAS, the computation of UAS movements, setups, and results validating the use of UAS mounted with vibrometer for transverse displacement measurement in the field.

4.1.1 Preliminary Testing

The purpose of the preliminary field test was to find the optimal distance of operation for the vibrometer from the target for a UAS based operation or rather to explore the effects of distance in the accuracy of the readings outdoors. The layout of the field testing is in Figure 4-1.
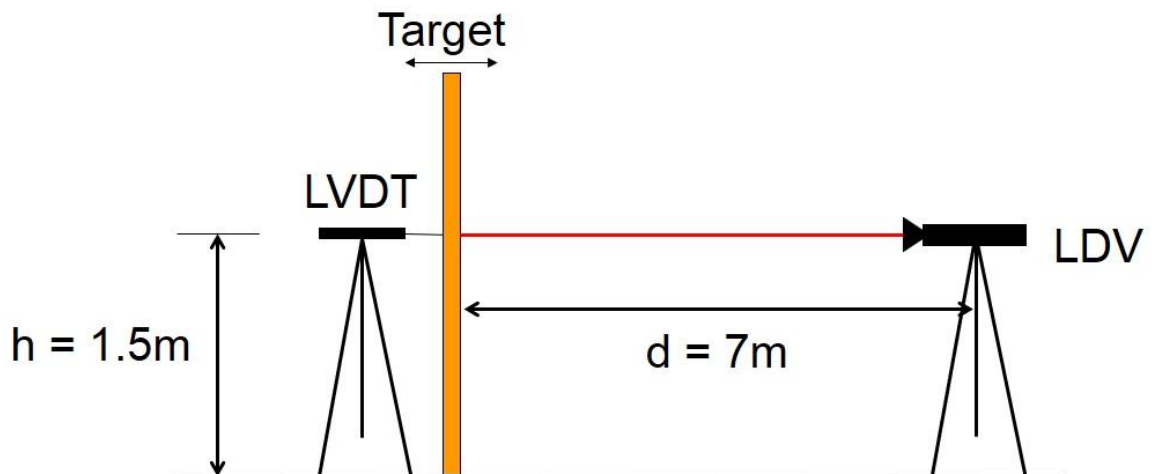
Figure 4-1. Test layout for preliminary vibrometer field testing

In the field setup, the vibrometer is arranged such that the height of the laser signal from the ground surface, is the same as the height of the LVDT. Figure 4-2 shows the field setup realization. In this test, 5 set of readings were taken from different distances of vibrometer from the target, ranging from 5 feet to 25 feet at an increment of 5 feet. The data acquisition system used for these experiments is vibpilot and the sampling frequency 1024 Hz. A wooden plank was used to simulate the dynamic displacement of the bridge.
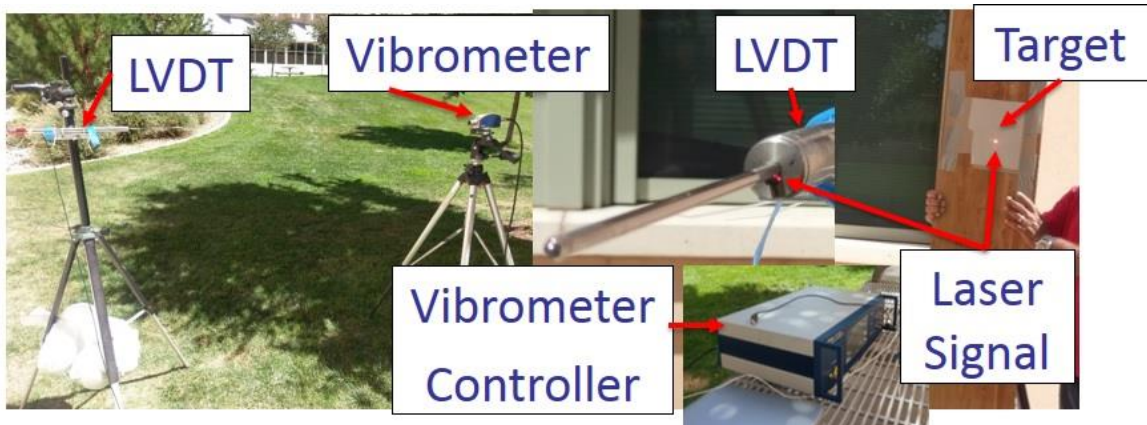
Figure 4-2. Field test setup for preliminary vibrometer testing

The maximum sensitivity of the controller module is 5 mm/V, and the Data Acquisition System (DAQ) has a range of ±10V. When the displacement recorded is more than ±50mm, the signal needs to be corrected. Figure 4-3 shows the actual vibration captured by the LVDT, and the measured reading of the vibrometer, for a displacement of more than -50mm. In the field, if the total displacements would exceed 50mm, the measurement would still be calculated. However, given the experience of the bridge researchers measuring displacements, this displacement is not expected to be exceeded
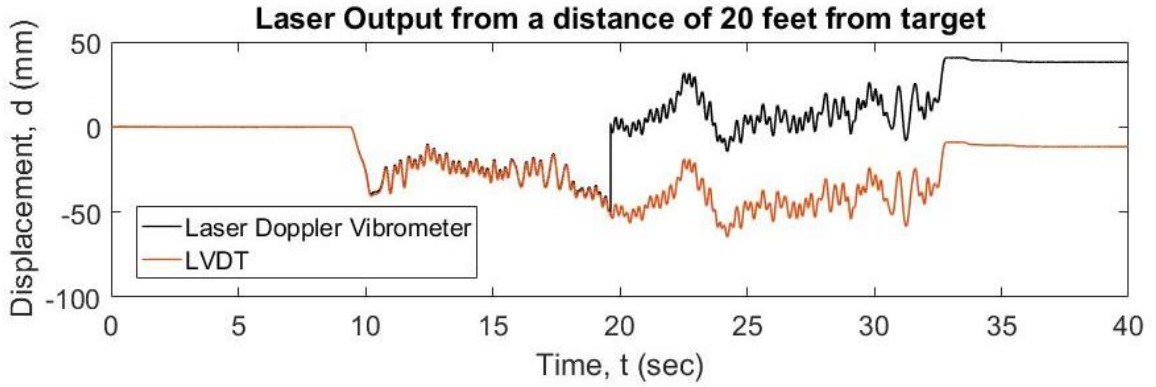
Figure 4-3. Measured output of Vibrometer at 20 feet from the target vs LVDT

Figure 4-4 shows the corrected readings for the measurements. It is observed that the corrected readings match the LVDT output.
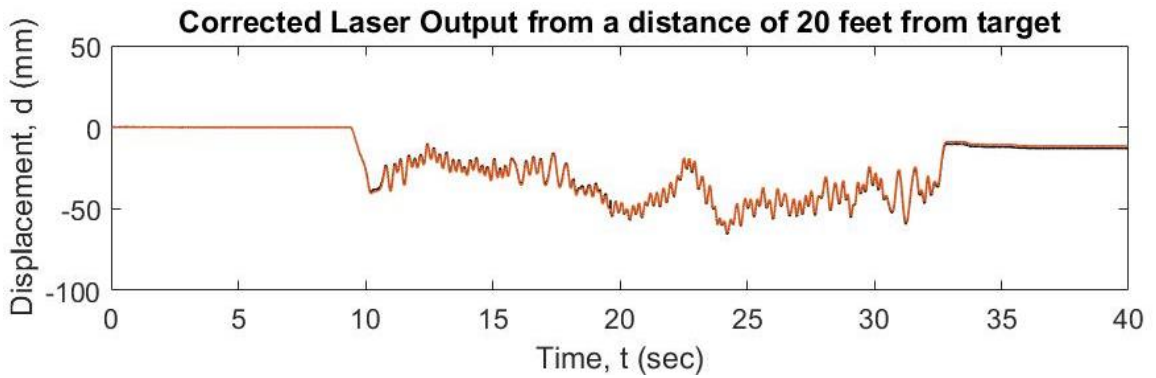
Figure 4-4. Corrected output of Vibrometer at 20 feet from the target vs LVDT

Figure 4-5 shows that the performance of the vibrometer is very close to that of the LVDT. Figure 4-6 shows that there is no significant change or definite increase in the signal difference of the with increase in the distance from the target.

(a)

(b)

(c)

(d)
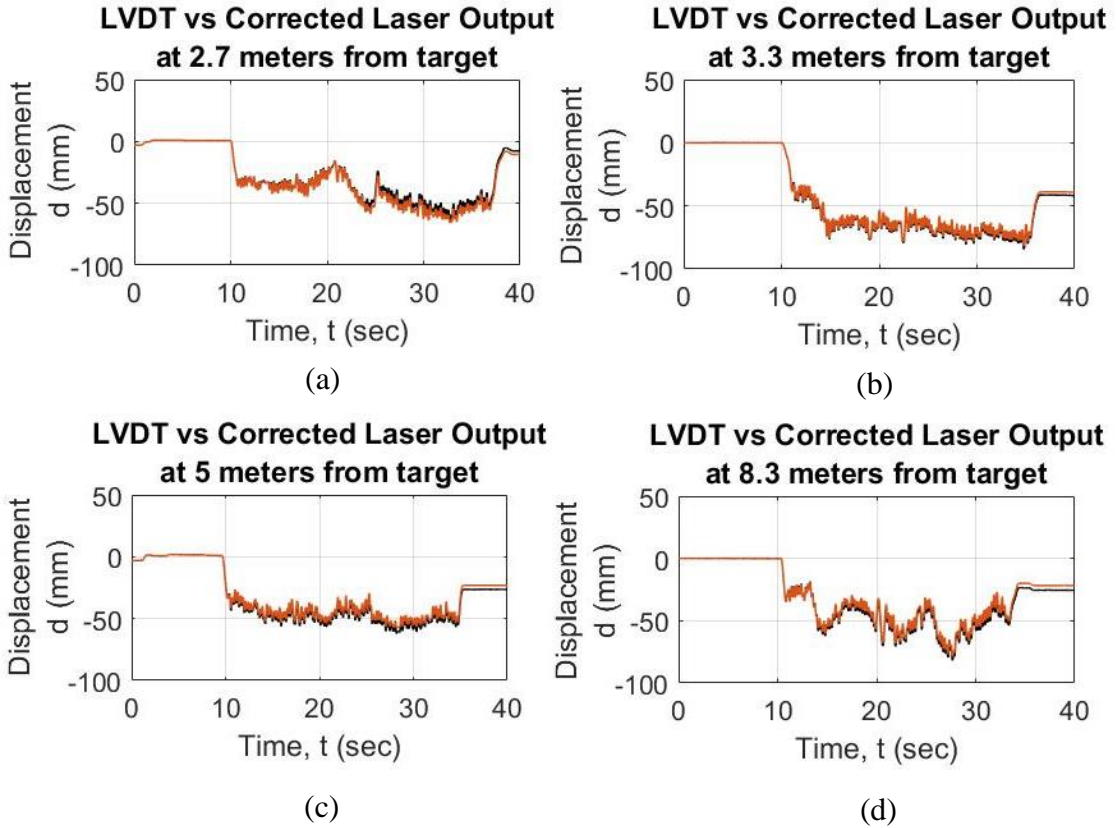
Figure 4-5. Corrected vibrometer output vs LVDT at (a) 2.7 meters from the target, (b) 3.3 meters from the target, (c) 5 meters from the target, and (d) 8.3 meters from the target

(a)

(b)
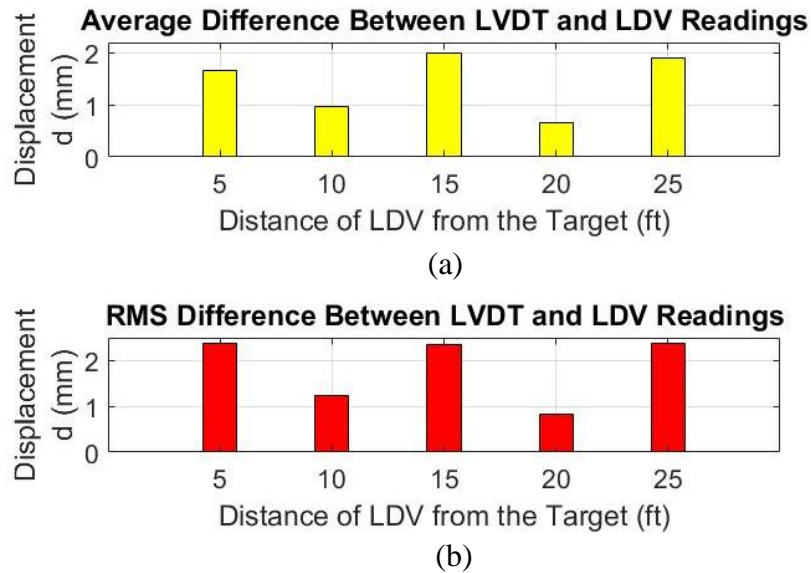
Figure 4-6. (a) Average signal difference between vibrometer and LVDT from different distances and (b) RMS signal difference between vibrometer and LVDT from different distances

Also, the spectral analysis of both the signal show that the output profile of the vibrometer is the same as that of the LVDT (Figure 4-7). From this, it can be concluded that the vibrometer does not add any frequency components to the output and it can be used to obtain total displacements in the field.
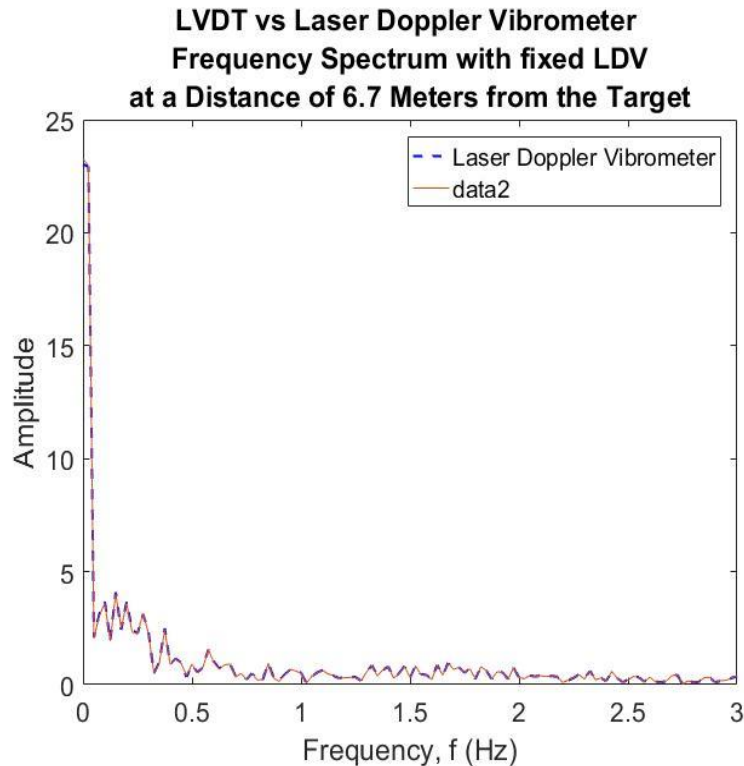
Figure 4-7: Frequency Spectrum of Vibrometer output vs LVDT output

4.1.2 UAS selection

The UAS selection included multiple considerations for its proper integration with LVD requirements. First, the UAS to be considered for the research should be capable of hovering with a payload of more than 5 pounds. Secondly, the integrated system will be used for testing of railroad bridges under dynamic loading, and average length of a conventional freight train is about 6600 feet (Joiner, S. 2010). Thus, to cross a 500 feet railroad bridge at 25 mph, will take the

69

train over 3 minutes. Accessing the bridge and finding the adequate location will take several minutes as well. Thus, to correctly obtain several complete train crossing events, the UAS-LDV assembly should be able to hover for more than 10 minutes. With these criteria, the UAS considered for this research are detailed in Table 4-1.

Table 4-1: Unmanned Aerial System details and selection criteria

Company	DraganFly	Asctec	Action Drone USA	DJI
Name	X4-P	Pelican	AD2-X8	Matrice 600 Pro
Image				
Website	www.draganfly.com	www.asctec.de/en	www.actiondroneusa.com	www.dji.com
Details	Payload Capacity: 800 gm Hovering Time: 16 mins	Payload Capacity: 650 gm Hovering Time: 16 mins	Payload Capacity: 18-30 lbs. Hovering Time: 15 mins	Payload Capacity: 5.5 kg Hovering Time: 18 mins
Cost	$23,285	$5,000	$18,999	$6,600

As seen from the comparison, Matrice pro 600 has a payload of 5.5 kg and a hovering time of around 18 minutes at full payload. It also has an enhanced Global Positioning System (GPS) and an inertial measurement unit (IMU), along with self-correction and stabilization capabilities. The author of this research selected the DJI Matrice 600 Pro to be integrated00 with the preselected LDV.

4.1.3 UAS familiarization

After the UAS selection and acquisition, several test flights were conducted to familiarize with its, movement and capabilities. Figure 4-8 shows the UAS in the air during one of the test flights.

Figure 4-8. DJI Matrice 600 Pro test flight

After the initial flight tests, UAS was attached with some weight and flight tested prior to the integration with the LDV. Figure 4-9 shows the weight assembly for the UAS. During the flight test with weight attached to the UAS system, it was observed that the dynamics of the system do not change extensively during the flight. The system response for the provided input does not affect the overall handling of the system. It was observed that attaching the weights directly to the

chassis of the UAS does not affect its stability. It was determined that the weight

should not be suspended from the UAS for better control of the overall system.

Figure 4-9. UAS attached with dead weight for test flight

During the preliminary validation of this UAS for LDV integration, several

mistakes were made. The lessons from these mistakes were used to develop the

research framework for the integration of the system. Table 4-2 shows the

summary of important mistakes and lessons from this research stage.

Table 4-2: Failures and Lessons from the UAS test flights

Failures	Causes
Drone flight and crash against the wall	• Return to home function failure due to GPS signal
Drone flight and crash at George J Maloof Airpark	• Landing on uneven surface • Improper GPS configuration

Figure 4-10 shows the damage to the UAS motors and propellers after the

UNM test flight crash. For these causes the author and the pilot of the UAS

observed that the flight in confined space causes weak GPS signal and learnt the

importance of configuring GPS antenna and system. They also learnt that during

imbalanced landings, it is important to abort the landing and make a fresh landing attempt.

Figure 4-10. Damage to the UAS propellers and front motors from UNM crash.

The remaining research steps included the generation of checklists and failsafe methods. Additionally, tethering was added from the drone to the ground to avoid damage to the vibrometer assembly or any injuries during the flight of the two integrated systems.

4.2 Methodology

4.2.1 UAS Hovering Data Measurement

To understand the movement of the UAS while hovering 2 feet in the air, the laser doppler vibrometer was used to measure the hovering movement of one UAS under normal outdoor conditions. The field test setup for measuring the UAS movement can be seen in the Figure 4-11.
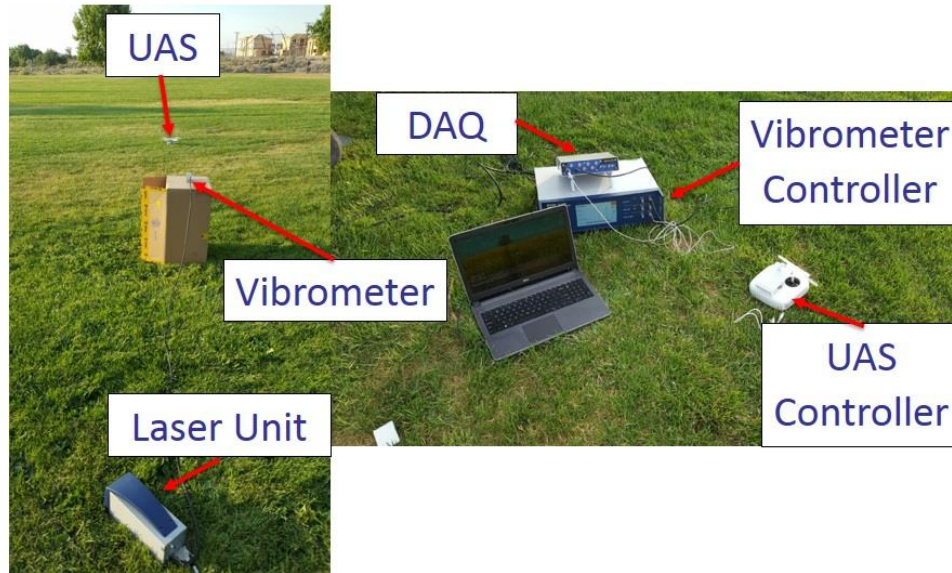
Figure 4-11. Field test setup to measure UAS hovering data

The DJI Phantom 3 Pro was used for this test. Figure 4-12 Shows the plot of UAS hovering data obtained in this test. Even when the two UAS are different in both hardware and software, this preliminary exploration was conducted for preparation purposes and only as exploratory research, given that there was no information available about the displacement of UAS using a fixed reference.
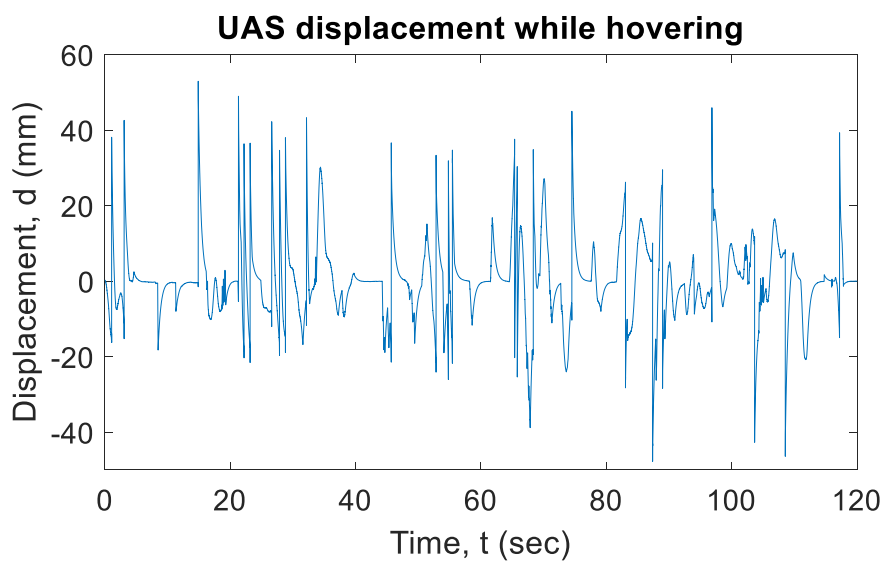
Figure 4-12. UAS displacement while hovering

It was noted that the small size of the UAS and the lack of flat surface as a target made it difficult for the vibrometer to be constantly focused on the sensing. The results show that the drift and corrections for the movement results in very low frequency movements in the direction of the laser. These results were used in the subsequent stage of the research to inform the requirements of sensing transverse displacements with UAS operations.

4.2.2 UAS Hovering Movement

To understand the hovering motion of the vibrometer, the time domain data is converted into frequency domain. This is done by using the Fourier transformation of the time domain signal. The conversion of the discrete signal is done using

$$X_k = \sum_{0}^{N-1} e^{-j2\pi kn/N} \tag{4.1}$$

Analyzing the signal in frequency domain gives a better understanding of the hovering performance. Figure 4-13 shows the conversion of the UAS hovering signal into the frequency domain. It is observed that most of the power in the hovering is concentrated on frequencies under 0.5 Hz. This motion will be filtered using a high pass filter to compare the dynamic motions of vibrometer and LVDT. Following research from Moreu et al. (2014), the measurement of the dynamic transverse displacements of railroad bridges can inform railroad managers of the condition of the bridges.
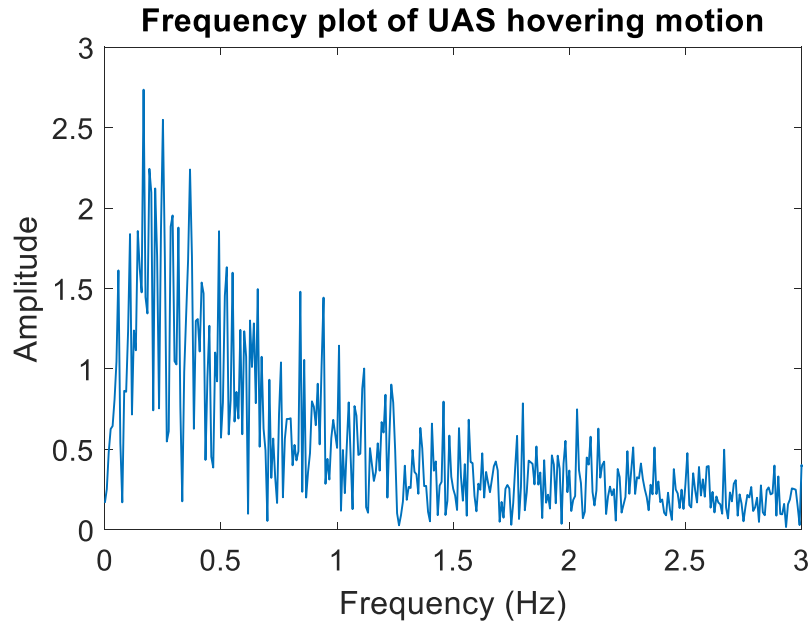
Figure 4-13. Frequency spectrum of UAS hovering motion

4.2.3 UAS Movement Compensation

Since the movement of the has low frequency, the movement of the UAS can be filtered out of the vibrometer signal to obtain the dynamic transverse displacement of the target.

A high pass Butterworth filter of order 3 is designed for this purpose, with a 3-dB (half-power) or cutoff frequency of 0.5 Hz. Figure 4-14 shows the magnitude response of the designed filter.

4.2.4 Performance Evaluation Criteria

To benchmark the operation capabilities of the vibrometer, the readings of the vibrometer are compared to those of the LVDT. For these experiments, two parameters are used for comparison between the two readings, the maximum difference (E_1) and the RMS difference (E_2).
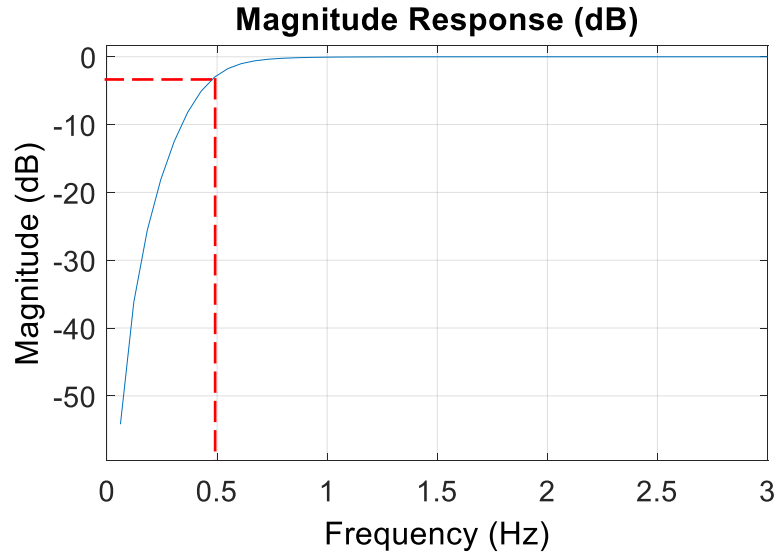
Figure 4-14. Magnitude response of 3rd order Butterworth high-pass filter with cut-off frequency 0.5Hz

The maximum difference between the signals is obtained by comparing the values at each of the sampling point and then finding the maximum of this value from these differences. For 'n' sampling points, the difference is obtained as:

$$\text{Max}(E_1(i)) = (abs(LVDT(i) - LDV(i))), \; 1 \le i \le n \tag{4.1}$$

The RMS difference for 'n' sampling points is obtained as

$$RMSD = \sqrt{\frac{\sum_{i=1}^{n}(LVDT(i)-LDV(i))^2}{n}} \tag{4.2}$$

These two parameters will be used to quantify the difference between the LVDT and LDV measurements.

4.3 Experimentation

4.3.1 Experimental Layout

Figure 4-15 shows the experimental layout for the field testing using a LDV mounted onto a UAS. In the field testing, the movement of the target is captured by the vibrometer mounted on a UAS. The measurements obtained by the vibrometer are compared to the actual displacements of the target measured by the LVDT.
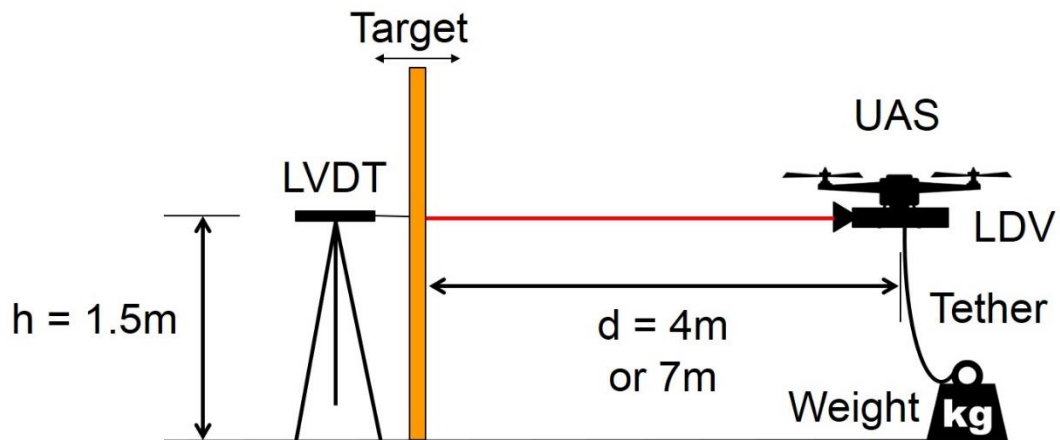
Figure 4-15. Experimental layout for the field testing using a LDV mounted on a UAS.

The connection between the vibrometer and its data acquisition unit is a fixed optical fiber cable. To protect the vibrometer and to prevent injuries in case of sudden and unexpected UAS movement, the UAS is tethered to the ground using a heavy weight cable. In this comparison, the UAS system is not attached with any sensor for tracking its movement. The movement compensation approach was based on the sensor. The future approach will include mounting acceleration and gyro based inertial navigation units mounted on the UAS system, and assisted with camera, to measure the precise movement of the UAS system while in flight.

The objective of this comparison in the current field test setup is the proof of concept measurement of dynamic transverse displacements of railroad bridges using an LDV mounted on a UAS.

4.3.2 Field Test Setup

The implementation of the experimental setup for field testing is shown in Figure 4-16.

Figure 4-16. Filed testing using a LDV mounted on a UAS

The pilot will command the UAS to hover approximately 1.5 meters from the ground and the LVDT is arranged accordingly to point to the same location on the target. The UAS is flown at 4 to 7 meters from the target. The UAS is attached with the vibrometer using zip ties on a carbon fiber plates. In the field, the cloth was used between the plate and the vibrometer to eliminate the vibrations from the UAS motor into the LDV. Figure 4-17 shows the vibrometer assembly on the UAS.

Figure 4-17. Vibrometer assembly to the UAS.

The UAS was tethered to the ground along with the vibrometer cable to protect the vibrometer assembly as well as to prevent injuries. Figure 4-18 shows the UAS tethering.

Figure 4-18. UAS tethered to the ground along with vibrometer cable.

The length of the connection between the LDV and the controller is fixed at 3 meters, and this is the optimal length of connection for the signal to travel through it without attenuation. The plank is manually moved in a way that simulates the movement of the railway bridge with various frequency and amplitude components

including the pseudo static displacement. In this way, the field testing results can

be used as a proof of concept prior to the testing of real railroad bridge.

4.4 Results

This section presents the results from the field testing. Three results

captured using the LDV mounted onto the UAS are analyzed. Of the three trials,

one was captured from a distance of four meters from the target, and two from a

distance of seven meters from the target. Figure 4-19 shows the data captured by

the vibrometer data acquisition system for these 3 trials.

The captured data of Figure 4-19 includes the distortion due to the out of

bounds condition of the signal obtained from the vibrometer. Figure 4-20 shows

the corrected signals for the three experiments.
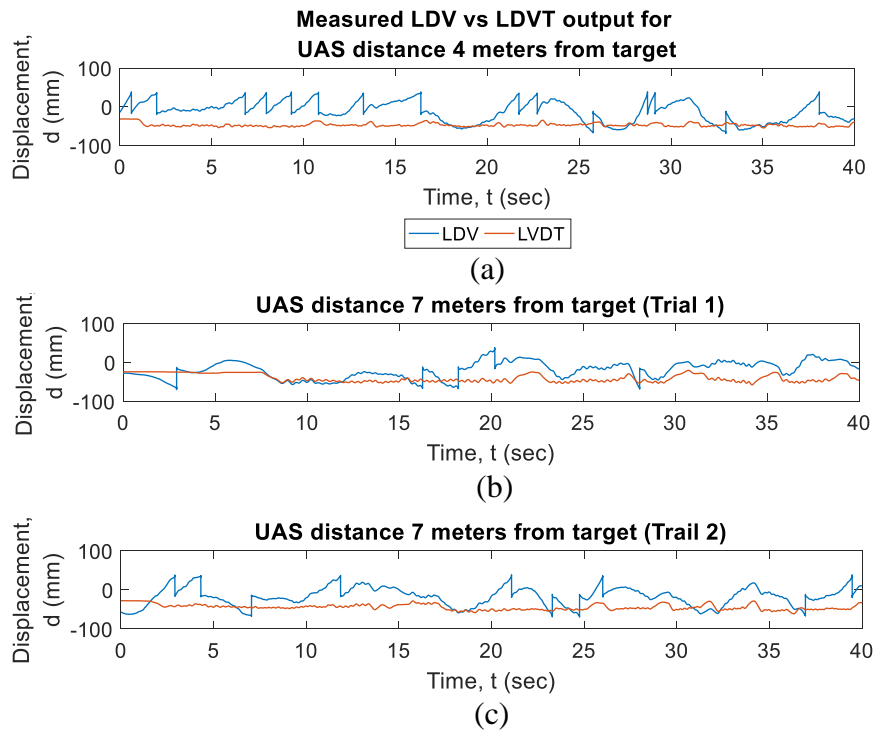
Figure 4-19. Actual data captured by the vibrometer vs LVDT with UAS flying at (a) 4 meters from the target, (b) 7 meters from the target (trial 1), and (c) 7 meters from the target (trial 2)
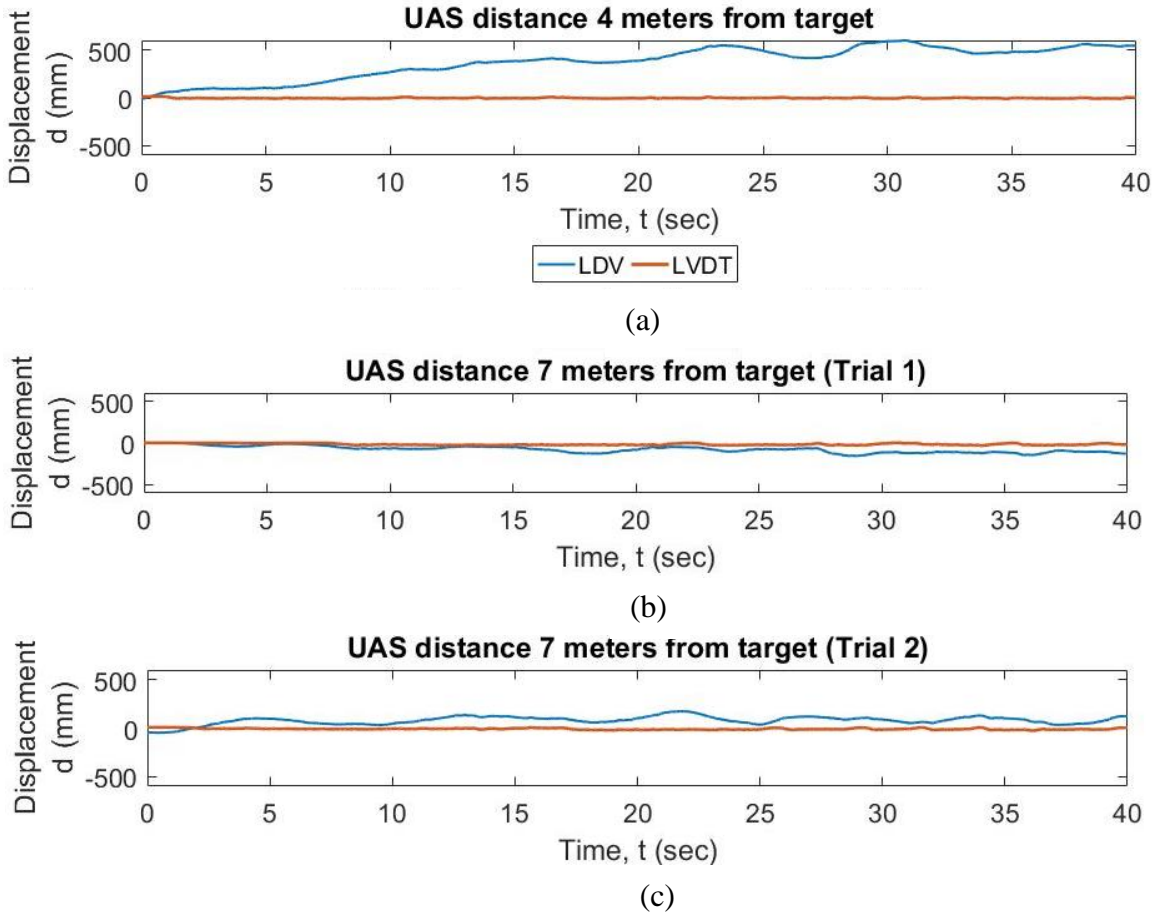
Figure 4-20. Corrected data from the vibrometer vs LVDT from the UAS distance of (a) 4 meters from the target, (b) 7 meters from the target (Trial 1), and (c) 7 meters from the target (Trail 2)

The analysis of the outputs reveals that the vibrometer signal is free distortions due to out of bound condition outside of the reflective tape used for these experiments. Figure 4-20 also revealed that the drifting motion of the UAS of a is very low frequency. The frequency domain analysis of the signals from the vibrometer and the LVDT are is shown in Figure 4-21. This plot shows that as recalled from Figure 4-7, vibrometer and LVDT have the same spectral output, their signals below 0.5 Hz are different on the frequency domain due to the hovering of the UAS. It can be concluded that the additional frequency components are added to the lower frequencies due to the motion of the UAS. However, at the

frequencies greater than 0.5 Hz, the signals from vibrometer as well as the LVDT

show similar profile.
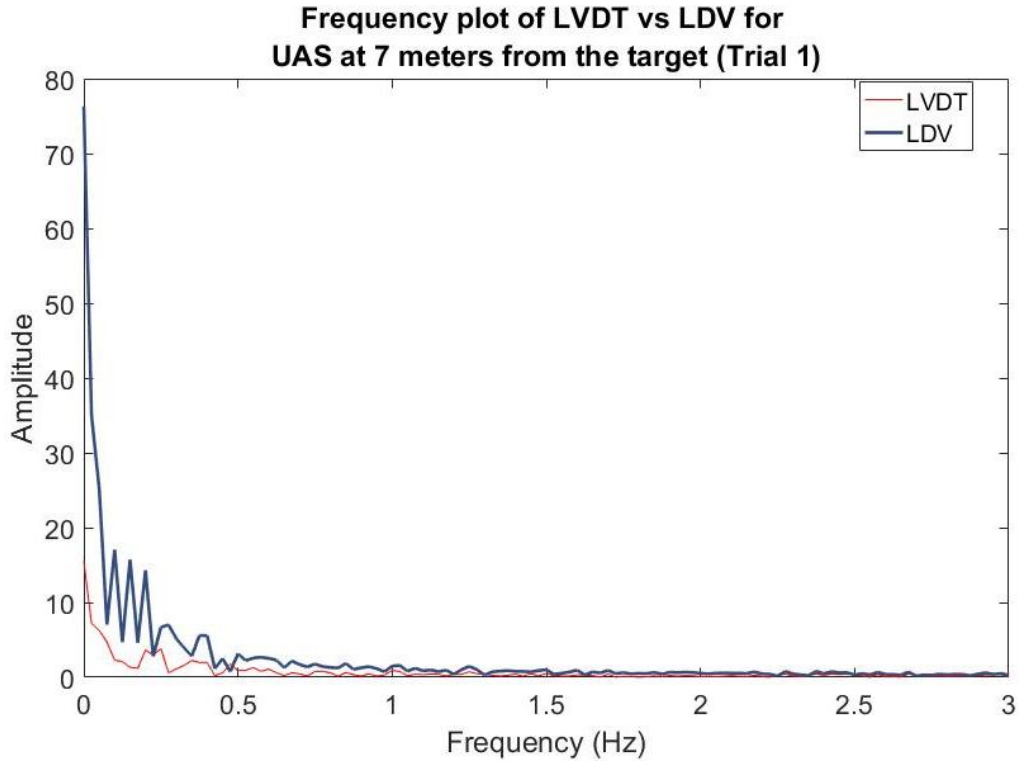
Figure 4-21. Frequency domain plot for corrected signal of the vibrometer mounted on a UAS 7 meters from the target vs LVDT

The signals are filtered using a high pass Butterworth filter with a cut off

frequency of 0.5Hz. Figure 4-22 shows the frequency spectrum of the vibrometer

and LVDT filtered data. The time domain plot of these signals is shown in Figure

4-23. It is observed that the filtered signals match very closely. This shows that the

dynamic data obtained from a hovering vibrometer matches closely with the

dynamic transverse displacement collected using a LVDT.
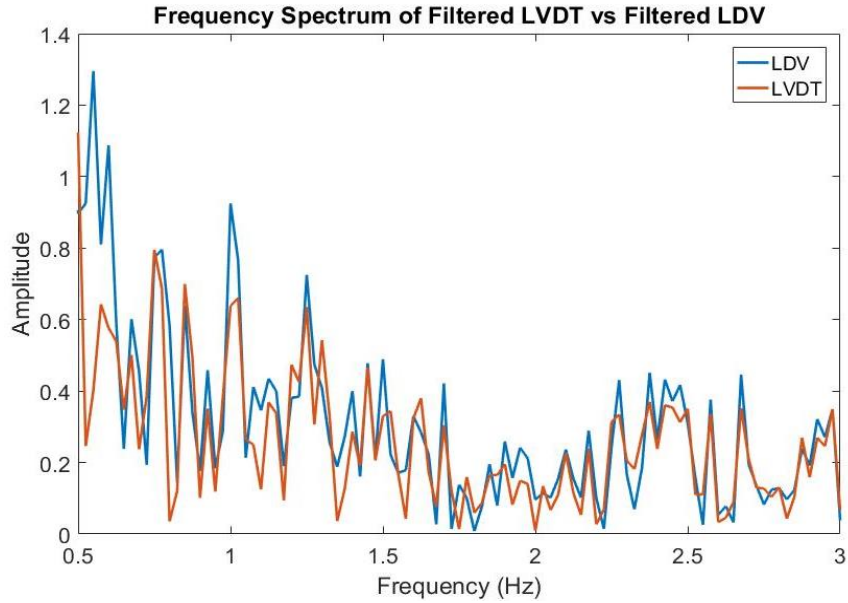
Figure 4-22. Spectral output of filtered LVDT and LDV signals
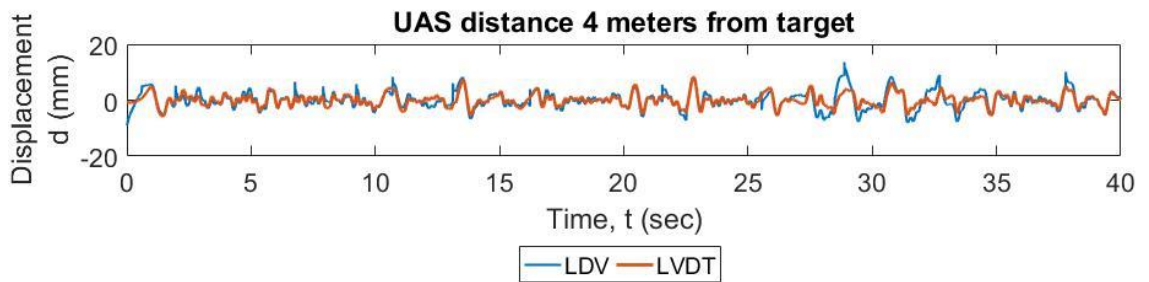
(a)
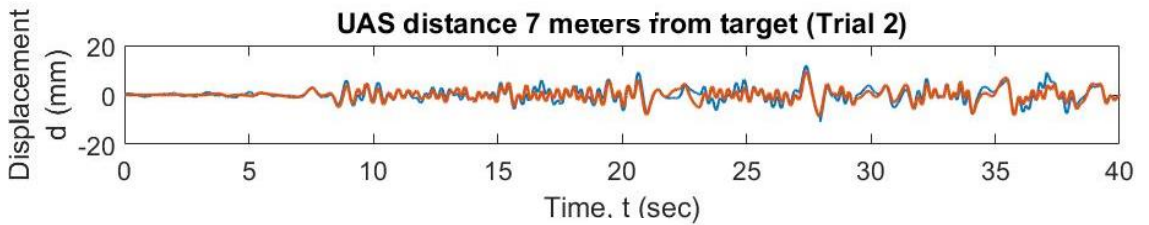
(b)
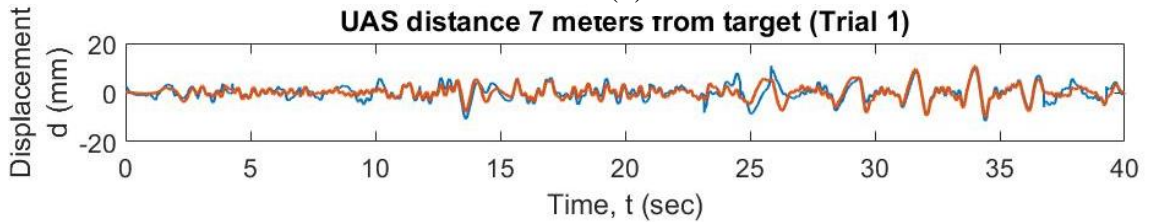
(c)

Figure 4-23. Comparison of dynamic displacements measured by LDVT and LDVT at (a) 4 meters from the target, (b) 7 meters from the target (trial 1), and (c) 7 meters from the target (Trial 2)

Based on the analysis and the observation of the readings that were measured inside the reflective area, the readings were only compared for those times where the laser fell within the limits of the reflective tape. When the filtered signals are enlarged to focus on that portion of the data, shown in Figure 4-24, it reveals the two signals matching in both amplitude and phase.

(a)

(b)

(c)
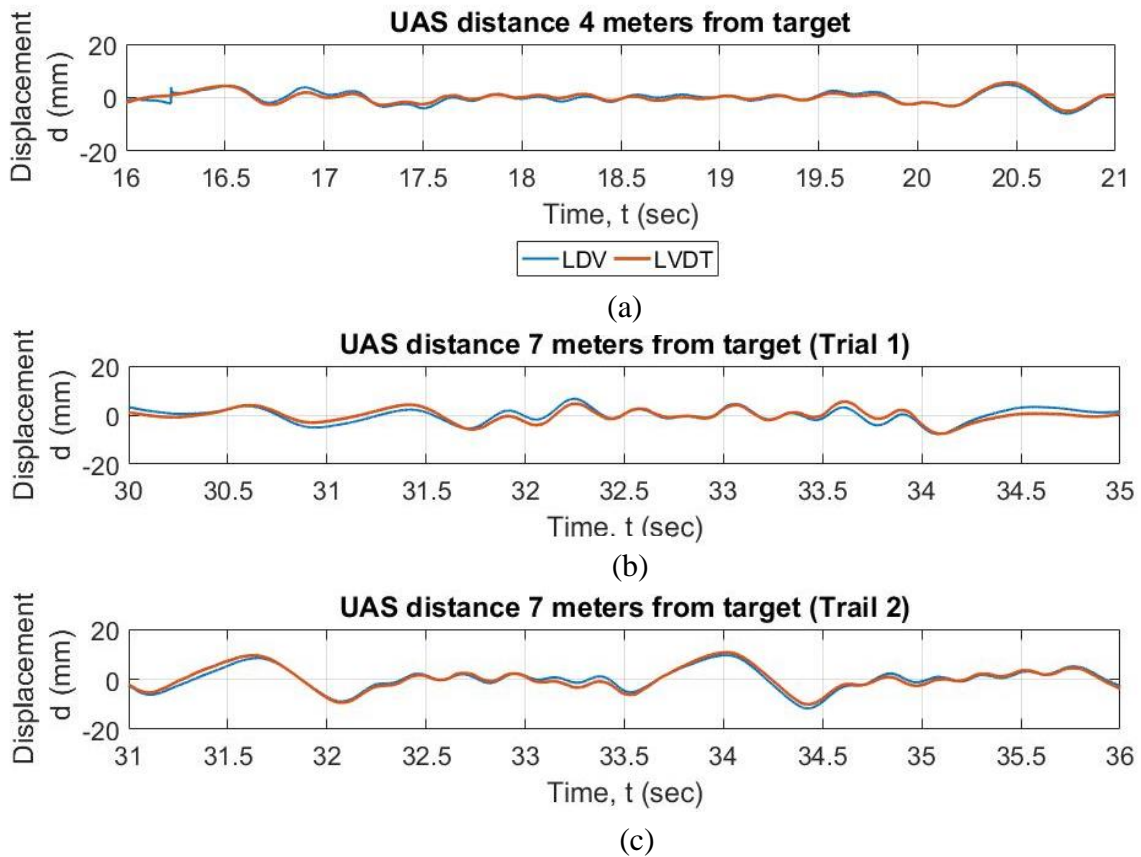
Figure 4-24. Focused dynamic displacements measured with LDV vs LVDT with UAS distance of (a) 4 meters from the target, (b) 7 meters from the target (Trial 1), and (c) 7 meters from the target (Trail 2)

When the signals are compared for peak and RMS differences, it is observed that both the peak as well as RMS difference is less than 2 mm (Figure 4-25). Figure 4-26 shows that the average output peak error of the three tests is about 10% and the average RMS difference is around 8%. These results are very

promising and prove that a LDV mounted on a UAS can be used for monitoring the

dynamic transverse bridge displacements under the discussed considerations.
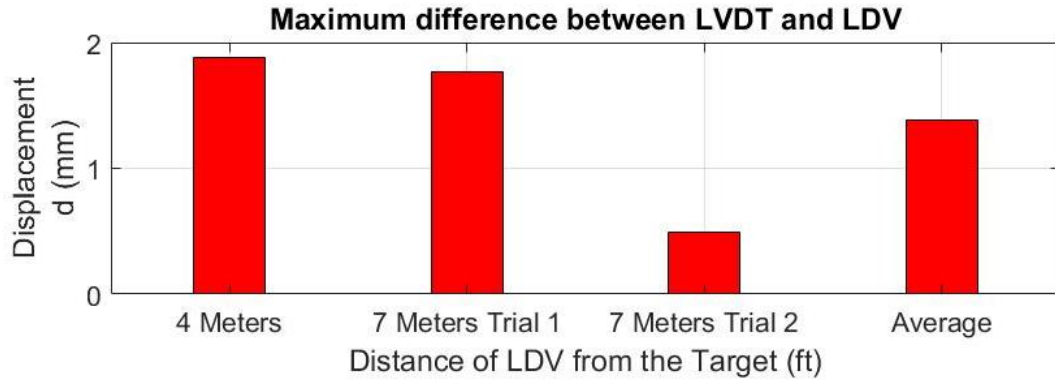
(a)
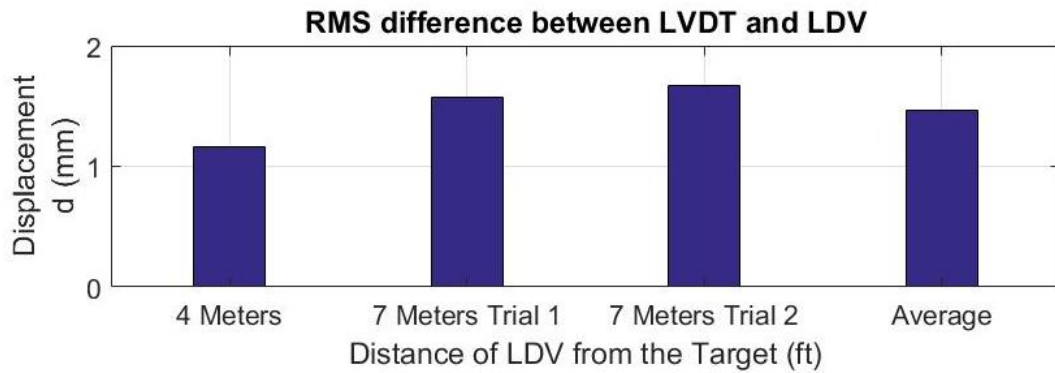
(b)

Figure 4-25.(a) Peak signal difference comparison between filtered vibrometer and LVDT signals and (b) RMS signal difference comparison between filtered vibrometer and LVDT signals

The last section of this chapter discusses the conclusion of these results in

the context of future applications measuring real train crossings over railroad

bridges.

Maximum difference between LVDT and LDV

(a)

RMS difference between LVDT and LDV
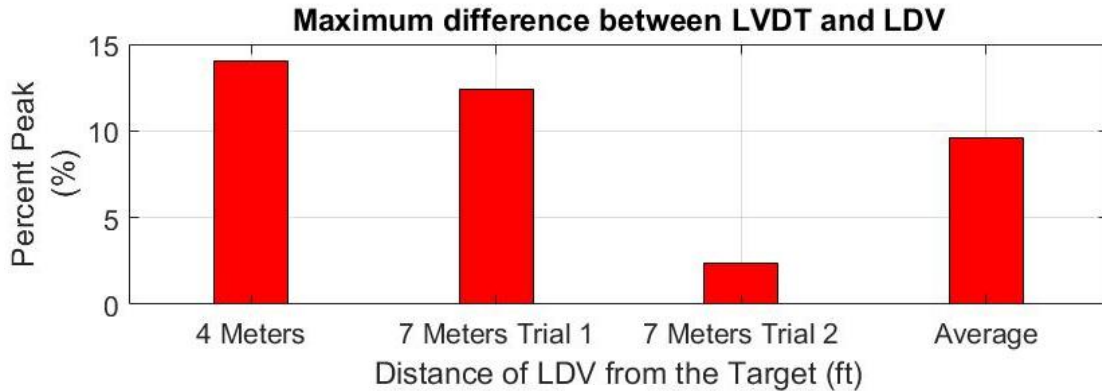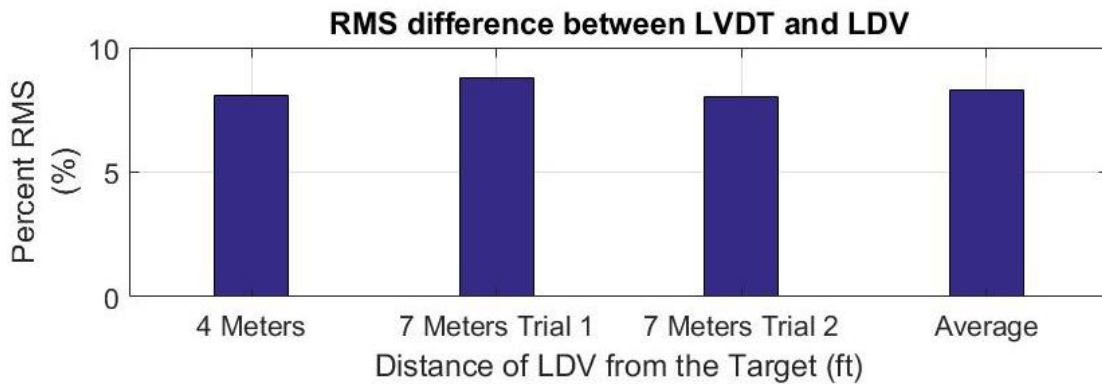
(b)

Figure 4-26. (a) Peak signal difference comparison between filtered vibrometer and LVDT signals and (b) RMS signal difference comparison between filtered vibrometer and LVDT signals

4.5 Conclusions

This chapter focused on measuring the dynamic transverse displacements of the target using a LDV mounted on a UAS. Initially, field tests were done to determine the optimal working distance of the vibrometer. The author observed that signal difference between LDVT and LDV does not change with the distance and there is no definite increase in the error. The UAS hovering test revealed that the UAS hovers with a displacement movement under 0.5Hz in frequency. DJI Matrice 600 Pro with an ability to lift a payload of 5.5 kg was selected for the research. During the field tests, the vibrometer was attached under the UAS and the entire assembly was tethered to the ground during the flight. The integrated

system was able to measure the dynamic transverse displacements of the target. The average of the maximum of the peak errors for the three trials is 10%. The average of the RMS difference for the three trials is 8%.

From these tests and their results, the author concluded that an integrated UAS-LDV system can measure dynamic transverse displacements of the target. The future stages of this research are described in the last chapter of this MS thesis that included field testing, integration of three systems to measure 3D displacements, and automatic monitoring of infrastructure using multiple UAS for safe and cost-effective monitoring of railroad critical infrastructure.

Chapter 5: Conclusion and Future Research

5.1 Summary

This research presents a novel method to measure dynamic transverse bridge displacement using an LDV with a UAS. The thesis introduced the problems of bridge transverse displacement measurement using contact and non-contact sensors. A new method for transverse bridge displacement measurement using a moving laser doppler vibrometer to be mounted on a drone was introduced. It was then established that the first step in this approach was to find the operation capabilities of a vibrometer subject to different motions. The algorithms were developed based on trigonometry to compensate for the motion of the vibrometer. These algorithms included correction of the static angular positioning of vibrometer, the dynamic angular motion of the vibrometer, and the random motion of the vibrometer. These algorithms were then used to test in different test scenarios. The vibrometer was tested for accuracy from different distances, for different frequencies and amplitudes, and different signal properties. The errors in these tests were found to be less than 10% peak and 2% RMS. The vibrometer was then tested for accuracy at angles with the target while being stationary with 5% peak and 2% RMS errors.

The correction algorithms were analyzed for dynamic pitching motion, and also for the random motion of the vibrometer. The differences for the dynamic pitching was less than 10% peak and less than 5% RMS, the difference of measurements between the proposed method and measured transverse

displacements for random motion were around 12% in peak and 1% in RMS. It was established from the results that the vibrometer can measure the target vibration from all these different configurations accurately under the described testing conditions.

The test setup was then designed to measure simulated displacement of railroad bridge under dynamic loading by train loads using LDV mounted on a UAS. The test setup also described how the tethering of UAS was used for protection of the vibrometer cables and assembly. The setup was successfully tested using a LDV mounted on a UAS. The results obtained were plotted and corrected for the out of bounds condition of the vibrometer. The corrected results were then analyzed in the frequency domain, and it was seen that the low frequency components of the vibrometer readings matched the movements of the drone. After filtering both signals for this low frequency component with a 3rd order high pass Butterworth with a 0.5Hz cut-off frequency, they were compared for the performance in the same frequency range. It was seen from this analysis that the signals matched closely to each other. Research results also showed that the peak difference between the actual displacement captured by the LVDT, and the displacement captured by the vibrometer is around 10%, and the RMS difference is around 8%, which is a promising result proving that the solution of using a LDV mounted UAS is suitable for dynamic transverse displacement measurement.

The major contributions of this research include the following: (1) selection of a laser sensor to be integrated with the UAS system. (2) design algorithms to correct the errors introduced due to the movement of the vibrometer, and

successful testing of transverse displacement measurement using a moving

vibrometer platform, as well as of the correction algorithms, (3) selection of a UAS

suitable for lifting the vibrometers, and (4) first attempts to use a LDV mounted on

a UAS for collection of dynamic transverse displacement data, and successful

testing and analysis of the data collected by the integrated UAS-LDV system. The

contributions of this MS Thesis are summarized in Figure 5-1
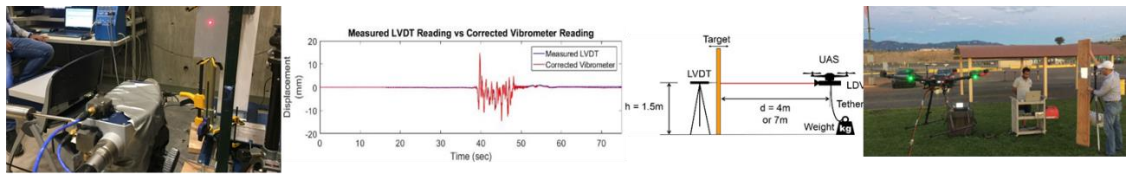
Displacement sensor selection	Development of correction algorithms	UAS-LDV system integration	Field testing of UAS-LDV system
Zero mean and non-zero mean signals Peak: 4% RMS: 1%	Angular motion correction: Peak: 10%, RMS: 5% Random motion correction: Peak: 10% RMS: 5%	LDV O/P not affected by distance between 5 and 25 feet from the target sUAS hovering freq. under 0.5 Hz	Target displacement measurement with integrated system: Peak: 10% RMS: 7%

Figure 5-1. Summary of contributions of the UAS-LDV integrated system

5.2 Future Research

5.2.1 Benchmarking and setting standards

This thesis has been complemented with constant guidance and

suggestions from the project review panel, and industry experts. As per their

feedback, the future work on this project includes benchmarking the UAS based

LDV operations for different operating and environmental conditions. This includes

benchmarking the operation of the UAS system on various types of steel reflective

surfaces, measurements on old rusty bridges with chipped paints, operating LDV based UAS in various lighting conditions, and in different weather. The other task will be to set standards for this system including the distance of operation from the target (25ft, 50ft, 75ft, 100ft, 125ft, 150ft) while flying to collect transverse target displacement. This will be done to improve the safety of UAS and infrastructure while operating next to a structure.

5.2.2 Field Testing

Field testing will be done on a real bridge under train passing events. The testing will be conducted in the test facility at Pueblo, CO. with a LDV mounted on a tethered UAS. Figure 5-2 shows the proposed test setup and layout of sensors for the field testing.
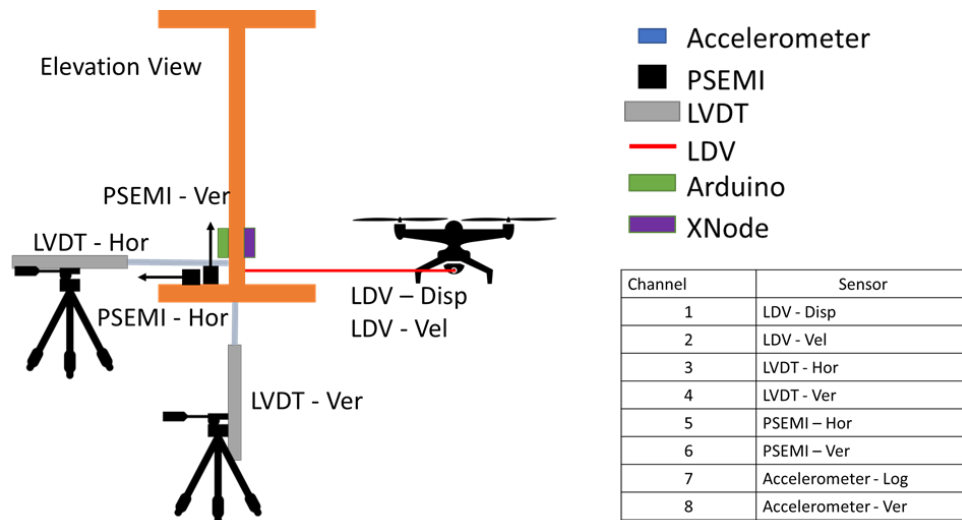
Figure 5-2. Elevation view proposed field testing setup and layout.

5.2.3 Integration of Three Systems

In the next step of this research, a third system will be added to the LDV and UAS. An Image processing based localization will be implemented for tracking

the movement of the UAS based on technology developed by Yoon, H. et al. 2016. The movements of the UAS will be calculated based on this approach, and these movements will be used for obtaining the horizontal movement of the UAS and the LDV for 3D displacement monitoring. Figure 5-3 shows the proposed UAS displacement monitoring technique using image processing of a checker board target.

$$s_1[x\ y\ 1] = [X\ Y\ Z\ 1]\begin{bmatrix} R_1 \\ t_1 \end{bmatrix} K$$

$$s_2[x_2\ y_2\ 1] = [X + dx, Y + dy, Z + dz, 1]\begin{bmatrix} R_2 \\ t_2 \end{bmatrix} K$$
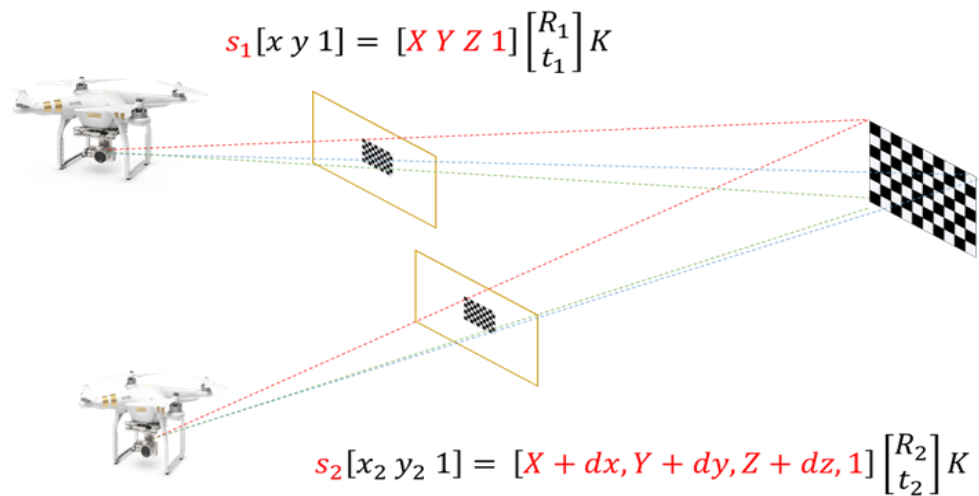
Figure 5-3. Proposed UAS 3D displacement monitoring technique using image processing of a checker board target (Yoon et al. 2016).

5.2.4 Automation

On future research steps, it is desired that the UAS will be programed to fly next to the railroad bridge and collect transverse displacements autonomously. This will save human effort involved in structural inspection. The automation of the UAS will have the capabilities to compensate for its movements under various environmental and mechanical conditions.

5.2.5 Swarm Robotics

Future developments from these integrated systems include simultaneously measuring the transverse displacement of the bridge at multiple points under

dynamic loading, as well as collection of the transverse train displacement during normal operations, automatically. To make this possible, a swarm system needs to be developed with multiple UAS-LDV systems for measuring the transverse bridge displacement such that the UAS work with each other and compensate for each other's movements. Also, the goal is to have these system housings in the train car itself for easier deployment and data acquisition for all the bridges along the path of the train for continuous monitoring.

5.3 Applications

The proposed method can be implemented with minimal training and basic data acquisition and flight knowledge. This technology has several applications such as real-time transverse displacement measurement of industrial buildings in operations such as oil and mining industries. The proposed technology reduces the efforts, risk, time, and cost involved in acquiring transverse displacements under loading operations and can be implemented for efficient infrastructure monitoring across various industries.

5.4 Publications

The results of this research are being reviewed for submission in reputed international journals. The results have also been presented at national and international technical conferences. The publications have been listed below:

a. *Journal publications (to be submitted in 2018)*

- Garg, P., Moreu, F., Ozdagli, A., Taha, M.R., and Mascarenas, D. (2017). Non-Contact Dynamic Displacement Measurement of Structures Using a Moving

Laser Doppler Vibrometer. (to be submitted to the Journal of Sound and Vibration Measurement) (Chapter 3)

- Garg, P., Moreu, F., Taha, M. R., Mascarenas, D. and Zhang, S. (2017). Dynamic Displacement Measurement Using a Laser Doppler Vibrometer Mounted on an Unmanned Aerial Vehicle. (To be submitted to Journal Mechanical Systems and Signal Processing) (Chapter 4)

b. Conference Proceedings

- Garg, P., Taylor, T., Moreu, F. (2018) "Transverse Bridge Displacement Measurement using Unmanned Aerial Vehicles" 7th World Conference on Structural Control and Monitoring, Qingdao, China (July 2018)

- Garg, P., Ozdagli, A. and Moreu, F. (2018) "Railroad Bridge Inspections for Maintenance and Replacement Prioritization Using Unmanned Aerial Vehicles (UAVs) with Laser Scanning Capabilities" TRB's Rail Safety IDEA Program: Sponsoring Innovation to Improve Railroad Safety and Performance. Transportation Research Board Annual Conference, Washington D. C. (January 2018)

- Garg, P., Ozdagli, A., and Moreu, F. Real-time Displacements of Railroad Bridges under Train Crossing Events Using Non-Contact, Reference-free Vibrometers. Structures Congress 2017 by American Society of Civil Engineers. Denver, CO, USA, Apr 6 – 8, 2017

- Garg, P., Gomez, J., Ozdagli, A., and Moreu, F. Optimal Bridge Displacement Controlled by Train Speed on Real-Time. IMAC XXXV conference by Society

of Experimental Mechanics (SEM). Garden Grove, CA, USA, Jan 30 – Feb 2, 2017 (Chapter 3)

- Garg, P., Gomez, J., Ozdagli, A., and Moreu, F. Non-Contact, Reference-Free Measurement of Bridge Displacement Using Vibrometer. 2nd Huixian International Forum on Earthquake Engineering for Young Researchers. Beijing, China. Aug 19 – 21, 2016 (Chapter 3)

- Ozdagli, A., Moreu, F., Vemuganti, S., Gomez, A., and Garg, P. Data Fusion of Accelerometers with Inclinometers for Reference-free High-Fidelity Displacement Estimation. 8th European Workshop on Structural Health Monitoring, Bilbao, Spain 2016

References

Agdas, D., Rice, J. A., Martinez, J. R., & Lasa, I. R. (2015). Comparison of visual inspection and structural-health monitoring as bridge condition assessment methods. Journal of Performance of Constructed Facilities, 30(3), 04015049.

Allen, J., & Walsh, B. (2008, May). Enhanced oil spill surveillance, detection and monitoring through the applied technology of unmanned air systems. In International oil spill conference (Vol. 2008, No. 1, pp. 113-120). American Petroleum Institute.

American Railway Engineering and Maintenance-of-Way Association (AREMA). (2003) 405 "Practical guide to railway engineering." Lanham: MD, 2003.

American Society of Civil Engineers (ASCE). (1988). "National Council on Public Works Improvement." Retrieved from https://www.infrastructurereportcard.org/wp-content/uploads/2017/03/1988-Fragile-Foundations-ExSum.pdf

American Society of Civil Engineers (ASCE). (1998). "1998 Report Card of America's Infrastructure." Retrieved from https://www.infrastructurereportcard.org/wp-content/uploads/2016/10/1998-ASCE-Report-Card-for-Americas-Infrastructure.pdf

American Society of Civil Engineers (ASCE). (2001). "2001 Report Card of America's Infrastructure." Retrieved from https://www.infrastructurereportcard.org/wp-content/uploads/2016/10/2001-ASCE-Report-Card-for-Americas-Infrastructure.pdf

American Society of Civil Engineers (ASCE). (2005). "2005 Report Card of America's Infrastructure." Retrieved from https://www.infrastructurereportcard.org/wp-content/uploads/2016/10/2005-ASCE-Report-Card-for-Americas-Infrastructure.pdf

American Society of Civil Engineers (ASCE). (2009). "2009 Report Card of America's Infrastructure." Retrieved from http://2013.infrastructurereportcard.org/2009/sites/default/files/RC2009_full_report.pdf

American Society of Civil Engineers (ASCE). (2013). "2013 Report Card of America's Infrastructure." Retrieved from http://2013.infrastructurereportcard.org/

American Society of Civil Engineers (ASCE). (2017). "2017 Report Card of America's Infrastructure." Retrieved from

https://www.infrastructurereportcard.org/wp-content/uploads/2016/10/Grades-Chart.png

Andrew Smyth, Meiliang Wu, Multi-rate Kalman filtering for the data fusion of displacement and acceleration response measurements in dynamic system monitoring, Mechanical Systems and Signal Processing, Volume 21, Issue 2, February 2007, Pages 706-723, ISSN 0888-3270, http://dx.doi.org/10.1016/j.ymssp.2006.03.005.

Ashkenazi, V., & Roberts, G. W. (1997). Experimental monitoring of the Humber Bridge using GPS. In Proceedings of the Institution of Civil Engineers-Civil Engineering (Vol. 120, No. 4, pp. 177-182). London: Published for the Institution of Civil Engineers by Thomas Telford Services, c1992

Association of American Railroads (AAR). (2013) "AAR 2013 Total Annual Spending Data". Retrieved from https://www.aar.org/Fact%20Sheets/Safety/2013-AAR_spending-graphic-fact-sheet.pdf

Association of American Railroads (AAR). (2013a) "Our Network, Economic and public benefits". Retrieved from https://www.aar.org/todays-railroads/our-network#maintain

Association of American Railroads (AAR). (2015) "AAR Outlook 2015". Retrieved from https://www.aar.org/Documents/Outlook%202015/2015OutlookReport.pdf

Association of American Railroads (AAR). (2016) "Bridging America: Maintaining Our Rail Bridges, Freight Rail Works.". Retrieved from http://archive.freightrailworks.org/videos/bridging-america/

Blanks, M. (2016). UAS Applications. Introduction to Unmanned Aircraft Systems, 19.

Bridge Access Specialties. (2017). "Railroads - Project Gallery". Retrieved from: http://www.bridgeaccessspecialties.com/railroads_project_gallery.php

Brumm, A. (2012). "Bluesky Purchases Innovative Optech Airborne Mapping System". Retrieved from: https://www.pobonline.com/articles/98667-bluesky-purchases-innovative-optech-airborne-mapping-system

Chan, B., Anstice, D., Pettigrew, T., & Saul, I. (2017, April). Photogrammetric modelling and drones for the effective inspection and management of major steel truss bridges: case study. In Austrosads Bridge Conference, 10th, 2017, Melbourne, Victoria, Australia.

Chen, L. C., & Lin, L. J. (2010). Detection of building changes from aerial images and light detection and ranging (LIDAR) data. Journal of Applied Remote Sensing, 4(1), 041870.

Chen, S. E., Hauser, E. W., & Boyle, C. G. (2015). U.S. Patent No. 9,014,415. Washington, DC: U.S. Patent and Trademark Office.

Cranenbroeck, J. V. (2015). "Long Bridge GNSS Monitoring by CGEOS". Retrieved from: http://www.wallonia.be/en/blog/long-bridge-gnss-monitoring-cgeos

Cummings, A. R., McKee, A., Kulkarni, K., & Markandey, N. (2017). The Rise of UAVs. Photogrammetric Engineering & Remote Sensing, 83(4), 317-325.

D. Ribeiro, R. Calçada, J. Ferreira, T. Martins, Non-contact measurement of the dynamic displacement of railway bridges using an advanced video-based system, Engineering Structures, Volume 75, 15 September 2014, Pages 164-180, ISSN 0141-0296, http://dx.doi.org/10.1016/j.engstruct.2014.04.051.

DJI (2017). "Matrice 600 Pro Specs". Matrice 600 Pro. Retrieved from https://www.dji.com/matrice600-pro/info#specs

d'Oleire-Oltmanns, S., Marzolff, I., Peter, K. D., & Ries, J. B. (2012). Unmanned aerial vehicle (UAV) for monitoring soil erosion in Morocco. Remote Sensing, 4(11), 3390-3416.

Ellenberg, A., Branco, L., Krick, A., Bartoli, I., & Kontsos, A. (2014). Use of unmanned aerial vehicle for quantitative infrastructure evaluation. Journal of Infrastructure Systems, 21(3), 04014054.

Ellenberg, A., Kontsos, A., Moon, F., & Bartoli, I. (2016). Bridge related damage quantification using unmanned aerial vehicle imagery. Structural Control and Health Monitoring, 23(9), 1168-1179.

Ellenberg, A. J. (2017). Structural Health Monitoring using Unmanned Aerial Systems (Doctoral dissertation, Drexel University).

Fanis Moschas, Stathis Stiros, Measurement of the dynamic displacements and of the modal frequencies of a short-span pedestrian bridge using GPS and an accelerometer, Engineering Structures, Volume 33, Issue 1, January 2011, Pages 10-17, ISSN 0141-0296, http://dx.doi.org/10.1016/j.engstruct.2010.09.013.

Federal Railroad Administration (FRA). (2010). "Bridge Safety Standards; Final Rule". Retrieved from http://www.fra.dot.gov/eLib/details/L03212

Federal Railroad Administration (FRA). (2015). "Freight Railroads Background" Office of Policy, Office of Rail Policy and Development, Federal Railroad Administration. Retrieved from https://www.fra.dot.gov/eLib/Details/L03011

Feng, D., Feng, M. Q., Ozer, E., & Fukuda, Y. (2015). A vision-based sensor for noncontact structural displacement measurement. Sensors, 15(7), 16557-16575.

Feng, M., Fukuda, Y., Feng, D., and Mizuta, M. (2015a). "Nontarget Vision Sensor for Remote Measurement of Bridge Dynamic Response." J. Bridge Eng., 10.1061/(ASCE)BE.1943-5592.0000747, 04015023.

Flammini, F., Pragliola, C., & Smarra, G. (2016, November). Railway infrastructure monitoring by drones. In Electrical Systems for Aircraft, Railway, Ship Propulsion and Road Vehicles & International Transportation Electrification Conference (ESARS-ITEC), International Conference on (pp. 1-6). IEEE.

Fukuda, Y., Feng, M. Q. and Shinozuka, M. (2010), Cost-effective vision-based system for monitoring dynamic response of civil engineering structures. Struct. Control Health Monit., 17: 918–936. doi:10.1002/stc.360

Garg, P., Gomez, J., Ozdagli, A., Moreu, F. (2016). Non-Contact, Reference-Free Measurement of Bridge Displacement Using Vibrometer. 2nd Huixian International Forum on Earthquake Engineering for Young Researchers. Beijing, China, August 19-21, 2016

Getzin, S., Nuske, R. S., & Wiegand, K. (2014). Using unmanned aerial vehicles (UAV) to quantify spatial gap patterns in forests. Remote Sensing, 6(8), 6988-7004.

Gomez, J. A., Ozdagli, A. I., & Moreu, F. (2017). Reference-free dynamic displacements of railroad bridges using low-cost sensors. Journal of Intelligent Material Systems and Structures, 1045389X17721375

Ham, Y., Han, K. K., Lin, J. J., & Golparvar-Fard, M. (2016). Visual monitoring of civil infrastructure systems via camera-equipped Unmanned Aerial Vehicles (UAVs): a review of related works. Visualization in Engineering, 4(1), 1.

Hani H. Nassif, Mayrai Gindy, Joe Davis, Comparison of laser Doppler vibrometer with contact sensors for monitoring bridge deflection and vibration, NDT & E International, Volume 38, Issue 3, April 2005, Pages 213-218, ISSN 0963-8695, http://dx.doi.org/10.1016/j.ndteint.2004.06.012.

Hawken, R., Nguyen, T., & Ivanyi, J. (2017, April). Bridge condition inspections using unmanned aerial vehicles: a trial project. In Austroads Bridge Conference, 10th, 2017, Melbourne, Victoria, Australia.

Hoag, A., Hoult, N. A., Take, W. A., Moreu, F., Le, H., & Tolikonda, V. (2017). Measuring displacements of a railroad bridge using DIC and accelerometers. SMART STRUCTURES AND SYSTEMS, 19(2), 225-236.

iMetrum. (2017). "Road Bridges". Retrieved from: https://www.imetrum.com/structural-testing/road-bridges/

Infrastructure Report Card. (2017) "Conditions and Capacity". Retrieved from https://www.infrastructurereportcard.org/cat-item/rail/

Joiner, S. (2010, February). "Is Bigger Better? 'Monster' Trains vs Freight Trains". Popular Mechanics. Retrieved from http://www.popularmechanics.com/technology/infrastructure/a5314/4345689/

Jong Jae Lee, Masanobu Shinozuka, A vision-based system for remote sensing of bridge displacement, NDT & E International, Volume 39, Issue 5, July 2006, Pages 425-431, ISSN 0963-8695, http://dx.doi.org/10.1016/j.ndteint.2005.12.003

Kim, H., Sim, S. H., & Cho, S. (2015, August). Unmanned aerial vehicle (UAV)-powered concrete crack detection based on Digital Image Processing. In 6th International Conference on Advances in Experimental Structural Engineering, 11th International Workshop on Advanced Smart Materials and Smart Structures Technology August (pp. 1-2).

Kogan, M. G., Kim, W. Y., Bock, Y., & Smyth, A. W. (2008). Load response on a large suspension bridge during the NYC Marathon revealed by GPS and accelerometers. Seismological Research Letters, 79(1), 12-19.

Lee, J. J., & Shinozuka, M. (2006). Real-time displacement measurement of a flexible bridge using digital image processing techniques. Experimental mechanics, 46(1), 105-114

Li, C. J., & Ling, H. (2016, June). High-resolution, downward-looking radar imaging using a small consumer drone. In Antennas and Propagation (APSURSI), 2016 IEEE International Symposium on (pp. 2037-2038). IEEE.

Liu, C., Li, W., Lei, W., Liu, L., & Hu, H. (2011, June). Architecture planning and geo-disasters assessment mapping of landslide by using airborne LiDAR data and UAV images. In Proc. SPIE (Vol. 8286, p. 82861Q).

M+P International. (2017). Bosch Hildesheim: m + p vibration control systems since 1991. Retrieved from: https://www.mpihome.com/de/nachrichten-termine/nachrichten/bosch-hildesheim-mp-schwingregelsysteme-seit-1991.html

Marshall, P. (2013). "How LIDAR is revolutionizing maps, geospatial data". Retrieved from: https://gcn.com/articles/2013/03/12/lidar-revolutionizing-maps-geospatial-data.aspx

Mason, J. D., Ayorinde, E. T., Mascarenas, D. D., & Moreu, F. (2016). Tap Testing Hammer using Unmanned Aerial Systems (UASs) (No. LA-UR-16-26204). Los Alamos National Laboratory (LANL).

Mascareñas, D., Flynn, E., Todd, M., Park, G., & Farrar, C. (2008). Wireless sensor technologies for monitoring civil structures. Sound and Vibration, 42(4), 16-21.

Mehrabi, A. B. (2006). In-service evaluation of cable-stayed bridges, overview of available methods and findings. Journal of Bridge Engineering, 11(6), 716-724.

Moreu, F., & Nagayama, T. (2008). Use of wireless sensors for timber trestle railroad bridges health monitoring assessment. In Proc., 2008 Structures Congress

Moreu, F., & LaFave, J. M. (2011). Survey of Current Research Topics--Railroad Bridges and Structural Engineering. Railway Track and Structures, 107(9)

Moreu, F., & LaFave, J. M. (2012). Current research topics: Railroad bridges and structural engineering. Newmark Structural Engineering Laboratory. University of Illinois at Urbana-Champaign

Moreu, F., Jo, H., Li, J., Kim, R. E., Cho, S., Kimmle, A., & LaFave, J. M. (2014). Dynamic assessment of timber railroad bridges using displacements. Journal of Bridge Engineering, 20(10), 04014114

Moreu, F. (2015). Framework for risk-based management and safety of railroad bridge infrastructure using wireless smart sensors (WSS) (Doctoral dissertation, University of Illinois at Urbana-Champaign)

Moreu, F., Li, J., Jo, H., Kim, R. E., Scola, S., Spencer Jr, B. F., & LaFave, J. M. (2015a). Reference-Free Displacements for Condition Assessment of Timber Railroad Bridges. Journal of Bridge Engineering, 21(2), 04015052

Moreu, F., Ayorinde, E., Mason, J., Farrar, C., & Mascarenas, D. (2017). Remote railroad bridge structural tap testing using aerial robots. International Journal of Intelligent Robotics and Applications. Retrieved from https://doi.org/10.1007/s41315-017-0041-7

Moschas, F., Psimoulis, P. A., & Stiros, S. C. (2013). GPS/RTS data fusion to overcome signal deficiencies in certain bridge dynamic monitoring projects. Smart Structures and Systems, 12(3_4), 251-269.

Nagayama, T., & Spencer Jr, B. F. (2007). Structural health monitoring using smart sensors. Newmark Structural Engineering Laboratory. University of Illinois at Urbana-Champaign.

Nakamura, S. (2000). "GPS Measurement of Wind-Induced Suspension Bridge Girder Displacements." J. Struct. Eng., 10.1061/(ASCE)0733-9445(2000)126:12(1413), 1413-1419.

National Oceanic and Atmospheric Administration (NOAA). (October 2017). "What is Lidar?" National Ocean Service website. Retrieved from https://oceanservice.noaa.gov/facts/lidar.html

Ozdagli, A. I., Gomez, J. A., & Moreu, F. (2017). Real-Time Reference-Free Displacement of Railroad Bridges during Train-Crossing Events. Journal of Bridge Engineering, 22(10), 04017073.

Paneque-Gálvez, J., McCall, M. K., Napoletano, B. M., Wich, S. A., & Koh, L. P. (2014). Small drones for community-based forest monitoring: An assessment of their feasibility and potential in tropical areas. Forests, 5(6), 1481-1507.

Panos A. Psimoulis, Stathis C. Stiros, Measurement of deflections and of oscillation frequencies of engineering structures using Robotic Theodolites (RTS), Engineering Structures, Volume 29, Issue 12, December 2007, Pages 3312-3324, ISSN 0141-0296, http://dx.doi.org/10.1016/j.engstruct.2007.09.006.

PCB Piezotronics. (2017). "Model: 311E1110G". Retrieved from https://www.pcb.com/products.aspx?m=3711E1110G

Piotr Olaszek, Investigation of the dynamic characteristic of bridge structures using a computer vision method, Measurement, Volume 25, Issue 3, 1 April 1999, Pages 227-236, ISSN 0263-2241, http://dx.doi.org/10.1016/S0263-2241(99)00006-8.

Psimoulis, P. and Stiros, S. (2013). "Measuring Deflections of a Short-Span Railway Bridge Using a Robotic Total Station." J. Bridge Eng., 10.1061/(ASCE)BE.1943-5592.0000334, 182-185.

Psimoulis, P. A., & Stiros, S. C. (2007). Measurement of deflections and of oscillation frequencies of engineering structures using Robotic Theodolites (RTS). Engineering Structures, 29(12), 3312-3324.

Polytec Inc. (2017). "Technical Data." OFV-534 Compact Sensor Head. Retrieved from http://www.polytec.com/fileadmin/user_uploads/Products/Vibrometers/OFV-534/Documents/OM_DS_OFV-534_E_42367.pdf

Polytec Inc (2017a). "Basic Principles of Vibrometry". Retrieved from http://www.polytec.com/us/solutions/vibration-measurement/basic-principles-of-vibrometry/

Quanser. (2017). "Overview". Shake Table II. Retrieved from https://www.quanser.com/products/shake-table-ii/

Reagan, D., Sabato, A., & Niezrecki, C. (2017, April). Unmanned aerial vehicle acquisition of three-dimensional digital image correlation measurements for structural health monitoring of bridges. In Nondestructive Characterization and Monitoring of Advanced Materials, Aerospace, and Civil Infrastructure 2017 (Vol. 10169, p. 1016909). International Society for Optics and Photonics.

RDP Group. (2017). "DCTH Series DC to DC LVDT Displacement Transducer". Retrieved from http://www.rdpe.com/ex/dcth.htm

Restas, A. (2015). Drone applications for supporting disaster management. World Journal of Engineering and Technology, 3(03), 316.

Stathis C. Stiros, Panos A. Psimoulis, Response of a historical short-span railway bridge to passing trains: 3-D deflections and dominant frequencies derived from Robotic Total Station (RTS) measurements, Engineering Structures,

Volume 45, December 2012, Pages 362-371, ISSN 0141-0296, http://dx.doi.org/10.1016/j.engstruct.2012.06.029.

Sheppard, L. (2010). "Innovative Infrastructure: Smart Bridges". Retrieved from: http://buildipedia.com/aec-pros/public-infrastructure/innovative-infrastructure-smart-bridges?print=1&tmpl=component

Siebert, S., & Teizer, J. (2014). Mobile 3D mapping for surveying earthwork projects using an Unmanned Aerial Vehicle (UAV) system. Automation in Construction, 41, 1-14.

Smartsensys. (2017). "Facade Monitoring". Retrieved from: http://smartsensys.com/suave/

Wang, T., Garg, V., and Chu, K. (1991). "Railway Bridge/Vehicle Interaction Studies with New Vehicle Model." J. Struct. Eng., 10.1061/(ASCE)0733-9445(1991)117:7(2099), 2099-2116.

Watson, C., Watson, T., and Coleman, R. (2007). "Structural Monitoring of Cable-Stayed Bridge: Analysis of GPS versus Modeled Deflections." J. Surv. Eng., 10.1061/(ASCE)0733-9453(2007)133:1(23), 23-28.

Woolard, J. W., & Colby, J. D. (2002). Spatial characterization, resolution, and volumetric change of coastal dunes using airborne LIDAR: Cape Hatteras, North Carolina. Geomorphology, 48(1), 269-287.

Ting-Hua Yi, Hong-Nan Li, Ming Gu, Experimental assessment of high-rate GPS receivers for deformation monitoring of bridge, Measurement, Volume 46, Issue 1, January 2013, Pages 420-432, ISSN 0263-2241, http://dx.doi.org/10.1016/j.measurement.2012.07.018.

Verma, V., Kumar, R., & Hsu, S. (2006). 3D building detection and modeling from aerial LIDAR data. In Computer Vision and Pattern Recognition, 2006 IEEE Computer Society Conference on (Vol. 2, pp. 2213-2220). IEEE.

Vian, J. L., Mansouri, A. R., & Saad, E. W. (2011). U.S. Patent No. 8,060,270. Washington, DC: U.S. Patent and Trademark Office.

Vu, T. T., Matsuoka, M., & Yamazaki, F. (2004, September). LIDAR-based change detection of buildings in dense urban areas. In Geoscience and Remote Sensing Symposium, 2004. IGARSS'04. Proceedings. 2004 IEEE International (Vol. 5, pp. 3413-3416). IEEE.

X. Meng, A.H. Dodson, G.W. Roberts, Detecting bridge dynamics with GPS and triaxial accelerometers, Engineering Structures, Volume 29, Issue 11, November 2007, Pages 3178-3184, ISSN 0141-0296, http://dx.doi.org/10.1016/j.engstruct.2007.03.012.

Yang, J., Li, J. B., and Lin, G. (2005). "A simple approach to integration of acceleration data for dynamic soil–structure interaction analysis." Soil Dyn.EarthquakeEng.,26(8),725–734

Yoon, H., Elanwar, H., Choi, H., Golparvar-Fard, M., & Spencer, B. F. (2016). Target-free approach for vision-based structural system identification using con sumer-grade cameras. Structural Control and Health Monitoring, 23(12), 1405-1416.

Yoon, H., Shin, J., & Spencer, B. F. (2017). Structural Displacement Measurement using an Unmanned Aerial System. Computer-Aided Civil and Infrastructure Engineering.

Zhang, S., & Bogus, S. M. (2014). Use of low-cost remote sensing for infrastructure management. In Construction Research Congress 2014: Construction in a Global Network (pp. 1299-1308).